JPRS L/9987

17 September 1981

USSR Report

EARTH SCIENCES

(FOUO 7/81)

FBIS FOREIGN BROADCAST INFORMATION SERVICE

NOTE

JPRS publications contain information primarily from foreign newspapers, periodicals and books, but also from news agency transmissions and broadcasts. Materials from foreign-language sources are translated; those from English-language sources are transcribed or reprinted, with the original phrasing and other characteristics retained.

Headlines, editorial reports, and material enclosed in brackets [] are supplied by JPRS. Processing indicators such as [Text] or [Excerpt] in the first line of each item, or following the last line of a brief, indicate how the original information was processed. Where no processing indicator is given, the information was summarized or extracted.

Unfamiliar names rendered phonetically or transliterated are enclosed in parentheses. Words or names preceded by a question mark and enclosed in parentheses were not clear in the original but have been supplied as appropriate in context. Other unattributed parenthetical notes within the body of an item originate with the source. Times within items are as given by source.

The contents of this publication in no way represent the policies, views or attitudes of the U.S. Government.

APPROVED FOR RELEASE: 2007/02/09: CIA-RDP82-00850R000400050037-2

JPRS L/9987

17 September 1981

USSR REPORT
EARTH SCIENCES
(FOUO 7/81)

CONTENTS

OCEANOGRAPHY

UDC 551.466.81

GENERATION OF INTERNAL WAVES BY LOCAL DISTURBANCES IN A FLUID WITH GIVEN VARIATION OF DENSITY OVER DEPTH

Moscow IZVESTIYA AKADEMII NAUK SSSR: FIZIKA ATMOSFERY I OKEANA in Russian Vol 17, No 6, Jun 81 pp 625-631

[Article by I. V. Sturova and V. A. Sukharev, Institute of Hydrodynamics, Siberian Department, USSR Academy of Sciences]

[Text] A method is proposed for calculating linear internal gravitational waves occurring in a nonviscous incompressible fluid with arbitrary continuous stable stratification during uniform flow over a source and runoff of equal intensity and during collapse of a "spot" by a completely mixed fluid.

Solution of the given problem has now been found only for some special cases of dense stratification of a fluid (see, for example [1-4]). Primarily retaining the postulation of the problem used in [4], let us investigate the behavior of internal waves for the general case of continuous (stable) variation of density over depth.

1. Let us consider the stead three-dimensional problem of uniform flow around a point source system at velocity U and runoff of equal intensity m located at depth h from an undisturbed free surface z = 0 of a horizontal layer of fluid $-\infty < x, y < \infty$ and $-H \leq z \leq 0$. The segment of the straight line connecting the source and the runoff has a length 2a and is parallel to the x axis coinciding with the direction of the velocity vector of the fluid far upstream.

The equation for the vertical velocity component v(x, y, z) has the following form in linear postulation using Bussinescu's approximation

$$\frac{\partial^2}{\partial x^2}\Delta v + \frac{N^2(z)}{U^2}\Delta_2 v = m\delta(y)\frac{\partial}{\partial z}\delta(z+h)\frac{\partial^2}{\partial x^2}[\delta(x+a)-\delta(x-a)] \qquad (1)$$

with boundary value conditions

$$v=0 \quad \text{at} \quad z=0,\ z=-H,$$
$$v\to 0 \quad \text{at} \quad x^2+y^2\to\infty.$$

where Δ and Δ_2 are the complete and horizontal Laplace operators, respectively, $N(z) = [-g\rho_0'(z)/\rho_s]^{1/2}$ is the Brent-Byaysyal' frequency, $\rho_0(z)$ is the density distribution in an undisturbed source and $\rho_s = \rho_0(0)$ and δ is a Dirac delta function.

It should be noted that introduction of Bussinescu's approximation and the condition of a "hard cover" on a free surface is not a significant simplification (see the solution of a similar plane problem in [5]).

Let us introduce the dimensionless variables, having taken as scale units of length and velocity the values of R(the radius of the mid-section of a body, flow around which is simulated by a given system of features (see [4] for details)) and U, and let us utilize the Fourier transform with respect to variables x and y with real parameters μ and ν, respectively. For the function $f(\mu, \nu, z)$--a double Fourier transform $v(x, y, z)$ we find an ordinary differential equation

$$f''-k^2[1-\Lambda\gamma(z)/\mu^2]f=2im\sin\mu a\delta'(z+h),$$
$$f=0 \quad \text{at} \quad z=0,\ z=-H, \tag{2}$$

where $k^2=\mu^2+\nu^2$, $\Lambda=gR/U^2$, $\gamma(z)=-\rho_0'(z)/\rho_*$. All the presently known solutions of the initial equation (1) with continuous density distribution were found for those cases when function $\gamma(z)$ is constant or piecewise constant.

In the general case for a smooth function $\gamma(z)$, the solution of equation (2) can be represented in the form (see (7.9) in [1])

$$f(z)=-2im\sin\mu a\sum_{n=1}^{\infty}\frac{W_n'(-h)W_n(z)}{(k_n^2-k^2)\int_{-H}^{0}W_n^2(s)\,ds},$$

where k_n and $W_n(z)$ are the eigen-values and eigen-functions, respectively, of the Sturm-Louisville problem

$$W''+\varkappa\Lambda\gamma(z)W=\lambda W,$$
$$W=0 \quad \text{at} \quad z=0,\ z=-H,\ \varkappa=k^2/\mu^2 \tag{3}$$

with $\lambda = k^2$ in the role of a spectral parameter. As is known (see, for example, [6]), the set of eigen-numbers of this problem is no more than denumerable, has no final limiting point and all the eigen-numbers are simple and real. Moreover, the set of eigen-numbers of this problem is bounded above (all eigen-numbers lie in the range $(-\infty, \varkappa\Lambda\gamma_m]$, where $\gamma_m=\max_{-H\le z\le 0}\gamma(z)$) and, consequently, there is a finite number of eigen-numbers λ_n (n = 1, 2, 3...) which increases with an increase of $\varkappa$ for a given value of $\varkappa$.

Knowing the value of f, from the linearized condition $\partial\eta/\partial x = v/U$ for the function $\eta(x, y, z)$ that describes vertical displacements of the liquid particle, we determine the function $\xi(\mu, \nu, z)$--the dual Fourier transform of function η and we make the inverse transformations similar to [4].

The behavior of internal waves at great distances from the source of the disturbance is investigated in the given paper; therefore, when performing integration in the complex k-plane, only single integrals that are residues at the real poles of the integrand will be left. According to the condition of radiation, all the real poles turn around small semicircles on which $\mathrm{Im}(k) < 0$. Accordingly,

$$\eta(r,\varphi,z)\approx-\frac{m}{\pi}\sum_{n=1}^{\infty}\left\{\int_0^{\pi/2}P_n\sin(rk_n\sin(\theta+\varphi))\,d\theta+\right.$$
$$\left.+\int^{\pi/2}P_n\sin(rk_n\sin(\theta-\varphi))\,d\theta\right\}, \tag{4}$$

where

$$P_n=\frac{\sin(ak_n\sin\theta)}{k_n\sin\theta}\frac{W'(k_n,\theta,-h)W(k_r,\theta,z)}{\int_{-H}^{0}W^2(k_n,\theta,s)\,ds}$$

and the variables are substituted

$$\mu=k\sin\theta,\ \nu=k\cos\theta,\ x=r\cos\varphi,\ y=r\sin\varphi.$$

The expressions for the other flow characteristics have similar form [4].

Asymptotic analysis of the integrals in (4) at $r\to\infty$ by the stationary phase method shows that the main contribution of order $O(r^{-1/2})$ introduces a second integral since it alone has stationary points in the integration interval. The contribution of the second integral has an order not less than $O(r^{-1})$. This statement can be proved in the following manner. The stationary points are determined from the equation $\Psi'(\theta)=0$ at $\Psi(\theta)=k_n(\theta)\sin(\theta\pm\phi)$, which may lead to the form $\operatorname{tg}\phi=\mp\Phi(\theta)$, where

$$\Phi(\theta)=\frac{\operatorname{tg}\theta\,dk_n/d\theta+k_n}{dk_n/d\theta-k_n\operatorname{tg}\theta}=\frac{\varkappa^2\sqrt{\varkappa-1}\,d(\lambda_n/\varkappa)/d\varkappa}{\varkappa(\varkappa-1)d\lambda_n/d\varkappa+\lambda_n}.$$

It is shown in [6] that $d(\lambda_n/\varkappa)/d\varkappa>0$ and consequently $\Phi(\theta)>0$ at all values of θ $(0<\theta<\pi/2)$ and the stationary points at $0<\phi<\pi/2$ may have only the second integral in (4) for which $\Psi(\theta)=k_n(\theta)\sin(\theta-\phi)$. However, direct use of the stationary phase method to calculate this integral is difficult since the function $\Psi(\theta)$ may in the general case have several extreme points in the integration interval and it is difficult to predict beforehand the number and multiple of them.

The proposed method of solving the given problem was realized numerically and consists of three steps: 1) determination of the positive eigen-values $\varkappa_n$ at $\lambda=0$ for a given number of wave modes, 2) finding the functions of $\lambda_n(\varkappa)$ and 3) performing numerical integration of (4) similar to [4].

To calculate the eigen-values of $\lambda_n(\varkappa)$ of problem (3), one can introduce the transforms

$$W_n(z)=e^{\psi_n(z)}\sin\omega_n(z),\ W_n'(z)=e^{\psi_n(z)}\cos\omega_n(z) \tag{5}$$

and one can find the following boundary-value problem:

$$\omega_n'=1+[\varkappa\Lambda\gamma(z)-\lambda_n-1]\sin^2\omega_n,$$
$$\omega_n=0 \quad \text{at} \quad z=-H,\ \omega_n=n\pi \quad \text{at} \quad z=0. \tag{6}$$

The equation for function $\psi_n(z)$ has the form

$$\psi_n'=0{,}5[1-\varkappa\Lambda\gamma(z)+\lambda_n]\sin 2\omega_n,$$
$$\psi_n=0 \quad \text{at} \quad z=-H.$$

The Runge-Kutta-Mersen method of fourth order of accuracy with automatic selection of the step was used for numerical solution of these equations and the derived eigen-numbers were refined by the adjustment method. It should be noted in this case that the infinite summation limit in (4) is replaced by a finite value of M for $\phi > 0$, determined from the relation

$$\varkappa_M(0)<\sin^{-2}\varphi<\varkappa_{M+1}(0).$$

To make specific calculations, as an example of density distribution in the undisturbed state, the thermocline model was selected for which

$$\gamma(z)=\gamma_0\{1+24\,\mathrm{ch}^{-2}[(z+10)/2]\} \quad \text{at} \quad -H\leqslant z\leqslant 0, \tag{7}$$

where $\gamma_0 = 2.484\cdot10^{-5}$ and H = 100. The first 10 values of $\varkappa_n(0)$ for the given density distribution at Λ = 12.26 are given in the table. The results obtained by the WKB method [7], according to which $\varkappa_n(0)=\left[n\pi\Big/\int_{-H}^{0}\sqrt{\Lambda\gamma(s)}\,ds\right]^2$, are also presented for comparison. For distribution (7) $\int_{-H}^{0}\sqrt{\Lambda\gamma(s)}\,ds=2{,}099.$ The values of $\varkappa_n(0)$ characterize the angles at which the corresponding wave modes are included. The relative accuracy in solving the differential equation was equal to 10^{-5} and that during adjustment was equal to n^{-4} in the calculations given here and below.

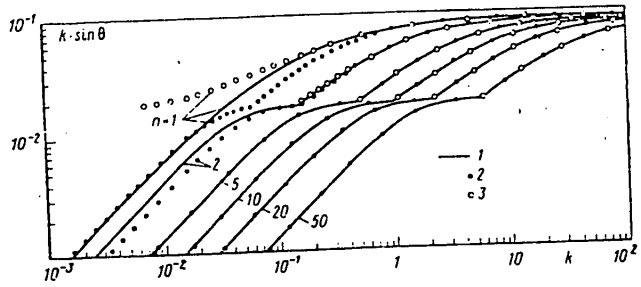

Figure 1. Variance Functions for Some Modes of Wave Motion (n = 1, 2, 5, 10, 20, 50): 1--numerical solution; 2--WKB approximation; 3--infinite fluid

The variance functions for some modes of wave motion are presented in Figure 1, where the solid lines indicate the results of numerical calculations and the dark points show the results of WKB approximation [7, 8] obtained by using the two-scale asymptotic expansion method. It is obvious that, beginning approximately from mode 5, the results of both solutions become very similar. The curves noted by the light points correspond to the solution of [9] for an infinite liquid. In this case the discrete spectrum exists only at $\sqrt{\Lambda\gamma_0}<k\sin\theta<\sqrt{\Lambda\gamma_m}$ for the density distribution in the form of (7).

Clearly marked "shelves," especially for the higher modes, are observed in the behavior of the variance curves, the appearance of which is accompanied by complex dependence of the group velocities of internal waves on frequency and a number of abnormal frequencies appears at which the group velocity reaches extreme values. This fact results in difficulties in using the stationary phase method. Similar anomalies in the behavior of variance curves are noted in [4, 10], where the frequency characteristics of internal waves in a fluid consisting of several layers with constant values of Brent-Vyaysyal' frequency in each layer were investigated.

It should be pointed out that there is now a number of papers (see the bibliography in [11]) devoted to calculation of variance curves and eigen-functions of wave motion in the case of an arbitrarily stratified fluid. The method used in this paper is similar to that in [11].

Eigen-Values of $\varkappa_n(0)$ for the First 10 Modes

n	(1) Численное решение	(2) Приближение ВКБ	n	Численное решение	Приближение ВКБ
1	2,39	2.24	6	80,1	80,6
2	5,89	8,96	7	109	110
3	17,3	20,2	8	148	143
4	36,6	35.8	9	187	181
5	59,8	56,0	10	225	224

Key:
1. Numerical solution
2. WKB approximation

Calculations of the vertical displacements of the liquid particles described by the function $\eta(x, y, z)$ were made at $y/R = 100$, $a/R = 9.49$ and $mR/U^2 = 3.16$. The disturbances that are the sum of the first 26 modes at $h/R = 20$ and $z/R = -4$, -10, -16 and -35 (curves 1-4) are shown in Figure 2, a. It is obvious that the most intensive and short-wave disturbances occur at $z/R = -10$, which corresponds to the level at which the maximum Brent-Vyaysyal' frequency is located. The oscillation amplitude decreases significantly as the distance from the center of the thermocline decreases. Comparison of the contributions of individual modes showed that the disturbances for values of z corresponding to the thermocline zone are mainly determined by the first mode, but higher modes contribute maximum disturbances outside the thermocline zone. If the submergence depth varies, the most intensive disturbances occur when the characteristics are in the thermocline zone. Thus, for

example, the oscillation amplitude at levels z/R = -10 increases fivefold at h/R = = 12 compared to the case of h/R = 20 and in this case the wavelength decreases somewhat and attenuation becomes very slow with an increase of x. The increase of amplitudes is not more than threefold at the other levels under consideration.

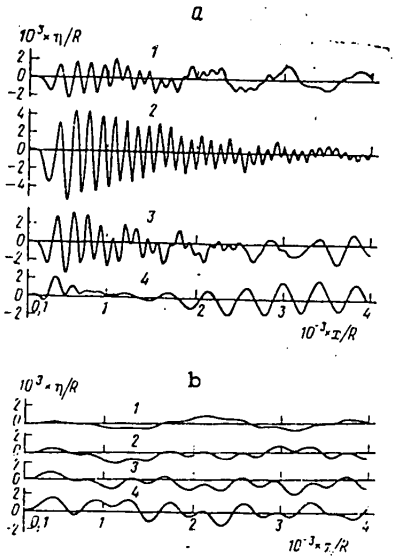

Figure 2. Vertical Displacements That Occur During Uniform Flow Around a Source-Runoff System for y/R = 100 and h/R = 20 in the case of a thermocline (a) and a linearly stratified fluid (b). Curves 1-4 correspond to values of z/R = -4, -10, -16 and -35

Similar disturbances occurring at the same parameters in the case of a linearly stratified fluid are presented in Figure 2, b for comparison, for which the function $\gamma(z)$ is a constant and is equal to γ_0. It is obvious that the disturbances have a greater wavelength and lower amplitudes in this case. The contributions of individual modes are approximately identical in nature.

2. To investigate internal waves induced by collapse of the mixing zone, let us consider the plane nonstationary problem on flow arising upon collapse of an initially round spot of a completely mixed fluid surrounded by a statified fluid.

Let us introduce the coordinate system y, z in the plane of motion (the y axis coincides as before with the upper boundary of the fluid and the z axis is aligned vertically upward). The fluid is mixed at initial moment of time t = 0 within a circle of radius R with center at the point y = 0, z = -h so that the disturbance of density has the form

$$\rho(y, z, 0) = \begin{cases} \rho_c - \rho_0(z) & \text{at } y^2+(z+h)^2<R^2, \\ 0 & \text{at } y^2+(z+h)^2>R^2, \end{cases}$$

where

$$\rho_c = \frac{2}{\pi R^2} \int_{-R-h}^{R-h} \rho_0(z) [R^2 - (z+h)^2]^{1/2} dz.$$

The density distribution outside the spot is described by the function $\rho_0(z)$. The method of solving the given problem is similar to item 1 (time t plays the role of longitudinal coordinate x and the values of R and $(R/g)^{1/2}$ are taken as the scalar units of length and time. The ordinary differential equation for the function $f(\nu, z, \mu)$, which is the double Fourier transform of function $v(y, z, t)$, has the form

$$f'' - \nu^2 [1 - \gamma(z)/\mu^2] f = F, \quad f = 0 \quad \text{at} \quad z = 0, \; z = -H,$$

where

$$F = -\frac{2\nu[\rho_c - \rho_0(z)]}{\rho_* \mu^2} \sin(\nu \sqrt{R^2 - (z+h)^2}) \, V(R+z+h) \, V(R-z-h),$$

V is a Heaviside step function. Similar to item 1, the final solution for function $\eta(r, \phi, z)$, which satisfies the linearized condition $\partial\eta/\partial t = v$ in the given problem, at $r \to \infty$ outside the spot has the form

$$\eta(r, \varphi, z) \approx -\frac{1}{\pi} \sum_{n=1}^{M} \int_{\varphi}^{\pi/2} \frac{W(k_n, \theta, z) \cos(r k_n \sin(\theta - \varphi)) \, d\theta}{k^2 \cos\theta \sin^3\theta \int_{-H}^{0} W_2 \, ds} \times \tag{8}$$

$$\times \int_{-(R+h)}^{R-h} \frac{\rho_0(s) - \rho_c}{\rho_*} W(k_n, \theta, s) \sin(k_n \sin\theta \sqrt{R^2 - (s+h)^2}) \, ds,$$

where

$$r = \sqrt{y^2 + t^2}, \quad \varphi = \operatorname{arctg}(y/t).$$

The function $W(k_n, \theta, z)$ is an eigen-function of the Sturm-Liuville problem similar to (3)

$$W'' + \bar{\varkappa}\gamma(z) W = \bar{\lambda} W, \quad W = 0 \quad \text{at} \quad z = 0, \; z = -H,$$

where $\bar{\varkappa} = \operatorname{ctg}^2\theta$ and $\bar{\lambda} = k^2 \cos^2\theta$. In the special case when the spot is located completely in the layer with constant density gradient, the internal integral in (8) is calculated analytically and, making use of transforms (5) for function W, we find

$$\eta(r, \varphi, z) \approx \sum_{n=1}^{M} \int_{\varphi}^{\pi/2} \frac{J_2(\sqrt{\alpha} \operatorname{ctg}\theta) \cos\{\omega(-h)) \sin(\omega(z)) \cos(r k_n \sin(\theta - \varphi)) \, d\theta}{k_n \sin\theta \cos^2\theta \int_{-H}^{0} \sin^2 \omega(s) \exp[2\psi(s) - \psi(-h) - \psi(z)] \, ds},$$

where $\alpha = \gamma(-h)$ and J_2 is a second-order Bessel function of first kind.

Numerical calculations of vertical displacements of liquid particles were made similar to item 1 for the function $\gamma(z)$ given by expression (7) at $y/R = 100$.

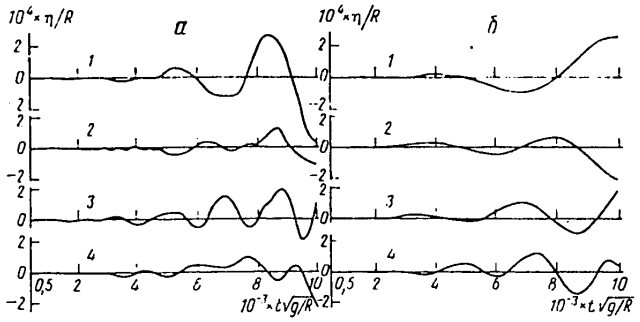

Figure 3. Vertical Displacements Caused by Collapse of "Spot" at y/R = 100 and h/R = 20 in the Case of a Thermocline (a) and a Linearly Stratified Fluid (b). Curves 1-4 correspond to values of z/R = = -4, -10, -16 and -35

The functions $\eta(y, z, t)$ at h/R = 20 and z/R = -4, -10, -16 and -35 (curves 1-4) are presented in Figure 3,a. Similar to Figure 2, a, the contribution of the first 26 modes is taken into account. Unlike the problem considered in section 1, the pattern of wave disturbances is hardly dependent on the location of the spot. Comparison of the contributions of individual modes showed that the first modes are negligible while the higher modes make the main contribution. Similar disturbances occurring at the same parameters in the case of a linearly stratified fluid are presented in Figure 3, b for comparison. It is obvious that the amplitude and frequency nature of the disturbances remains the same as in the case of a thermocline in the reciprocal to the first problem.

It should be noted that the described behavior of internal waves generated by local disturbances of both types coincides qualitatively with the earlier considered case of a three-layer fluid, in each layer of which the Brent-Vyaysyal' frequency was constant and maximum in the middle layer [4].

The outlined method of calculation can also be used to investigate internal waves generated by other types of disturbances, for example, by bottom unevennesses or atmospheric disturbances, since analysis of these problems is made by the same method [12].

Bibliography

1. Miles, J. W., "Internal Waves Generated By a Horizontally Moving Source," GEOPHYSICS AND FLUID DYNAMICS, Vol 2, No 1, 1971.

2. Schooley, A. H. and B. A. Hughes, "An Experimental and Theoretical Study of Internal Waves Generated by the Collapse of a Two-Dimensional Mixed Region in a Density Gradient," JOURNAL OF FLUID MECHANICS, Vol 51, Part 1, 1972.

3. Dokuchayev, V. P. and I. S. Dolina, "Radiation of Internal Waves by Sources in an Exponentially Stratified Fluid," IZVESTIYA AN SSSR, FAO, Vol 13, No 6, 1977.

4. Sturova, I. V., "Internal Waves Generated by Local Disturbances in a Stratified Fluid," in "Dinamika sploshnoy sredy" [The Dynamics of a Continuous Medium], Issue 35, Novosibirsk, Izdatel'stvo Instituta gidrodinamiki SO AN SSSR, 1978.

5. Sturova, I. V. and V. A. Sukharev, "The Plane Problem of Wave Motions Occurring in a Continuously Stratified Fluid During Flow Around a Submerged Body," IZVESTIYA AN SSSR, MZHG, No 4, 1978.

6. Dotsenko, S. F., "The Structure of Wave Motion in a Flow During Arbitrary Variation of Density Over Depth," MORSKIYE GIDROFIZICHESKIYE ISSLEDOVANIYE, No 3, 1973.

7. Hyun, J. M., "Internal Wave Dispersion in Deep Oceans Calculated by Means of Two-Variable Expansion Techniques," JOURNAL OF THE OCEANOGRAPHIC SOCIETY OF JAPAN, Vol 32, No 1, 1976.

8. Kulakov, A. V., "Applying the Method of Two-Scale Asymptotic Expansions to Investigate the Problem of the Vertical Structure of Free Oscillations in the Ocean," TRUDY GMTS SSSR, No 197, 1977.

9. Zaytsev, A. A., "The Thermocline as a Waveguide Channel," in "Issledovaniye otkrytoy chasti Atlanticheskogo okeana" [Investigating the Open Part of the Atlantic Ocean], Moscow, Izdatel'stvo Instituta okeanologii AN SSSR, 1978.

10. Goncharov, V. V., "Some Characteristics of Internal Waves in the Ocean," in "Tsunami i vnutrenniye volny" [Tsunamis and Internal Waves], Sevastopol', Izdatel'stvo MGI AN USSR, 1976.

11. Kulakov, A. V., "Numerical Method of Calculating the Vertical Structure of Oscillations in the Ocean," OKEANOLOGIYA, Vol 17, No 5, 1977.

12. Dotsenko, S. F., "Asymptotic Analysis of Transient Waves from Beginning, Periodic and Moving Disturbances," MORSKIYE GIDROFIZICHESKIYE ISSLEDOVANIYE, No 3, 1977.

6521
CSO: 1865/210

UDC 551.466.31

INTERPRETING MEASUREMENTS OF WIND WAVE DISPERSION CHARACTERISTICS

Moscow IZVESTIYA AKADEMII NAUK SSSR: FIZIKA ATMOSFERY I OKEANA in Russian Vol 17, No 6, Jun 81 pp 639-646

[Article by M. M. Zaslavskiy and I. A. Leykin, Institute of Oceanology, USSR Academy of Sciences]

[Text] Analysis of available experimental data shows that the mean position of the dispersion crest for the energy-bearing components of developed seas coincides with the dispersion ratio for linear free waves $\omega^2 = gk$, while the relative value of the blurring of the dispersion crest is low ($\Delta\omega/\omega \ll 1$). According to laboratory measurement, the values of blurring for wind waves during the initial stage of development are comparable to the mean value of frequency ($\Delta\omega/\omega \sim 1$), which makes short waves similar to turbulence in their dispersion properties.

The problem of the similarity of real wind waves in dispersion characteristics to linear free waves was discussed in [1]. The qualitative analyses given in [1] show that an ordinary dispersion relation should be performed with acceptable accuracy for linear free gravity waves only for the energy-bearing components of developed seas ($\omega_m U_a/g \sim 1$, where ω_m is the frequency corresponding to the maximum wave spectrum, U_a is wind velocity far from the surface and g is the acceleration of gravity)

$$\omega = \pm\sigma(k) = \pm(gk)^{1/2}. \tag{1}$$

One should expect significant blurring of the dispersion relation through the plane (k, ω) for the short-wave components of developed seas and for wind waves during the initial stages of formation when the phase velocity of waves is $c = g/\omega \ll U_a$, which makes these waves more similar to ordinary turbulence.

Specific difficulties arise when these conclusions are compared to observation data. As is known, if there is a relationship of frequency ω the modulus of the wave vector k of type 1 for a statistically stationary and horizontal-homogeneous random gradient field $\zeta(x, t)$, $x = (x_1, x_2)$, then the space-time spectrum of this field $E(k, \omega)$ is represented in the form

$$E(\mathbf{k}, \omega) = {}^1/_2[F(\mathbf{k})\delta(\omega-\sigma(k)) + F(-\mathbf{k})\delta(\omega+\sigma(k))] \tag{2}$$

and accordingly is localized on the dispersion surface $\omega = \sigma(k)$ in a three-dimensional space (k, ω) $(k = (k_1 = k\cos\theta, k_2 = k\sin\theta))$. Therefore, the most natural method of checking dispersion relation (1) experimentally for wind waves consists in determining their space-time spectrum $E(k, \omega)$. In this case violations of dispersion relation (1) will be found both in deviation of the real dispersion surface $\omega_c(k)$ from $\sigma(k)$ and in blurring of the spectrum $E(k, \omega)$ in some vicinity $\Delta\omega(k)$ of this dispersion surface. The dispersion surface $\omega_c(k)$ may generally not be detected in observations with sufficiently extensive blurring $\Delta\omega \approx \omega$.

Simultaneous measurements of the surface rise $\zeta(x, t)$ at many points is necessary in the general case to determine the space-time spectrum of wind waves $E(k, \omega)$, which is technically very complex and is not used even under laboratory conditions. The principal capability of determining the spectrum of $E(k, \omega)$ using a small number of sensors (on the order of 10) appeared with development of adaptive methods of spectral analysis [2, 3]. These methods were used in [4] for direct determination of frequency ω_m and the wind vector k_m, corresponding to the spectral maximum of storm waves, in application to investigation of the dispersion relation for wind waves. The data obtained in [4] are represented in Figure 1 in the form of the function $\omega(k)$; some additional data that characterize the conditions of making these and other full-scale measurements of wave action analyzed below are presented in the table.

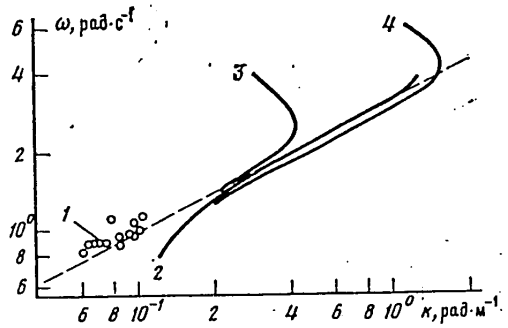

Figure 1. Mean Position of Dispersion Crest $_c(k)$ From Full-Scale Measurement Data: 1--Konyayev and Leykin [4]; 2--Grose et al [6]; 3--Yefimov and Khristoforov [7]; 4--Kiseleva [5]. The dashed line is the dispersion relation of free waves $\omega^2 = gk$.

The results of [4] show that the mean position of the dispersion crest for the energy-bearing components of developed seas coincides well with dispersion relation (1); the slight systematic excess of $\omega_c(k)$ over $\sigma(k)$ is obviously related to the presence of drift currents that always accompany the real wave-formation process.

The main volume of experimental data at our disposal on the dispersion characteristics of developed seas are indirect in nature. When interpreting these data, one must exercise some care since the effects of blurring of the dispersion relation frequently cannot be separated from the effects of shifting of the dispersion surface $\omega_c(k)$ with respect to $\sigma(k)$ when using them.

(1) Литература	U_α, м/с (2)	$\omega_m/2\pi$, Гц (3)	$\frac{\omega_m U_\alpha}{g}$	Диапазон ω (или λ) (4)	(5) Примечание
(6) Коняев, Лейкин [4]	12	~0,15	1,1	$\omega=\omega_m$	(7) Штормовые волны
Киселева [5] (8)	6÷9,5	~0,2	–	$\omega\geqslant\omega_m$	Смешанное волнение (9)
Гроуз и др. [6] (10)	–	–	–	$\omega>\omega_m$	Развитое волнение (11)
Ефимов, Христофоров [7] (12)	–	–	–	$\omega\geqslant\omega_m$	–
Ефимов и др. [8] (13)	–	0,21÷0,29	–	$\omega\geqslant\omega_m$	–
Коняев, Назаров [9] (14)	–	~0,2	–	$\lambda=38$ и 56 см	Смешанное волнение
Лейкин, Розенберг [10] (15)	1÷5	~0,2	–	$\lambda=6$ см	» »

Note. The dash in the table means an absence of the required data in the paper; the value of $\omega_m U_a/g$ was not calculated for cases of mixed seas.

Key:

1. Literature
2. m/s
3. Hertz
4. Range of ω (or of λ)
5. Remarks
6. Konyayev and Leykin [4]
7. Storm waves
8. Kiseleva [5]
9. Mixed seas
10. Grose et al [6]
11. Developed seas
12. Yefimov and Khristoforov [7]
13. Yefimov et al [8]
14. Konyayev and Nazarov [9]
15. Leykin and Rozenberg [10]

Let us first consider one of the simplest methods of an indirect check of dispersion relation (1) for wind waves by the frequency spectra of the rise of level $S(\omega)$ and by slope spectra $S_{x_1}(\omega)$ and $S_{x_2}(\omega)$ corresponding to the spatial derivatives $\partial\zeta/\partial x_1$ and $\partial\zeta/\partial x_2$ in two mutually perpendicular directions ox_1 and ox_2. Since the space-time spectrum $E_{x_\alpha}(k, \omega)$ of a random field $\partial\zeta/\partial x_\alpha$ ($\alpha = 1, 2$) is related to $E(k, \omega)$ by the relation

$$E_{x_\alpha}(k, \omega)=k_\alpha^2 E(k, \omega),$$

then

$$E_x(k, \omega)=E_{x_1}(k, \omega)+E_{x_2}(k, \omega)=k^2 E(k, \omega).$$

By integrating with respect to k the latter equality in relation to (2), we find the relationship of the frequency spectra $S(\omega)$ and $S_x(\omega) = S_{x_1}(\omega) + S_{x_2}(\omega)$ in the form

$$S_x(\omega)=(\omega^4/g^2)S(\omega). \tag{3}$$

An experimental check of relation (3) permits one to judge whether the dispersion relation for wind waves is actually fulfilled.

The usual presentation of experimental data of this type consists in finding the "dispersion relation"

$$k=k_e(\omega)=[S_x(\omega)/S(\omega)]^{1/4}, \tag{4}$$

found upon replacement of multiplier ω^4/g^2 by k on the right side of (3). Similar data from [5, 6] are presented in Figure 1 that show that dispersion relation (4)

coincides approximately with (1) in some frequency range near frequency ω_m, corresponding to the maximum spectrum of sea state, while function $\omega_c(k)$ determined according to (4) in the region of smaller scales systematically exceeds the value of $\sigma(k)$. However, it is impossible to relate this effect to displacement of the real dispersion surface $\omega_c(k)$: first, deviation of $\omega_c(k)$ from $\sigma(k)$ may be related to increasing errors of determining the spectra of $S_x(\omega)$ and $S(\omega)$ (the spread of experimental points in this frequency range usually significantly increases and the mean path of the derived function is represented in Figure 1 for the data of [5]) and second, blurring of the space-time spectrum $E(k,\omega)$ with respect to an undistorted dispersion surface $\sigma(k)$ also produces a similar effect.

Similar results from the methodical viewpoint were found in [7] upon comparison of velocity spectra $S_{w1}(\omega)$ and $S_{w2}(\omega)$, which were calculated by simultaneous recordings of the vertical velocity component at two levels in the surface layer, separated vertically by distance z. Based on the relation for attenuation of wave motion with depth, which follows from linear theory, one can find

$$k(\omega)=(1/2\Delta z)\ln\left(S_{w1}(\omega)/S_{w2}(\omega)\right). \tag{5}$$

The values of $k(\omega)$ calculated according to (5) [7] are also presented in Figure 1. Consideration of function $k(\omega)$ shows that dispersion relation $\omega^2 = gk$ is fulfilled in the frequency range $\omega \approx 1\text{-}2.5$ rad/s. A systematic deviation of $\omega_c(k)$ from $\sigma(k)$ appears with an increase of frequency; as the authors of [7] note, this indicates that the velocity field in this frequency band is determined to a significant degree by turbulent motion. In terms of the present paper, this means increased blurring of spectrum $E(k, \omega)$.

Let us discuss another method of determining the dispersion relation for wind waves, consisting of simultaneous recording of the surface rise $\zeta_1(t)$ and $\zeta_2(t)$ at two points separated by a short distance l_0 (compared to the length of the waves being measured) in the main direction of wave propagation. The phase shift function $\phi = \text{arctg}\,(-Q(\omega)/C(\omega))$ (where $C(\omega)$ and $Q(\omega)$ are real and imaginary parts of the mutual spectrum) is calculated by means of mutual spectral analysis and the phase velocity of the spectral components is determined

$$c(\omega)=l_0\omega/\varphi(\omega). \tag{6}$$

Full-scale data of this type, related to developed seas [8], are presented in Figure 2. A systematic excess of experimental function $c(\omega)$ over the dispersion function for free waves $c = g/\omega$ is partly related to the measurement method--it turns out that $c_m \approx g/\omega_m$ when the real angular distribution of wave energy is considered. However, the difference of experimental values of $c(\omega)$ from calculated values cannot be explained in this manner in the range of higher frequencies ($\omega > \omega_m$) and the authors of [8] relate the observed effect to the presence of nonlinear harmonics of the energy-bearing components of wave action among the high-frequency components of the spectrum.

One should bear in mind in this regard that even this method has the same disadvantages (although in a more subtle form) as methods based on a check of relations (4) and (5). Actually, the proposition of the existence of dispersion relation (1) is used a priori in the expressions that link frequency spectra $C(\omega)$ and $Q(\omega)$ to

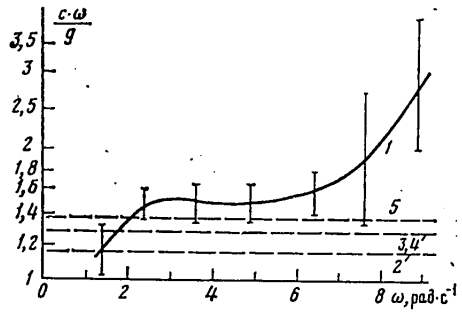

Figure 2. Ratio of Phase Velocity $c(\omega)$ of Spectral Components of Sea States to Phase Velocity $c = g/\omega$ of Free Waves (measurements of Yefimov et al [8]): 1--experimental values; 2-5--calculated values for different approximations of the angular distribution of wave energy $S(\theta)$ (2--$S(\theta) \sim \cos^2\theta$, 3--$s(\theta) \sim \cos\theta$, 4--$S(\theta) \sim \cos^2(0.8\theta)$ and 5--$S(\theta) \sim \cos(0.8\theta)$)

spectrum $E(k, \omega)$. Therefore, the given expression (6) for $c(\omega)$, like dispersion relations (4) and (5), can be used only as an indicator of the similarity of the real dispersion relation to (1). Approximate fulfillment of the equality $l_0\omega/\phi(\omega) = g/\omega$ (with additional consideration of the angular distribution of wave energy) denotes the minor nature of the effects of blurring of the dispersion relation and its similarity to the function $\sigma(k) = (gk)^{1/2}$, but if this equality is violated, the values of $c(\omega)$ determined according to (6) no longer describe the real dispersion relation. Specifically, inequality $l_0(\omega)/\phi(\omega) > g/\omega$ can be explained only by the effects of blurring the dispersion relation with respect to the undistorted mean proposition $c(\omega) = g/\omega$.

Thus, the experimental data at our disposal (Figures 1 and 2), related to the case of sufficiently developed seas ($\omega_m U_a/g \sim 1$), indicates that dispersion relation (1) is fulfilled with acceptable accuracy in this case for the energy-bearing components ($k \approx k_m$), although analysis of the degree of smallness of the effects of blurring $\Delta\omega(k)$ of real dispersion curve $\omega_c(k)$ and its deviation from function (1) is difficult.

Determination of dispersion characteristics is made difficult for small-scale components ($k >> k_m$) of developed seas by the complexity of conducting measurements in the presence of powerful energy-bearing components. On the other hand, the design complexities related to the use of multicomponent wave sensor systems having selectivity by wave number k and direction of wave arrival θ under full scale conditions have already been overcome for measurements in this range of scales [9]. Using these systems--two-dimensional interference arrays--one can measure the cross-section $S_{k_i}(\omega)$ of the space-time spectrum $E(k, \omega)$ for a selected wave number k_i, which essentially permits one to determine both the mean position of the dispersion surface at $k = k_i$ and its effective blurring, which can be determined, for example, for symmetrical spectra $S_{k_i}(\omega)$ as the width of spectrum $S_{k_i}(\omega)$ by the half-power level.

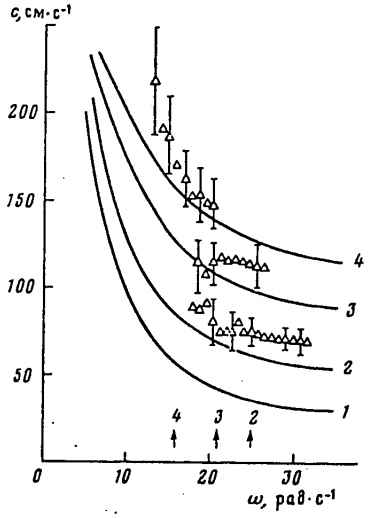

Figure 3. Dependence of Phase Velocity of Waves on Frequency $c(\omega)$ (laboratory measurements of Kononkova and Pokazeyev [11]): 1--dispersion curve for free waves $c = g/\omega$; 2, 3 and 4--dispersion curves calculated with regard to drift current for values of dynamic wind velocity $u_* = 20.8$, 63 and 99 cm/s, respectively; the symbols are the experimental values of $c(\omega)$; the errors show the position of the frequency of the energy-bearing waves ω_m

The spectra of $S_{ki}(\omega)$ for components with $\lambda = 38$ and 56 cm, obtained during measurements in the coastal zone in a slight wind are presented in [9]. The data of [9] show that the mean position of the dispersion crest for the investigated c-state components is similar to the calculated value; at the same time some broadening of the experimental spectra of $S_{ki}(\omega)$ is noted compared to the calculated spectra, the final width of which is related to the spatial resolution of the arrays used. Similar measurements for even smaller scale components ($\lambda = 6$ cm) showed [10] that the broadening of the frequency spectra of these components of $S_{ki}(\omega)$ is so great at $U_a > 1$-2 m/s that it is generally impossible to determine the mean position of the dispersion crest.

Thus, the sparse available data [9, 10] qualitatively confirm the concept of blurring of the dispersion relation for the short-wave crest of the spectrum whose value increases with an increase of the wave number k of short waves and, according to the authors of [9, 10], is related mainly to modulation of the ripple frequency by long waves. However, quantitative analyses of the magnitude of this blurring cannot be found.

Let us judge the experimental data on the dispersion characteristics of wind waves during the initial stages of development ($c_m/U_a \ll 1$) which are usually studied under laboratory conditions. The most widespread method of measuring the dispersion

relation in laboratory basins is the method already considered of determining the phase velocity $c(\omega)$ by means of two separated sensors. The values of $c(\omega)$ found in [11] and determined by this method are presented in Figure 3; a systematic excess of the measured values $c(\omega)$ over the dispersion function $c(\omega) = g/\omega$ for the energy-bearing components of sea state ($\omega \approx \omega_m$) is easily explained by the doppler frequency shift due to a drift current in the channel. Similar results for components with $\omega \sim \omega_m$ were found by the same method in [12].

At the same time the values of $c(\omega)$ decrease more slowly with an increase of frequency for components with $\omega > \omega_m$, which follows from linear theory even with regard to drift (see the data of Figure 3 for $u_* = 63$ and 99 cm/s). According to the authors of [12], who also obtained a similar result, this is related to nonlinear effects--to the presence of harmonics of the main frequency ω_m in the spectrum.*

However, as noted above, an excess of the measured values of $c(\omega)$ over the calculated values with the given measurement method can also be explained by the presence of blurring of the dispersion relation with respect to the mean position (with regard to drift). Some data on blurring of the dispersion relation for developed wind waves with $c_m/U_a \ll 1$ are presented in [14], where broadening of the spectra of $S_{ki}(\omega)$ measured by interference arrays for sea-state components with $\lambda = 3$ and 6 cm in a slight wind ($U_a = 3$-5 m/s), was noted.

Information on the extent of blurring $\Delta\omega$ can also be obtained from radiophysics papers related to investigation of the doppler spectra of radio (acoustic) signals scattered by a disturbed water surface. From the viewpoint of spatial analysis of the wave spectrum, the doppler locater is equivalent to a two-dimensional interference array, but provides better spatial selectivity and permits one to realize the advantages of the noncontact method. Special investigations on blurring of the dispersion relation using doppler equipment have not yet been carried out, although similar measurements of the spectra of developed wind waves have already been carried out by the method (see, for example, survey [15]). Nevertheless, it it has been established that observed broadening of scattered doppler spectra of $s(\omega)$ cannot be explained by scattering effects, but is related mainly to blurring of the dispersion relation of wind waves.

This conclusion is formulated more clearly in [16], where "coherent" broadening (related to the presence of long-wave components) and "noncoherent" broadening (related to the turbulent nature of wave formation) of the dispersion relation of short-wave components ($\lambda \approx$ 1-10 cm) of wind waves during the initial stages of development were determined.

Taking the foregoing into account, the values obtained in [16-18] for the relative width of the spectra of $s(\omega)$, which comprise from 0.1 to 0.8, can be taken as a somewhat exaggerated estimate of the relative width of the dispersion crest of

---

*Since the drift current is not uniform in depth, there is some ambiguity in selecting the values of flow velocity u_0. A value of $u_0 = 0.6\, u_*$ (u_* is the dynamic wind velocity) was selected in [11], which coincides, according to [13], to the drift current velocity in a thin surface layer.

short waves $\Delta\omega/\omega$. The observed increase in the values of $\Delta\omega/\omega$ with an increase of wave acceleration F and of wind velocity U_a is apparently related to the modulating effect of the long-wave components, the role of which also increases with an increase of F and U_a.

Conclusions. The given consideration of experimental data on the dispersion characteristics of wind waves shows that available full-scale data are very sparse and were obtained by different (mainly indirect) methods, which makes comparison of their results difficult. Part of these measurements corresponds to the case of mixed seas; the values of wind velocity U_a or of the frequency of the spectral maximum $_m$ are not presented in some papers, which does not permit one to estimate the degree of development of seas. Therefore, it is presently impossible to obtain quantitative estimates of the shifting of the mean position of the dispersion crest and of its blurring for different components of developed seas.

Nevertheless the considered experimental data confirm the analyses presented in [1], according to which the mean position of the dispersion crest for the energy-bearing components of developed seas whose phase velocity is similar to wind velocity ($c \sim U_a$) coincides with the dispersion relation for linear free waves $\omega^2 = gk$, while the magnitude of the blurring is small ($\Delta\omega/\omega \ll 1$), although it is difficult to estimate the degree of smallness of blurring effects.

The values of blurring according to laboratory measurement data are comparable for wind waves during the initial stage of development to the mean value of frequency ($\Delta\omega/\omega \sim 1$), which makes short waves similar to turbulence in their dispersion properties. Further experimental investigations are required to determine the dispersion characteristics of the short-wave components of developed seas, which are strongly dependent on the orbital motion of long-wave components.

Note. After the given article was sent to press, paper [19] was published in which the results of direct determination of the dispersion relation for developed wind waves were presented from data of simultaneous measurements of sea states at several separate points. The results of this paper, obtained by adaptive methods of spectral analysis, agree with the conclusions of this article and show that the mean position of the dispersion crest is well described by the dispersion relation $\omega^2 = gk$ while the magnitude of blurring of the crest is small for the energy-bearing components of seas and those similar to them ($\omega_m \leq \omega < 2\omega_m$). In the higher frequency range ($\omega \geq 2\omega_m$), the mean position of the dispersion crest deviates from the curve $\omega^2 = gk$ and at the same time there is an increase of the blurring of the crest, which the authors feel is related to nonlinear effects (the contribution of the harmonics of the main frequency, especially discernible in the range of $\omega \approx 2\omega_m$) and to the nonpotential nature of wave motion.

BIBLIOGRAPHY

1. Zaslavskiy, M. M., "The Dispersion Characteristics of Wind Waves," IZVESTIYA AN SSSR, FAO, Vol 17, No 1, 1981.

2. Davis, R. E. and L. A. Regier, "Methods for Estimating Directional Wave Spectra from Multielement Arrays," JOURNAL OF MARINE RESEARCH, Vol 35, No 3, 1977.

3. Kozubskaya, G. I., and K. V. Konyayev, "Adaptive Spectral Analysis of Random Processes and Fields," IZVESTIYA AN SSSR, FAO, Vol 13, No 1, 1977.

4. Konyayev, K. V. and I. A. Leykin, "The Three-Dimensional Structure of Storm Waves at Sea," IZVESTIYA AN SSSR, FAO, Vol 14, No 12, 1978.

5. Kiseleva, O. A., "Experimental Investigation of the Two-Dimensional Energy Spectrum of Marine Wind Seas," MORSKIYE GIDROFIZICHESKIYA ISSLEDOVANIYA, No 3 (59), 1972.

6. Grose, P. L., K. L. Warsh and M. Garstang, "Dispersion Relations and Wave Shapes," JOURNAL OF GEOPHYSICAL RESEARCH, Vol 77, No 21, 1972.

7. Yefimov, V. V. and G. N. Khristoforov, "Wave and Turbulent Components of the Velocity Spectrum in the Upper Layer of the Ocean," IZVESTIYA AN SSSR, FAO, Vol 7, No 2, 1971.

8. Yefimov, V. V., Yu. P. Solov'yev and G. N. Khristoforov, "Experimental Determination of the Phase Propagation Velocity of the Spectral Components of Marine Wind Seas," IZVESTIYA AN SSSR, FAO, Vol 8, No 4, 1972.

9. Konyayev, K. V. and A. A. Nazarov, "Measuring the Space-Time Structure of High-Frequency Components of Wind Seas," IZVESTIYA AN SSSR, FAO, Vol 6, No 1, 1970.

10. Leykin, I. A. and A. D. Rozenberg, "Measuring the Angular Spectra of the High-Frequency Part of Seas," IZVESTIYA AN SSSR, FAO, Vol 7, No 1, 1971.

11. Kononkova, G. Ye. and K. V. Pokazeyev, "Experimental Investigation of the Dispersion Relation for the Components of the Frequency Spectrum of Wind Waves," VESTNIK MGU, SERIYA FIZIKA, ASTRONOMIYA, Vol 19, No 1, 1978.

12. Ramamonjiarisoa, A. and M. Coantic, "Loi experimentale de dispersion des vagues par le vent sur une faible longueur d'action," C. R. ACAD. SCI. PARIS, SER. B, Vol 282, 1976.

13. Wu, J., "Wind-Induced Currents," JOURNAL OF FLUID MECHANICS, Vol 68, Part 1, 1965.

14. Leykin, I. A., "Experimental Investigation of the Space-Time Structure of Marine Wind Seas in the High-Frequency Part of the Spectrum," Candidate of Physicomathematical Sciences Dissertation, Moscow, IO AN SSSR, 1973.

15. Wright, J. W., "Detection of Ocean Waves by Microwave Radar: The Modulation of Short Gravity-Capillary Waves," BOUNDARY-LAYER METEOROLOGY, Vol 13, Parts 1-4, 1978.

16. Zel'dis, V. I., I. A. Leykin, I. Ye. Ostrovskiy, A. D. Rozenberg and V. G. Ruskevich, "Investigating the Fluctuation Characteristics of Hydroacoustic Signals Scattered by a Disturbed Water Surface," TRUDY 8-Y VSESOYUZNOY AKUSTICHESKOY KONFERENTSII, Moscow, 1973.

17. Wright, J. W. and W. C. Keller, "Doppler Spectra in Microwave Scattering From Wind Waves," PHYSICS OF FLUIDS, Vol 14, No 3, 1971.

18. Duncan, J. R., W. C. Keller and J. W. Wright, "Fetch and Wind Speed Dependence of Doppler Spectra," RADIO SCIENCE, Vol 9, No 10, 1974.

19. Yefimov, V. V. and Yu. P. Solov'yev, "The Dispersion Relation and Frequency-Angular Spectra of Wind Waves," IZVESTIYA AN SSSR, FAO, Vol 15, No 11, 1979.

6521
CSO: 1865/210

UDC 629.127.066

ANNOTATION, ABSTRACTS FROM BOOK 'BASIC ELEMENTS OF UNDERWATER APPARATUS AND ROBOTS'

Moscow ELEMENTNAYA BAZA PODVODNYKH APPARATOV I ROBOTOV in Russian 1980 (signed to press 31 Oct 80) pp 2, 141-144

[Annotation of book "Basic Elements of Underwater Apparatus and Robots" edited by professor V. S. Yastrebov, doctor of technical sciences, USSR Academy of Sciences, Izdatel'stvo "Nauka", 1,000 copies, 144 pages]

[Text] The present collection contains reports given at the second Plenum of the section on "Underwater Apparatus and Robots" of the Oceanographic Commission of the USSR Academy of Sciences. The plenum was devoted to the problems and challenges of developing the basic elements of these new technical means of ocean research. The concept of basic elements [literally "element base"] includes not only the actual elements and systems of underwater apparatus and robots, but also the elements of their theory. It should be noted that the theory of underwater robots is in the very initial stage of development. Many of the fundamental issues are being decided at the present time on the basis of theoretical principles that relate to manned underwater vehicles.

The articles in this collection consider the state of the basic elements for these devices and propose some successful solutions. The book is intended for scientific workers and engineers engaged in designing technical means of developing the world ocean.

The book was ratified for printing by the Scientific Council on the Theory and Principles of the Design of Robots and Manipulators of the USSR Academy of Sciences and the Institute of Oceanology imeni P. P. Shirshov.

UDC 629.127.065

INTERACTIVE SYSTEMS FOR CONTROLLING UNDERWATER ROBOTS

[Abstract of article by Popov, Ye. P., and Kuleshov, V. S.]

[Text] This article considers the basic principles of building interactive systems to control the movements of underwater manipulating robots which function purposefully in the ocean environment under conditions of high hydrostatic pressure. The article has one illustration and three bibliographic entries.

UDC 629.127.066

PURPOSEFUL MECHANICS AS A STANDARDIZED APPARATUS FOR THEORETICAL SUBSTANTIATION OF MANIPULATOR DESIGNS

[Abstract of article by Korenev, G. V.]

[Text] This article reviews the basic principles of purposeful [tselenapravlennaya] mechanics for manipulators and techniques of using this knowledge for effective design of systems to control the movement of manipulators operating in an extreme ocean environment. The article has one illustration for bibliographic entries.

UDC 629.127.066

BASIC ELEMENTS OF THE SOFTWARE OF AN ALGORITHM TO CONTROL THE MOVEMENTS OF AN UNDERWATER CARRYING ROBOT IN A MARINE ENVIRONMENT STRATIFIED BY DENSITY

[Abstract of article by Chirskov, S. N.]

[Text] This article reviews the principles of formation of the file structure of an algorithm to control the movements of underwater robots. It discusses the elementary command of the file to accomplish vertical movements by an underwater robot in a stratified environment. The article has four bibliographic entries.

UDC 629.127.066

EQUATIONS OF THE MOVEMENT OF A SOLID BODY IN A MARINE ENVIRONMENT STRATIFIED BY DENSITY

[Abstract of article by Chirskov, S. N.]

[Text] This article reviews the principles of the dynamics of motion by a solid body in a stratified environment. The author investigates the characteristic phenomena that occur when a solid body moves in a stratified liquid. The article has two bibliographic entries.

UDC 629.127.066

A LINEAR MODEL OF A RESTRICTED UNDERWATER APPARATUS-MANIPULATOR SYSTEM

[Abstract of article by Krylov, G. K.]

[Text] This article considers an underwater apparatus, secured in a current by a line and receiving disturbances from the work of a manipulator. By analysis of the dynamics of the apparatus a system of three scalar differential equations was derived for planar disturbed motion. By excluding the binding reaction, a linear system of two heterogeneous differential equations is shown, and then they are represented in generalized form. The system of equations permits study of the motion of a restricted underwater apparatus. The article has one illustration and three bibliographic entries.

UDC 629.127.066

METHOD OF CONSTRUCTION AND STRUCTURE OF AUTONOMOUS SYSTEMS FOR CONTROL OF THE MOTION OF UNDERWATER APPARATUSES

[Abstract of article by Popov, O. S.]

[Text] Underwater apparatuses can be highly efficient only when control of their movement is automated. The distinctive problems are tracking the bottom and holding the apparatus at an assigned depth. This article proposes a combined method to synthesize autonomous control systems. The method is based on combined use of the techniques of optimal control and autonomous regulation.

UDC 629.127.066

PRINCIPLES OF CONSTRUCTION OF SPECIALIZED COMPUTERS FOR POSITIONAL SUPERVISORY CONTROL OF UNDERWATER MANIPULATORS

[Abstract of article by Vereshchagin, A. F., and Minayev, L. N.]

[Text] Control of contemporary manipulating robots involves the use of new sources of command data: coordinating handles, light pens, and displays. With the computer they convert supervisory information into signals to control the actuating units. This article reviews the theoretical foundation, control algorithms, and principles of construction of specialized computers which perform these conversions for positional (static) control systems. The job of these systems is to switch the gripping device of the manipulator automatically. The article has two illustrations and five bibliographic entries.

UDC 629.127.066

COMBINED CONTROL OF REMOTE-CONTROLLED UNDERWATER APPARATUSES IN THE DYNAMIC POSITIONING REGIME

[Abstract of article by Lomonosov, Yu. I.]

[Text] This article is devoted to the questions of automatic stabilization of an underwater apparatus near the work site in the presence of disturbances by the manipulator that affect the apparatus. The author considers the possibility of building devices to measure the disturbances created by the working manipulator. He demonstrates the possibility of devising a combined system to stabilize the position of the apparatus relative to the work site when the apparatus has a device to analyze disturbing forces and moments created by the working manipulator. The article has one illustration and two bibliographic entries.

UDC 629.127.066

SOME QUESTIONS OF STUDYING SYSTEMS TO CONTROL SECOND-GENERATION APPARATUSES AND ROBOTS

[Abstract of article by Vasil'yev, V. A.]

[Text] This article considers characteristics of the process of solving problems related to devising systems to control underwater apparatuses and robots. The author gives a block diagram of their hierarchy and analyzes the constituent elements. This analysis makes it possible to propose regimes and methods of examining an assigned region using underwater robots. The article has one illustration and five bibliographic entries.

UDC 629.127.066

DETERMINATION OF THE DYNAMIC CHARACTERISTICS OF A REMOTE-CONTROLLED APPARATUS IN THE STAGE OF ROUGH DESIGN

[Abstract of article by Stefanov, G. A.]

[Text] This article reviews the possibility of determining the dynamic characteristics of a remote-controlled apparatus based on the characteristics of the actuating, receiving, and transmitting devices of a television system, the persistence of the operator's visual analyzer, and the rate of updating of the information content of the television image. Based on the persistence of the transmitting tubes, the author derives equations for maximum rates of the most typical movement of remote-controlled underwater apparatuses (forward and rotating) around the axis of symmetry. These equations are recommended for rough calculations when determining the maximum tolerable speeds of movement of remote-controlled underwater apparatuses and, therefore, for determining the parameters of the propelling unit and selecting the electrical drive of the propeller aggregates when studying the work regimes of remote-controlled underwater apparatuses near the bottom, when the operator is making observations or searching for an object using a television communications channel. The article has three illustrations and four bibliographic entries.

UDC 629.127.066

HYDROACOUSTIC SYSTEMS OF A DEEP-WATER COMPLEX

[Abstract of article by Lomonosov, Yu. I., and Sychev, V. A.]

[Text] This article presents a classification of the problems solved by the hydroacoustic systems of a deep-water complex. The authors review the systems used to solve these problems and give their basic parameters. The article has four bibliographic entries.

UDC 629.127.066

SECTOR SURVEILLANCE SONAR FOR REMOTE-CONTROLLED UNDERWATER APPARATUSES

[Abstract of article by Zhavoronkov, S. V., Lomonosov, Yu. I., Rimskiy-Korsakc , M. A., Stefanov, G. A., and Sychev, V. A.]

[Text] This article gives a description of a sector surveillance sonar unit designed for use in remote controlled underwater apparatuses. The authors set forth its operating principles and describe the interaction of the primary assemblies of the unit. The article has one illustration and two bibliographic entries.

UDC 629.127.066

THE POSSIBILITY OF USING THE STEREO METHOD FOR SURVEYING THE BOTTOM WITH A SIDE-LOOKING SONAR

[Abstract of article by Lomonosov, Yu. I., and Sychev, V. A.]

[Text] This article considers the possibilities of using the stereo method to obtain an image of the sector of the bottom being investigated with a side-looking sonar unit. Expressions are given for determining the magnitude of displacement beyond the topography owing to the conditions of surveying. The authors consider two alternatives for obtaining a stereo image and analyze the images obtained using them. The article has five illustrations and four bibliographic entries.

UDC 62.52

SOME CHARACTERISTICS OF CONSTRUCTING CONTROL SYSTEMS FOR REMOTE-CONTROLLED UNDERWATER APPARATUSES

[Abstract of article by Stefanov, G. A.]

[Text] This article reviews the functions of the human operator as an element of the control system for remote-controlled underwater apparatuses, characteristics of the operator, and the working conditions. Recommendations are given for reducing the operator's workload and fatigue by means of automatic elements and computers that make it possible to use internal potential operator reserves to solve more complex problems that require fast, operational action. The article has one illustration and 14 bibliographic entries.

UDC 62.514.5

COMMAND AND ACTUATING ELEMENTS OF SYSTEMS TO CONTROL THE MOVEMENT OF REMOTE-CONTROLLED UNDERWATER APPARATUSES AND SOFTWARE FOR OPERATORS

[Abstract of article by Stafanov, G. A.]

[Text] This article reviews the development of control systems depending on the complexity of the problems which the particular remote-controlled underwater

apparatus is to solve. The broadening range of jobs done by such apparatuses, the increasing complexity of their design and equipment, and the growing number of degrees of freedom of the apparatus and its manipulating devices have made it much more difficult to control them. It is suggested that ways to increase the efficiency of the operator's multifunctional activity should be sought not so much in improvements of data display equipment as in identifying new principles of control which also contain new forms of information. The article considers a fundamentally new information-controlling biotechnical system that has been developed. This system involves creating a multistep suspension system for the operator's console which simulates the spatial movement of the apparatus and also has a television image. The article has 19 bibliographic entries.

UDC 629.127.066

PRINCIPLES OF CONSTRUCTION OF PASSIVE DIVING SYSTEMS FOR UNDERWATER APPARATUSES

[Abstract of article by Smirnov, A. V., and Yastrebov, V. S.]

[Text] Passive diving systems include oil-filled electrical drive systems, control systems, and systems for electrical power supply. This article presents the results of the study of their characteristics under conditions of high hydrostatic pressure and reviews the interrelationship and mutual dependence of these systems and of their individual elements within a diving complex. The authors formulate 10 principles for the construction of passive diving systems. The article has three illustrations and one bibliographic entry.

UDC 629.127.066

PRINCIPLES OF CONSTRUCTING HYDRAULIC DIVING SYSTEMS FOR UNDERWATER APPARATUSES

[Abstract of article by Smirnov, A. V., and Yastrebov, V. S.]

[Text] This article presents the results of studies of all the basic elements of a hydraulic diving system under conditions of high hydrostatic pressure. The mutual influence of particular elements is also investigated. As a result, the authors propose basic principles for designing a deep-water hydraulic drive system. The "Skat" robot, which was designed on the basis of a hydraulic diving system, is given as an example. The article has three illustrations and two bibliographic entries.

UDC 629.127.066

PHOTOGRAPHIC COMPLEXES OF UNDERWATER ROBOT-APPARATUSES AND THEIR BASIC ELEMENTS

[Abstract of article by Kalinin, Yu. S.]

[Text] This article considers the working conditions and requirements of photographic complexes in underwater apparatuses. The author gives different alternatives of optical systems and also a number of types of light sources and their characteristics in a marine environment with different optical properties.

UDC 629.127.066

ANALYSIS OF THE CHARACTERISTICS OF THE POWER PLANTS OF UNDERWATER APPARATUSES

[Abstract of article by Gorlov, A. A., and Siminskiy, V. V.]

[Text] This article reviews the structural elements of the energy complex of an underwater apparatus: the engine installation, the onboard energy unit, the power supply installation, and the ship support system. The authors give a system of equations that determine the weight and dimension characteristics of the sources of various types of energy for the general case where they are arranged in the solid, spherical body of an underwater apparatus. The article has two bibliographic entries.

UDC 629.129:620.91

SOURCES OF ENERGY FOR DEEP-WATER APPARATUSES

[Abstract of article by Brilliantov, A. N.]

[Text] This article considers storage batteries, fuel cells, thermal energy systems, and atomic and radioisotope energy sources. Their energy and weight-dimension characteristics, strong and weak points, feasibility, and promise for use as energy sources for deep-water apparatuses are compared. The article has two illustrations and five bibliographic entries.

UDC 629.1.075

SOME CHARACTERISTICS OF THE MOVEMENT OF A TOWED BODY

[Abstract of article by Yagodzinskiy, V. A.]

[Text] This article investigates change in the resulting hydrodynamic force of interaction between liquid and a body traveling close to the bottom. The author establishes the relationship between the magnitude of the Kelvin force that arises and the dimensions of the dome and distance from the ocean floor when a carrier of scientific-technical apparatus is towed in the vertical plane. The article has two illustrations and two bibliographic entries.

11,176
CSO: 1863/181

UDC 551.465:551.464.621

NONLINEAR MODEL OF THE CARBON CYCLE IN THE OCEAN

Moscow DOKLADY AKADEMII NAUK SSSR in Russian Vol 285, No 1, 1981 (manuscript received 24 Jul 80) pp 212-215

/Article by B.A. Kagan and V.A. Ryabchenko, Leningrad Branch, Institute of Oceanology imeni P.P. Shirshov, USSR Academy of Sciences/

/Text/ A model of the carbon cycle in the ocean that claims to be an adequate reproduction of actuality must describe the interrelated changes in temperature[1], the total carbon content, the destruction and production of organic matter that is the source of the flow of carbon of organic origin, the behavior of CO_2 in solution, gas exchange with the atmosphere, the thickness of the upper quasihomogeneous layer, and the processes of exchange between that layer and the deep layer, as well as between the areas where the cold, deep waters are formed and the rest of the ocean. The existing models (an analysis can be found in /1,2/) do not satisfy this requirement. To some extent, their flaws are overcome in the model discussed below.

As is usual, we will describe the carbon cycle within the framework of a reservoir model of the ocean. In contrast to the traditional approach, however, we will relinquish the unjustified fixation of the upper quasihomogeneous layer's thickness, the water temperature, and the coefficients of exchange between the upper quasihomogeneous and deep layers. We will regard their values, as with the value of the CO_2 flow at the water-air interface, as being subject to determination. We will divide the ocean into two areas: the area of the formation of the cold, deep waters and all the rest of the ocean, within the limits of which there occur rising vertical movements that compensate for the arrival of cold, deep waters from the areas where they originate. Let the effect of the first of these areas be distributed uniformly on the second--a local source is replaced by a distributed one. In view of the condition of conservation of mass, the rate of upwelling in the second area will then be W/S, where W is the volume flow rate of the source of the cold, deep waters and S is the actual area of the second area. In this latter area we will now distinguish two layers--the upper quasihomogeneous layer and the deep layer--and examine them together with the area of cold, deep water formation as a system of interconnected reservoirs. We will further make use of the following assumptions, which have been accepted in the theory of the upper quasihomogeneous layer (see, for example, /3,4/. We will assume that there is no turbulence in the seasonal thermocline and the deep layer underlying it; that turbulent flows on the upper quasihomogeneous layer's lower boundary are caused by the involvement of liquid from the seasonal thermocline as the upper quasihomogeneous layer deepens and are otherwise equal to zero; that the integral dissipation and

production of turbulent energy of mechanical and convective origin are proportional to each other, it being the case that the dissipation of the mechanical turbulent energy is concentrated in the Ekman boundary layer; that the seasonal thermocline can be approximated by a temperature jump. As a result, we approach the solution of the nonlinear problem, which includes the equations for the water temperature T in each of the reservoirs[2]:

$$\frac{d}{dt} T_0 H = q_{s0}^T + \frac{S}{S_0} w(T_1 - T_0), \tag{1}$$

$$\frac{d}{dt} T_1 h - T_1 \left(\frac{dh}{dt} + w \right) = q_{s1}^T - q_{h-0}^T - wT_1, \tag{2}$$

$$\frac{d}{dt} T_2 (H - h) + T_2 \left(\frac{dh}{dt} + w \right) = q_{h+0}^T + wT_0, \tag{3}$$

the equations for the total carbon concentration $/\overline{C}/$:

$$\frac{d}{dt} [C_0] H = q_{s0}^C + \frac{S}{S_0} w([C_1] - [C_0]) + B_0, \tag{4}$$

$$\frac{d}{dt} [C_1] h - [C_1] \left(\frac{dh}{dt} + w \right) = q_{s1}^C - q_{h-0}^C - w[C_1] + B_1, \tag{5}$$

$$\frac{d}{dt} [C_2] (H - h) + [C_2] \left(\frac{dh}{dt} + w \right) = q_{h+0}^C + w[C_0] + B_2, \tag{6}$$

the expression for the gas flow q_s^C at the ocean's surface:

$$q_s^C = Du_*(c_p - [CO_2]), \tag{7}$$

the condition of conservation of the sea water ions' charges:

$$\text{Alk} = \frac{K_1[H^+] + 2K_1K_2}{[H^+]^2 + K_1[H^+] + K_1K_2} \cdot [C] + \text{Alk}_B + \frac{K_w}{[H^+]} - [H^+], \tag{8}$$

the relationship between the concentration of carbon dioxide dissolved in the water $/\overline{CO_2}/$ and $/\overline{C}/$:

$$[CO_2] = \frac{[H^+]^2 [C]}{[H^+]^2 + K_1[H^+] + K_1K_2}, \tag{9}$$

the expression for the turbulent flows $q^{t,C}$ of heat and carbon at the lower boundary of the upper quasihomogeneous layer:

$$q_{h-0}^{T,C} = \begin{cases} \left(\begin{pmatrix} T_1 \\ [C_1] \end{pmatrix} - \begin{pmatrix} T_2 \\ [C_2] \end{pmatrix} \right) \left(\frac{dh}{dt} + w \right) & \text{for } \left(\frac{dh}{dt} + w \right) > 0, \\ 0 & \text{for } \left(\frac{dh}{dt} + w \right) \leqslant 0, \end{cases} \tag{10}$$

the expressions for the equivalent flows $q_{h+0}^{t,C}$ of heat and carbon at the upper boundary of the deep layer, which parametrize the formation process of the so-called multiple thermocline[3]:

$$q_{h+0}^{T,C} = \begin{cases} 0 & \text{for } \left(\frac{dh}{dt} + w \right) > 0, \\ -\left(\begin{pmatrix} T_1 \\ [C_1] \end{pmatrix} - \begin{pmatrix} T_2 \\ [C_2] \end{pmatrix} \right) \left(\frac{dh}{dt} + w \right) & \text{for } \left(\frac{dh}{dt} + w \right) \leqslant 0, \end{cases} \tag{11}$$

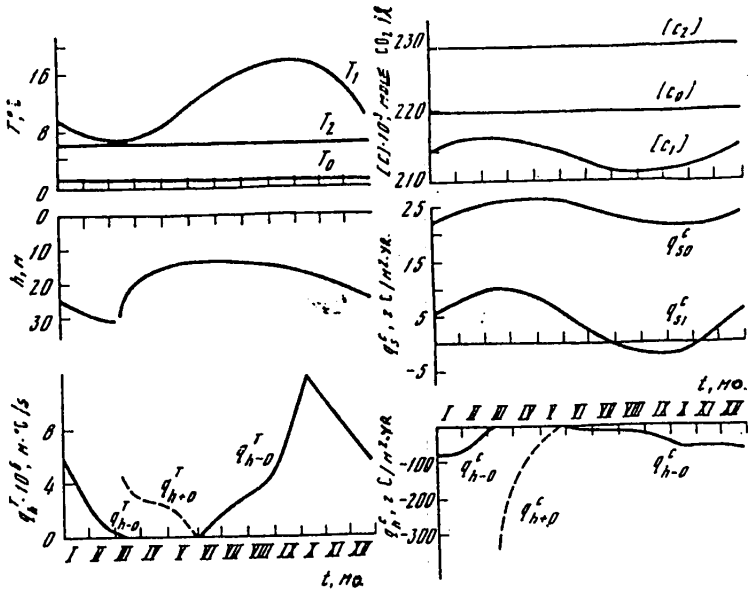

Figure 1. Annual pattern of the model's basic variables.

and, finally, for determininn the upper quasihomogeneous layer's thickness h:

$$\frac{dh}{dt} + w = \frac{1}{(T_1 - T_2)}\left[-C_1 q_{s1}^T - C_2 \frac{u_*^3}{g\alpha_T h} F\left(\frac{h}{h_e}\right)\right] \quad \text{for} \quad \left(\frac{dh}{dt} + w\right) > 0, \qquad (12')$$

$$h = -\frac{C_2}{C_1}\frac{u_*^3}{g\alpha_T q_{s1}^T}\left(1 - \frac{C_2}{C_1}\frac{u_*^3}{g\alpha_T h_e q_{s1}^T}\right)^{-1} \quad \text{for} \quad \left(\frac{dh}{dt} + w\right) \leq 0. \qquad (12'')$$

where D = coefficient of gas exchange with the atmosphere; c_p = equilibrium concentration of CO_2 in the water, which depends on the water's temperature and salinity and the partial pressure (p_{CO_2}) in the atmosphere; $/\overline{H^*}/$ = hydrogen ion concentration; K_1, K_2 = first and second carbonic acid dissociation constants; K_w = dissociation constant of sea water; Alk, Alk_B = common alkalinity and borate alkalinity; $F(h/h_e) = (1 - h/h_e)$ for $h < h_e$ and 0 for $h \geq h_e$ ($h_e = u_*/C_3|f|$ = thickness of the Ekman boundary layer); f = average (in the area under discussion) value of the Coriolis parameter; α_T = thermal coefficient of expansion of sea water; g = free-fall acceleration; C_1, C_2, C_3 = numerical constants; t = time.

The solution of system (1)-(12) makes it possible to reproduce temporal evolution T_i (i = 0, 1, 2), $/\overline{C_i}/$, $/\overline{CO_2}/$, $/\overline{H^+}/$, q_s^C, $q_{h-0}^{t,C}$, $q_{h+0}^{t,C}$ and h if the following values are given: heat flow q_s^t on the ocean's surface, the partial pressure p_{CO_2} in the atmosphere, the dynamic wind speed u_*, the sources and flows B_i of the carbon of organic origin, the ocean's depth H, the ratio S/S_0 of the areas of the "hot" and "cold" reservoirs, and the capacity of the source of the cold, deep waters or the upwelling rate w.

In this report we present the results of a numerical experiment on the seasonal variability of the natural carbon cycle in the ocean in the Northern Hemisphere. The required values of q_s^t and p_{CO_2} were taken from /5-7/. At first they were

Table 1. Average Annual Values of the Model's Basic Variables.

T_0	T_1	T_2	h, m	$q^t_{h-0}\cdot10^6$	$q^t_{h+0}\cdot10^6$	$\overline{/C_0/}\cdot10^3$	$\overline{/C_1/}\cdot10^3$	$\overline{/C_2/}\cdot10^3$
°C				m·°C/s		mole CO_2/ℓ		
0.87	12.27	6.18	20.1	3.73	0.50	2.20	2.13	2.29

q^C_{s0}	q^C_{s1}	q^C_{h-0}	q^C_{h+0}
g C/m^2·year			
23.8	3.64	-34.6	-22.9

presented in the form of a temporal Fourier series, and subsequently only the first four terms of the series for q^t_s and the first two of the series for p_{CO_2} were used. Parameters B_i (except for B_0, which was considered to be equal to zero)[2] were assumed to be equal to their average annual values; that is, B_1 = -34 g C/m^2·year, B_2 = -28 g C/m^2·year. (see /8/). An analogous assumption was made with respect to u_* and w. The former was assigned the value of 0.27 m/s in the area of formation of the cold, deep waters and 0.17 m/s in the rest of the ocean (values of D equal to $5.5\cdot10^{-5}$ and $5.14\cdot10^{-5}$ (see /9/) correspond to these u_*), while the latter was taken to be 10^{-5} cm/s. The values of H and S/S_0 were taken to be equal to 4,000 m and 10, respectively. The dependence of constants K_1, K_2 and K_w on temperature for a fixed salinity of 35 °/oo was taken according to Merbach /10/. The value taken for Alk was $2.4\cdot10^{-3}$ equiv/ℓ; Alk_B, which is a tabular function of T, $\overline{/H^+/}$ and salinity (see /10/), was computed during the solution process; in accordance with /4/, the values of C_1, C_2 and C_3 were assumed to be 0.1, $0.24\cdot10^{-3}$ and 100.

For the given initial values of T_i, $\overline{/C_i/}$ and h, the system of equations was integrated by the Runge-(Kutt) method. The calculations were continued, with a temporal spacing of 1 day, until the solution reached a periodic mode. The latter was considered to be a steady-state mode when the relative difference in T_i for the next two annual periods was 0.01 percent. This condition was achieved when 560 years had passed. The results of the calculation of the annual pattern of the model's basic variables is shown in Figure 1. Table 1 gives their average annual values. As is obvious, they agree qualitatively with the experimental data.

The authors are grateful to A.S. Monin for his constant attention to their work and to E.K. Byutner for his assistance in selecting the initial information and his helpful comments.

FOOTNOTES

1. In comparison with temperature, the salinity of sea water is a more conservative characteristic, and its value in the first approximation can be regarded as given.

2. The characteristics of the areas of the source of cold, deep waters, the upper quasihomogeneous layer and the deep layer are indicated by the subscripts 0, 1 and 2, respectively.

3. What is meant here is the formation of a new upper quasihomogeneous layer against the background of the old one and the formation of a stepped temperature profile in the thermocline displacement layer. The new thermocline insulates part of the old upper quasihomogeneous layer from the direct effect of processes taking place in the atmosphere, as a result of which the amount of carbon contained in the layer between the new and old thermoclines is gradually redistributed in the entire deep layer, primarily as the result of comparatively rare outbursts of turbulence that accompany the overturning of subsurface waves.

BIBLIOGRAPHY

1. Bolin, B., in "Fizicheskiye osnovy teorii klimata i yego modelirovaniya" /Physical Principles of the Theory of Climate and Its Modeling, collection of works/, Leningrad, 1977.

2. Bolin, B., et al., in "SCOPE Papers," Vol 13, Chapter 1, 1978.

3. Niiler, P.P., and Kraus, E.B., in "Modelirovaniye i prognoz verkhnikh sloyev okeana" /Modeling and Predicting the Upper Layers of the Ocean, collection of works/, Leningrad, 1979.

4. Kagan, B.A., et al., METEOROLOGIYA I GIDROLOGIYA, No 12, 1979, p 67.

5. Strokina, L.A., METEOROLOGIYA I GIDROLOGIYA, No 1, 1963, p 25.

6. Lowe, D.C., et al., TELLUS, Vol 31, 1979, p 58.

7. Bolin, B., and Bischof, W., TELLUS, Vol 22, 1970, p 431.

8. Skopintsev, B.A., OKEANOLOGIYA, Vol 15, 1975, p 830.

9. Ariyel', N.Z., et al., METEOROLOGIYA I GIDROLOGIYA, No 2, 1979, p 57.

10. Popov, N.I., et al., "Morskaya voda" /Sea Water/, Moscow, 1979.

11746
CSO: 8144/1395

UDC 535.2:551.463.5

RETURN SIGNAL MAGNITUDE DURING REMOTE LASER SOUNDING OF NATURAL WATER MEDIUMS

Moscow VESTNIK MOSKOVSKOGO UNIVERSITETA: SERIYA FIZIKA, ASTRONOMIYA in Russian
Vol 19, No 4, Jul-Aug 78 pp 64-70

/Article by A.A. Demidov, D.N. Klyshko and V.V. Fadeyev, Department of Wave Processes, Moscow State University/

/Text/ The development of methods of remote diagnostics for natural water mediums is becoming an ever more urgent problem, the solution of which is a matter of interest to many branches of the national economy. The composition of such mediums is extraordinarily complex and, in accordance with this, so is the spectrum of the return signal formed as the result of the different mechanisms of light interaction with the medium. In this spectrum, special attention is attracted by the lines of combination scattering (KR) of light by water (H_2O) molecules, which in a number of cases can serve as convenient reference points when determining the concentration of foreign bodies (such as phytoplankton) in the water /1-3/.

In this article we calculate the return signal formed during laser sounding of a natural water medium. Quantitative estimates are made for the return signal's spectral component, which corresponds to the Stokes component of the KR of water with a shift $\tilde{\nu} = 3{,}440\ \text{cm}^{-1}$ relative to the sounding radiation's wave number. The theoretical results are then compared with the experimental results obtained by the authors on the 18th voyage of the scientific research ship "Dmitriy Mendeleyev."

Calculation of the Return Signal. Let us discuss the propagation of a laser beam in a water medium and the formation of the return signal arising as the result of the light's interaction with water molecules and foreign bodies in the water. The sounding setup is shown in Figure 1.

The radiation source is characterized by a flow of emitted photons F_1 (photons per second), linear aperture $\Delta\rho_1$ and a radiation pattern of width $\Delta\theta_1$ with a maximum in direction n_1. The receiver's analogous parameters are indicated by the subscript "2." It is assumed that a large part of the beams are propagated at small angles to the z axis so that $n_{1z} \approx n_{2z} \approx 1$ (a small-angle approach /4/). The test object occupies an infinite layer between planes $z = z_0'$ and $z = z_{max}'$. The object of the investigation is a layer with thickness $\Delta z = z_{max}' - z_0'$. Refraction and reflection on the boundaries z_0' and z_{max}' will be ignored.

The medium is assumed to be turbid; that is, in addition to luminescing and non-elastically scattering centers such as molecules of a certain foreign body

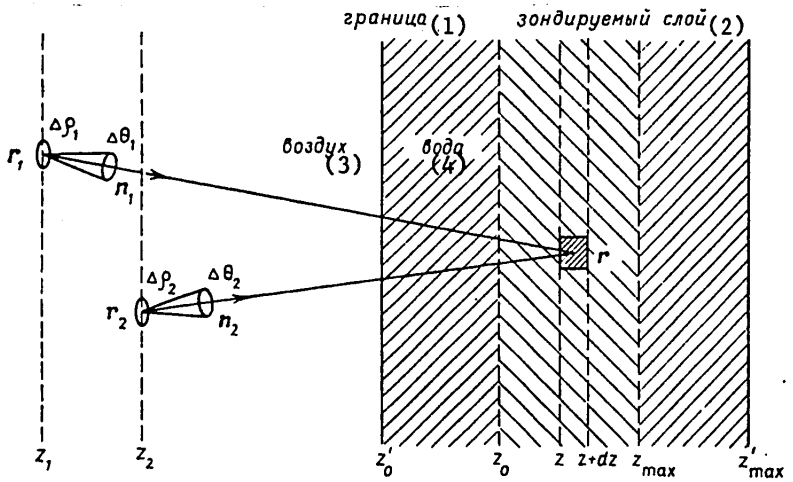

Figure 1. Diagram of remote laser sounding of natural water mediums.

Key:

1. Boundary
2. Sounded layer
3. Air
4. Water

(phytoplankton, for example), it also contains absorbing and elastically scattering particles. The scattering takes place on large (in comparison with the light's wavelength) particles, so it is directed forward at small angles to the z axis (Mie scattering).

It is necessary for us to determine the magnitude of the answering signal that is registered by the receiver and caused by any mechanism (type) of light interaction with the medium (fluorescence, KR, Mie and Rayleigh scattering so so forth) that is of interest to us.

The special features of light scattering in natural water mediums makes it possible to proceed from the general radiant energy transfer equation to the equation for transfer with a small-angle approach /4/:

$$\left(\frac{\partial}{\partial z} + 0\nabla_\perp + \varepsilon\right) B(\mathrm{r}, 0) = \frac{\sigma}{4\pi} \iint_{-\infty}^{\infty} d^2 0' B(\mathrm{r}, 0') \chi(0'), \tag{1}$$

where B(r,n) = brightness at point r in direction n; $\varepsilon = \sigma + \alpha$ = total attenuation (extinction) factor; σ = elastic scattering coefficient; α = absorption coefficient; $\chi(nn')$ = scattering indicatrix; $0 \equiv n_1$.

This equation can be solved by the Fourier method (see /3/), assuming that the scattering indicatrix is described by the exponential function (see /4/)

$$\chi(0) = \frac{2}{0^2} e^{-\frac{0}{\delta}} \tag{2}$$

and the transmitter's (laser's) and receiver's radiation patterns have a Gaussian shape.

In connection with this, we take into consideration the fact that when laser radiation strikes a unit of surface in the sounded layer (of thickness dz) of the medium and interacts with the particles in the medium, it causes answering radiation

$$dB_2(r, 0) = \sigma(0, z)\, n(z)\, \tilde{F}_1(r)\, \hbar\omega_2 dz,$$

where n(z) = the concentration of particles (cm^{-3}); $\tilde{F}_1(r)$ = density of the flow of exciting radiation (photons$\cdot cm^{-2}\cdot s^{-1}$); $\sigma(\theta,z)$ (cm^2/sr) = cross-section of the process of laser radiation interaction with the particles in the medium, which process was chosen in order to identify them. In the case where the particles are identified by their fluorescence, the indicatrix of which is (as a rule) a sphere, $\sigma \equiv \sigma_{f1}/4\pi$ (cm^2/sr), while σ_{f1} (cm^2) in the simplest case, where the same molecules both absorb and fluoresce, equals $\sigma_a\eta$, where σ_a (cm^2) is the absorption cross-section and η is the quantum efficiency of the fluorescence. For the case of combination scattering (in particular, the scattering particles can be water: $n_z = n_{H_2O} = 3.3\cdot 10^{22}$ cm^{-3} under normal conditions), $\sigma \equiv \sigma_{KR}(\theta)$ = the KR cross-section in the given observation direction (as a rule, KR has an elongated indicatrix that has a maximum in the forward and backward directions).

Then, by using the theory of reciprocity [5], we find the flow of photons registered by the receiver:

$$F_2 = F_1 \Delta\rho_2^2 \Delta\theta_2^2 \int_{z_0}^{z_{max}} dz \int_0^{\infty}\int dx dy \sigma(z)\, n(z) \cos[x\varphi_1(z)] \times$$

$$\times \cos[y\varphi_2(z)] \exp\left\{-(\varepsilon_1 + \varepsilon_2)z - \frac{1}{4}(x^2 a_x^2 + y^2 a_y^2) + \right.$$

$$\left. + \frac{\sigma_1 z}{\sqrt{1 + \sigma_1^2 (x^2 + y^2) z^2}} + \frac{\sigma_2 z}{\sqrt{1 + \delta_2^2 (x^2 + y^2) z^2}}\right\},$$

where

$$\varphi_1(z) = x_1 - x_2 + (z - z_1)\theta_{1x} - (z - z_2)\theta_{2x},$$
$$\varphi_2(z) = y_1 - y_2 + (z - z_1)\theta_{1y} - (z - z_2)\theta_{2y},$$
$$a_x^2 = \Delta\rho_1^2 + (z - z_1)^2 \Delta\theta_1^2 + \Delta x_2^2 + (z - z_2)^2 \Delta\theta_{2x}^2, \qquad (3)$$
$$a_y^2 = \Delta\rho_1^2 + (z - z_1)^2 \Delta\theta_1^2 + \Delta y_2^2 + (z - z_2)^2 \Delta\theta_{2y},$$
$$\Delta\rho_2^2 = \Delta x_2 \Delta y_2, \quad \Delta\theta_2^2 = \Delta\theta_{2x}\Delta\theta_{2y}.$$

In formula (3), ε, σ and δ are the primary hydro-optic characteristics of water on the wavelengths of the exciting laser radiation (subscript "1") and the return signal (subscript "2"); coordinate origin z = 0 is set at the point $z = z_0'$.

In the case of a coaxial system, where $r_1 = r_2$ and $n_1 = n_2$, and assuming that $\Delta\theta_{2x} = \Delta\theta_{2y} = \Delta\theta_2$, $\Delta x_2 = \Delta y_2 = \Delta\rho_2$, $\delta_1 = \delta_2 = \delta$ and $\sigma(z)n(z)$ is a constant in the sounded layer Δz, we obtain

$$F_2 = \frac{\pi}{4} F_1 \sigma n \Delta\theta_2^2 \Delta\rho_2^2 \int_{z_0}^{z_{max}} dz \int_0^{\infty} dx \exp\left\{-(\varepsilon_1 + \varepsilon_2)z - \frac{1}{4}a^2 x + \frac{(\sigma_1 + \sigma_2)z}{\sqrt{1 + \delta^2 z^2 x}}\right\}, \qquad (4)$$

where $a^2 = \Delta\rho_1^2 + \Delta\rho_2^2 + (z - z_1)^2(\Delta\theta_1^2 + \Delta\theta_2^2)$.

The effect of the air interval is not taken into consideration in formula (3); that is, $\sigma_{air} \simeq \varepsilon_{air} \simeq 0$.

It is interesting to note the characteristic dependence of the received signal on the distance $|z_1|$ from the laser to the water's surface during the sounding of a layer of a water medium (Δz). It is not difficult to show that the magnitude of the received signal is $\sim \Delta z/(|z_1|(|z_1| + \Delta z))$. In connection with this, at great distances ($|z_1| \gg \Delta z$) the signal magnitude is $\sim 1/|z_1|^2$, while at short distances ($|z_1| \ll \Delta z$), it is $\sim 1/|z_1|$. Analogous results are obtained when the asymptotes of formula (4) are examined:

$$\frac{F_2}{F_1} = \frac{\pi}{2} - \operatorname{arctg}\left(\frac{\Delta\theta}{\Delta\rho}|z_1|\right) \simeq \left(\frac{\Delta\rho}{\Delta\theta}\right)\frac{1}{|z_1|} \sim \frac{1}{|z_1|}, \quad |z_1| \ll \Delta z, \tag{5}$$

$$\frac{F_2}{F_1} \sim \frac{\Delta z}{\Delta\rho^2 + \Delta\theta^2|z_1|^2} \sim \frac{1}{|z_1|^2}, \quad |z_1| \gg \Delta z. \tag{6}$$

In principle, expression (3) makes it possible to determine particle concentration n by registering the return signal from them. However, even in the coaxial system that is simplest to analyze, it is necessary to check a large number of parameters, which in practice is (as a rule) impossible.

A comparison method in which a measurement of the relationship of the return signal's spectral components that are caused by KR of the water and fluorescence or KR of the foreign body makes it possible to avoid the necessity of checking these parameters and determine the concentraction n of the foreign body that is of interest was proposed in [1], tested experimentally in [1-2] and substantiated mathematically in [3].

Optimization of the Laser Radar's Optical Arrangement. Expression (3) gives the magnitude of the received signal during laser sounding of water mediums. It contains parameters characterizing the investigated object (the water medium) and the geometric factors in the experiment (angular and linear apertures of the laser and the receiver and their relative positions).

Let us optimize the geometry of the experiment for the purpose of obtaining a registered return signal of maximum magnitude. It is obvious that the first step in the optimization process is the creation of a coaxial system where the laser and the receiver are located at the same point (formula (4)).

When using a lens system, the receiver's (and transmitter's) linear and angular apertures $\Delta\rho_2$ and $\Delta\theta_2$ are related to the original aperture values $\Delta\rho_{20}$ and $\Delta\theta_{20}$ by relationships $\Delta\rho_2 = f\Delta\theta_{20}$ and $\Delta\theta_2 = \Delta\rho_{20}/f$, where f is the lens system's focal length.

By substituting $\Delta\rho_2$ and $\Delta\theta_2$ into equation (4) and differentiating it with respect to f, it is not difficult to find an equation for determining the optimum focus:

$$f^4 = \frac{\Delta\rho_{20}^2}{\Delta\theta_{20}^2} \frac{\int_{z_0}^{z_{max}} dz \int_0^\infty dx\, x (z - z_1)^2 e^{\psi(f,x,z)}}{\int_{z_0}^{z_{max}} dz \int_0^\infty dx x e^{\psi(f,x,z)}}, \tag{7}$$

where

$$\psi(f, x, z) = -(\varepsilon_1 + \varepsilon_2)z - \frac{x}{4}\left[\Delta\rho_1^2 + \Delta\theta_{20}^2 f^2 + (z - z_1)^2 \times \right.$$
$$\left. \times \left(\Delta\theta_1^2 + \frac{\Delta\rho_{20}^2}{f^2}\right)\right] + (\sigma_1 + \sigma_2)z/\sqrt{1 + \delta^2 z^2 x}. \tag{8}$$

By using the mean-value theorem, it is not hard to obtain an estimate for f_{opt} from formula (7):

$$f_{opt}^2 \simeq \frac{\Delta\rho_{20}}{\Delta\theta_{20}}(z_0 + |z_1|). \tag{9}$$

When sounding the layer near the surface or at great distances ($|z_1| \gg z_0$):

$$f_{opt} \simeq \sqrt{\frac{\Delta\rho_{20}}{\Delta\theta_{20}}|z_1|}. \tag{10}$$

Formula (10) is also correct in the case of sounding the entire water stratum ($z_0 = 0$, $z_{max} = \infty$) from great distances, since the integrand in (4) diminishes rapidly as the depth (z) increases and only the layers near the surface operate effectively (the thickness of the effectively working layer is ~10 m, while the deeper layers make a contribution of $\lesssim$5 percent).

Table 1.

No	$\lvert z_1\rvert$, m	$\Delta\theta_{20}$, rad	$\Delta\rho_{20}$, cm	F_2/F_1 for $f = f_{opt}$	f_{opt}, cm	$f_{opt}\sqrt{(\Delta\rho_{20}/\Delta\theta_{20})\lvert z_1\rvert}$, cm
1	10	0.25	0.05	$1.0\cdot10^{-8}$	16	14
2	30	0.25	0.05	$1.9\cdot10^{-9}$	27	24
3	30	1	1	$0.75\cdot10^{-6}$	66	55

Table 1 shows the results of the calculation of f_{opt}, on a BESM-4 high-speed computer, as a function of the receiver's aperture and distance $|z_1|$, as well as the value of F_2/F_1 as computed according to formula (4) (the case of sounding the entire water stratum) and the estimated value of f_{opt} (formula (10)).

The calculations were made for $\varepsilon_1 = 2.5\cdot10^{-4}$ cm^{-1}, $\varepsilon_2 = 2.6\cdot10^{-3}$ cm^{-1}, $\sigma_1 = 1.5\cdot10^{-5}$ cm^{-1}, $\sigma_2 = 0.7\cdot10^{-5}$ cm^{-1} and for $\delta_1 = 0.1$. The data were taken from [6].

In Table 1, line 3 corresponds to the case of signal registration by a broad-aperture spectrometer (of the interference filter type).

The transmitter's lens system is optimized analogously. In the general case the optimum focal lengths for the transmitter (subscript "1") and the receiver (subscript "2") can be found from the solution of the system

$$f_1^4 = \frac{\Delta\rho_{10}^2}{\Delta\theta_{10}^2}\,\frac{\iint x\,(z - z_1)^2\, e^{\psi(f_1, f_2, x, z)}\,dxdz}{\iint x e^{\psi(f_1, f_2, x, z)}\,dxdz},$$
$$f_2^4 = \frac{\Delta\rho_{20}^2}{\Delta\theta_{20}^2}\,\frac{\iint x\,(z - z_1)^2\, e^{\psi(f_1, f_2, x, z)}\,dxdz}{\iint x e^{\psi(f_1, f_2, x, z)}\,dxdz}, \tag{11}$$

where

$$\psi(f_1, f_2, x, z) = -(\varepsilon_1 + \varepsilon_2)z - \frac{1}{4}x\left[\Delta\theta_{10}^2 f_1^2 + \Delta\theta_{20}^2 f_2^2 + (z - z_1)^2\left(\frac{\Delta\rho_{10}^2}{f_1^2} + \frac{\Delta\rho_{20}^2}{f_2^2}\right)\right] + \frac{(\sigma_1 + \sigma_2)z}{\sqrt{1 + \delta^2 z^2 x}}.$$

From system (11) it is not difficult to derive the relationship between f_{1opt} and f_{2opt}:

$$f_{1opt} = f_{2opt}\sqrt{\frac{\Delta\theta_{20}}{\Delta\theta_{10}}\frac{\Delta\rho_{10}}{\Delta\rho_{20}}}, \tag{12}$$

which--in contrast to (10)--is precise and can replace any of the equations in system (11).

Comparison of Theory and Experiment. Experiments in the remote laser sounding of sea water for the purpose of making a quantitative determination of the amount of phytoplankton present were conducted on the 4th voyage of the scientific research ship "Akademik Petrovskiy" [1] and the 18th voyage of the scientific research ship "Dmitriy Mendeleyev." On the latter occasion we had an opportunity to vary the distance from the laser radar (lidar) to the ocean's surface and to evaluate the absolute magnitude of the signal that was received.

Below we present the numerical estimates of the theoretically derived values as applied to the lidar parameters and experimental conditions on the 18th voyage of the "Dmitriy Mendeleyev." The lidar had the following characteristics: wavelength of the sounding radiation -- 532 nm, laser pulse duration -- 10 ns, maximum energy in a pulse -- 10^{-2} J; the linear ($\Delta\rho_0$) and angular ($\Delta\theta_0$) apertures of the laser transmitter (subscript "1") and the receiver (subscript "2") were: $\Delta\rho_{10}$ = 0.5 cm, $\Delta\theta_0 = 5.8 \cdot 10^{-3}$, $\Delta\varphi_{20}$ = 0.05 cm, $\Delta\theta_{20}$ = 0.25.

The receiver was gated by a pulse with duration τ_{str} = 1 μs, so it registered the integral number of return signal photons formed in the layer from the surface (z = $= z_0 = 0$) to $z_{max} = \tau_{str}c \simeq 100$ m ($c \simeq 2 \cdot 10^{10}$ cm$\cdot$s^{-1}, which is the speed of light in a water medium.

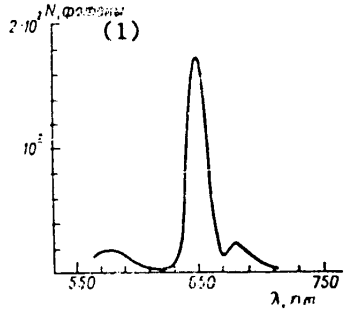

Figure 2. Spectrum of return signal during remote sounding (λ_{air} = 532 nm) of the ocean's surface at a distance of 10 m.
Key: 1. N, photons

One of the return signal spectrograms obtained during the sounding of the ocean's surface is presented in Figure 2. The peak on wavelength λ = 650 nm was caused by the water's KR signal, while the lesser one at λ = 680 nm was caused by the fluorescence of the marine phytoplankton's chlorophyll "A."

We also conducted an experiment in remote laser sounding in which we determined the signal's dependence on distance and the maximum working distance of our lidar (return signal registration was carried out with an OMA-1 system). The distance was changed by turning the lidar on a ring mount (which also changed the laser beam's angle of incidence on the water's surface). The results of these measurements are presented in Table 2.

Table 2.

Angle of laser beam incidence on the water's surface (degrees)	0	5	10	25	45	55	62	73
Distance z_1, m	10	10.05	10.15	11	14	17.5	21	35
KR signal of H_2O, photons, rel. units	175	202	188	202	106	34	24	3

The signal's dependence on the distance, which was even stronger than $|z_1|^{-2}$, is explained by the noncoaxiality of the system and the fact that when the ring mount's platform was turned, there was no optical alignment of the receiving system.

For sounding at a distance of 10 m, the water's KR signal was N_2 = 15,000 photons. ($N_2 = \int_{\tau_{str}} F_2(t)dt$) or $N_2/N_1 \simeq F_2/F_1 \simeq 1.4 \cdot 10^{-11}$, whereas a theoretical calculation with formula (4) gives $N_2/N_1 \simeq 8.6 \cdot 10^{-9}$; that is, a discrepancy factor of 600. Such a large discrepancy is explained by the ignoring of the terms characterizing the noncoaxiality of the system, the effect of the air interval, and (obviously) the larger values of ε and σ for the real case than those we used in our calculations (see above).

An accurate allowance for noncoaxiality requires the computation of the triple integral in (3). A gross estimate of the noncoaxiality factors shows that, in actuality, for $|z_1| \simeq 10$ m the result can differ by 2-3 orders of magnitude.

From what has been said, it follows that a change to a coaxial system will bring into play a large reserve for increasing the maximum range of answering signal detection. There is also another reserve: increasing the receiving system's sensitivity by using high-transmission (broad-aperture) spectrometers that are analogous to an interference filter (see Table 1) and more sensitive photoelectronic converters (FEP).

Computer calculations showed that when the water's KR signal is registered by a broad-aperture receiver ($\Delta\varphi_2$ = 1 cm, $\Delta\theta_2$ - 1 rad) with a photoelectronic converter equal in sensitivity to the OMA-1 system (photoconductive camera tube 1205D) and a lens (telescope) 60 cm in diameter with a focal length of 60 cm is used, the working distance z_1 can be increased to 3 km. A further improvement is possible by increasing the FEP's sensitivity and the laser's energy (F_1).

BIBLIOGRAPHY

1. Fadeyev, V.V., "Sb. tezisov konferentsii po lyuminestsentsii" /Collection of Summaries From the Conference on Luminescence/, Szeged, Hungarian People's Republic, 1976, p 7.

2. Klyshko, D.N., Rubin, L.B., Fadeyev, V.V., Kharitonov, L.A., Chekalyuk, A.M., and Chubarov, V.V., "Sb. tezisov VII konferentsii po spektroskopii" /Collection of Summaries From the Seventh Conference on Spectroscopy/, People's Republic of Bulgaria, 1976, p 204.

3. Klyshko, D.N., and Fadeyev, V.V., DAN SSSR, Vol 238, No 2, 1978, p 320.

4. Dolin, L.S., IZV. VUZOV. RADIOFIZIKA, Vol 7, 1964, p 380.

5. Yermakov, B.V., and Il'inskiy, Yu.A., IZV. VUZOV. RADIOFIZIKA, Vol 11, 1968, p 624.

6. Ivanov, A.P., "Fizicheskiye osnovy gidrooptiki" /Physical Principles of Hydro-Optics/, Minsk, 1975.

11746
CSO: 8144/1425

UDC 551.465.53

SPECTRA OF POLIMODE CURRENTS

Moscow DOKLADY AKADEMII NAUK SSSR in Russian Vol 258, No 2, 1981 (manuscript received 2 Feb 81) pp 331-334

[Article by V. N. Drozdov, A. S. Monin, corresponding member, USSR Academy of Sciences, and I. G. Yushina, Institute of Oceanology imeni P. P. Shirshov, USSR Academy of Sciences]

[Text] In accordance with the program of the Soviet-American oceanological experiment POLIMODE (named after the Soviet "POLIGON" experiment of 1970, which resulted in the discovery of synoptic eddies in the ocean, and the American MODE or "Mid-Ocean Dynamics Experiment" of 1973, duplicating it at a somewhat lesser scale), a number of institutes of the USSR Academy of Sciences and the Ukrainian Academy of Sciences carried out long-term measurements of oceanographic parameters in the Bermuda Triangle of the Sargasso Sea in a polygon measuring 300 x 300 km with its center at the point 29°N, 70°W during the 13 months from July 1977 through August 1978. The principal current measurements were made at 19 anchored buoy stations with measuring instruments at the four depths 100, 400, 700 and 1400 m (200 digital current meters were fabricated especially for this purpose).

With a frequency of registry of currents of 3-4 readings per hour there was an accumulation of about $3 \cdot 10^{-6}$ values of the current velocity vector. Thus, 21 synoptic eddies with diameters of 150-300 km with velocities of rotation in the upper layers averaging 30-35 cm/sec and velocities of movement of 3-10 km/day, primarily to the west, as well as a number of smaller eddies, were registered as passing through the polygon. Some results of the processing were published in [1, 2].

The experimentally collected data were introduced into an NR-3000 SKh computer in the form of a data recovery system allowing interrogations with respect to 23 parameters and their combinations. The series of mean hourly values of the zonal and meridional components of current velocity u and v present in this bank (152 series with 10 000 u and v values at four depths at each of 19 buoys) were used in this study in computing the frequency spectra of currents in the range of periods from 4 to 4 000 hours. We computed the spectra of u, v and kinetic energy $1/2(u^2 + v^2)$ for a total of 228 spectra.

In the mentioned series there were gaps created both by failure of the instruments to trigger and also due to the rejection of nonconforming values. As an average their percentage was 16.9% (including 13.7% at a depth of 100 m; 21.0% at 400 m;

11.4% at 700 m; 19.4% at 1400 m).

Individual gaps were filled by interpolation on the basis of adjacent values; group gaps were filled with the mean (~ mean annual) values of the corresponding series. The spectral densities of u and v were computed as the mean squares of the Fourier transforms of the corresponding series and then smoothed by contraction using a four-term Blackman-Harris "window" with a minimum level of the side lobes.

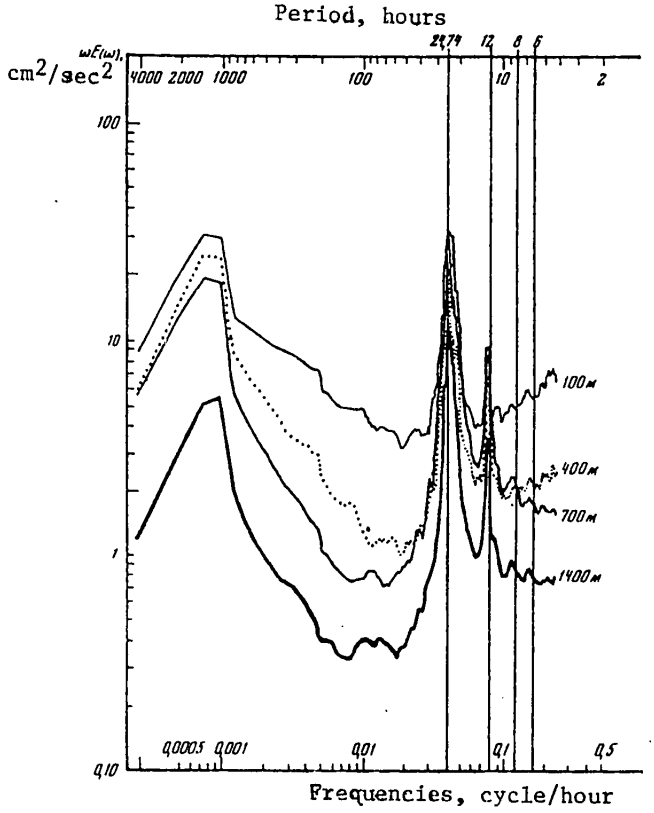

Fig. 1.

We computed the energy spectra $\omega E(\omega)$ (in cm^2/sec^2), where ω is the frequency (in cycles/hour), and $E(\omega)$ is the spectral density. They are convenient because on a graph with the abscissa $\ln \omega$ the areas under the $y = \omega E(\omega)$ curve give the contributions of the corresponding frequency intervals to the total dispersion of fluctuations of the parameter to be analyzed. However, since the $\omega E(\omega)$ values varied by two orders of magnitude, these values must be represented on the graphs at a logarithmic scale as well.

It was found that all 152 u and v spectra for four depths for the 19 buoy stations with an accuracy to small and irregular insignificant extrema have an extremely similar form with three distinct maxima in the region of the periods of synoptic

eddies (on the average τ = 1365.3 hours $\approx$ 56.9 days), diurnal and semidiurnal tidal periods (on the average τ = 24.7 and 12.6 hours), separated by deep minima at periods of about 57.7 and 14.2 hours and with a minimum immediately beyond the semidiurnal period ($\tau \sim$ 11.9 hours). As a rule the v spectra were a little above the u spectra; for example, as an average for 19 buoys at a depth of 100 m the $y = \omega E(\omega)$ values for the periods τ for u(y_u) and for v(y_v) were as follows

τ, hours	1365.3	57.7	24.7	14.2	12.6	11.9	4.1
y_u, cm^2/sec^2	23.60	3.49	30.78	3.55	9.18	4.11	6.32
y_v, cm^2/sec^2	36.28	3.70	32.26	4.32	9.55	4.90	6.58

Table 1

τ hours	y_{mean}, cm^2/sec^2 Depth	$y_{n-1} - y_2$, cm^2/sec^2 100 м	y_{mean} cm^2/sec^2 Depth	$y_{n-1} - y_2$, cm^2/sec^2 400 м
1365,3	30,52	53,59 – 16,81 = 36,78	23,58	58,68 – 5,86 = 52,82
57,7	3,59	5,05 – 2,41 = 2,65	1,20	2,18 – 0,64 = 1,53
24,7	31,63	56,44 – 13,68 = 42,76	19,00	39,72 – 5,30 = 34,42
14,2	4,04	6,57 – 2,05 = 4,52	2,21	3,01 – 1,44 = 1,57
12,6	9,46	12,51 – 7,26 = 5,25	6,81	11,07 – 4,12 = 6,95
11,9	4,54	5,79 – 3,02 = 2,76	2,39	4,15 – 1,18 = 2,97
4,1	6,45	9,77 – 3,11 = 6,65	2,46	4,75 – 1,28 = 3,47
	Depth 700 м		Depth 1400 м	
1365,3	19,30	35,04 – 10,43 = 24,61	5,60	8,93 – 1,76 = 7,18
57,7	0,74	1,06 – 0,47 = 0,59	0,36	0,58 – 0,17 = 0,41
24,7	33,61	49,46 – 16,61 = 32,84	11,88	17,80 – 6,59 = 11,21
14,2	2,61	3,60 – 1,86 = 1,74	1,00	1,46 – 0,68 = 0,78
12,6	8,79	11,50 – 6,35 = 5,15	3,63	5,65 – 2,08 = 3,57
11,9	1,98	2,89 – 1,55 = 1,35	1,31	1,93 – 0,97 = 0,96
4,1	1,62	1,96 – 1,21 = 0,76	0,80	1,19 – 0,62 = 0,57

Henceforth we will limit ourselves only to an examination of the spectra of kinetic energy $1/2(u^2 + v^2)$. The mean y_{mean} values and the variability characteristics $y_{n-1} - y_2$ of the significant extrema of these spectra for 19 buoys at four depths are given in Table 1 and curves for the mean spectra for 19 buoys at four depths are given in Fig. 1. These data show that the mean energy spectra for all buoys decrease monotonically with depth at all periods, exceot for the diurnal and semidiurnal periods (and in the interval between them), where the fluctuations were maximum at a depth of 700 m. The synoptic maximum in the layer 100-700 m decreases with depth very slowly (30.52 - 23.58 - 19.30), and at a depth of 1400 m it already has a considerably lesser value (5.60). The minimum between the synoptic and diurnal maxima at periods of about 57.7 hours, already detected on the basis of data from "POLIGON-70" [3], is exceedingly deep (3.59 - 1.20 - 0.74 - 0.36); this is the lowest level of the spectra in the entire considered range of periods. A little to the left of it on some individual spectra there were special maxima evidently created by atmospheric synoptic processes.

The highest maximum for almost all the spectra is observed near the diurnal period where the tidal lines σ_1, Q_1, ρ_1, O_1, NO_1, P_1, K_1, J_1, OO_1 are situated; these are enumerated here in the order of their increasing frequency (on the basis of

the decrease in amplitudes of tide-forming forces they are arranged in the order K_1, O_1, P_1, Q_1,...) and the line with the inertial period $\tau_i = 12/\sin\varphi$ hours, where φ is latitude (the POLIMODE buoys were at latitudes from 27°42' to 30°18', so that the inertial period τ_i varied from 25.8 to 23.8 hours). On individual spectra this maximum broke down into individual peaks, but their identification requires the use of spectroscopy with a higher resolution.

A maximum which is three times lower is observed near the semidiurnal period, where we find the tidal lines $2N_2$, μ_2, N_2, ν_2, M_2, L_2, T_2, S_2, K_2 in the order of an increase in their frequencies or M_2, S_2, N_2, K_2,... in the order of a decrease in the amplitudes of the tide-forming forces. To the right of τ_i in the spectrum a contribution is already made by internal waves; nevertheless, the minimum with τ = 14.2 hours between the diurnal and semidiurnal maxima and the first minimum to the right of the semidiurnal maximum with τ = 11.9 hours are extremely deep, which indicates a relatively poor development of internal waves of a nontidal origin. To the right of the minimum τ = 11.9 hours the spectra at depths of 700-1400 m drop off, whereas at depths of 100-400 m they rise. This is the sole appreciable effect of the "noise" created by the high-frequency fluctuations of surface buoys; at tidal and especially synoptic periods this noise is not reflected, so that the deeply submerged buoys used by American oceanologists for contending with this noise lead only to a loss of information on the dynamically most important upper layer of the ocean. Here on the spectra it is possible to see small special maxima at periods of 6 and 8 hours, possibly subharmonics of tidal periods.

The spatial variability of the values of the spectral extrema (for different buoys) is given in Table 1 as the difference $y_{n-1} - y_2$ of the second greatest and the second least values. It is greatest at the maxima, especially in the diurnal and then in the synoptic periods (whereas the minima are relatively stable), and decreases with depth together with the values of the mean spectra. A comparison of the spectra at individual buoys with the mean spectra indicated that usually a buoy is characterized by increased or decreased spectral values simultaneously at all periods and at all depths. The highest spectral levels were observed in the northwestern corner of the polygon, in the immediate neighborhood of the Gulf Stream, whereas the lowest levels were observed in the southwestern and especially in the northeastern corners of the polygon.

BIBLIOGRAPHY

1. Grachev, Yu. M., Yenikeyev, V. Kh. et al., DAN (Reports of the USSR Academy of Sciences), Vol 243, No 4, 1978.

2. Koshlyakov, M. N., Grachev, Yu. M. and Yenikeyev, V. Kh., DAN, Vol 252, No 3, 1980.

3. Vasilenko, V. M., Mirabel', A. P. and Ozmidov, R. V., OKEANOLOGIYA (Oceanology), Vol 16, 55, 1976.

5303
CSO: 8144/1581

UDC 534.24; 534.87

SPATIAL VARIABILITY OF THE ACOUSTIC FIELD REFLECTED FROM THE OCEAN FLOOR

Moscow DOKLADY AKADEMII NAUK SSSR in Russian Vol 259, No 1, Jul-Aug 81 (manuscript received 24 Nov 80) pp 205-208

[Article by L. M. Brekhovskikh, academician, V. I. Volovov and Yu. P. Lysanov, Acoustics Institute imeni N. N. Andreyev and Institute of Oceanology imeni P. P. Shirshov, USSR Academy of Sciences]

[Text] As indicated by numerous experimental investigations, the coefficient of reflection of an acoustic wave from the ocean floor experiences substantial changes with a change in the position of the research ship. [In this article reference is to wave reflection with normal incidence on the bottom.] It has now been established that there are at least three spatial scales of such variability, each of which has its own nature, its own characteristic properties and its own sphere of practical applications.

The greatest scale is some tens and hundreds of kilometers and corresponds to a change in general ocean floor relief. For example, with movement from regions with a level bottom to regions of oceanic ridges the effective reflection coefficient decreases by 6-16 db [1, 2].

The minimum spatial scale of change in the reflection coefficient falls in the range from fractions to tens of the wavelengths of sound. For example, at a frequency of 10 KHz it varies in dependence on the region from 0.1 to 2-3 m. A number of studies have been devoted to an investigation of the characteristics of this scale of variability, in particular the generalizing studies [1, 3]. The physical cause of the variability is that the reflected signal at the point of reception is formed as a superposing of the waves scattered by individual irregularities on the bottom and nonuniformities in the thickness of sediment. During movement of the receiving-radiating system there will be a redistribution of the phase difference of individual components, which will lead to a change in the amplitude of the reflected signal.

The discovery of small-scale variability of the reflection coefficient and the determination of the statistical nature of the reflection process have served as a basis for a new direction in acoustic investigations of the ocean floor and made it possible to propose new methods for solution of the problem of great practical importance of remote determination of the parameters of bottom microrelief ([1, 3, 4] and others), and also measurements of the absolute speed of the ship relative

to the bottom, its speed on course and at drift [5, 6].

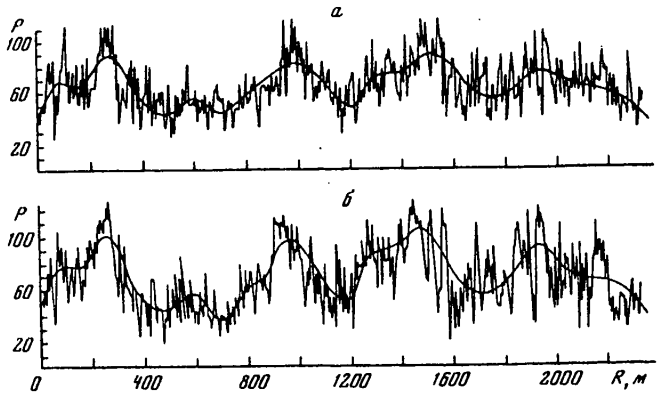

Fig. 1. Fluctuations of amplitude of signals reflected from bottom, received by different detectors (a and b) with great duration of process. Linear scale.

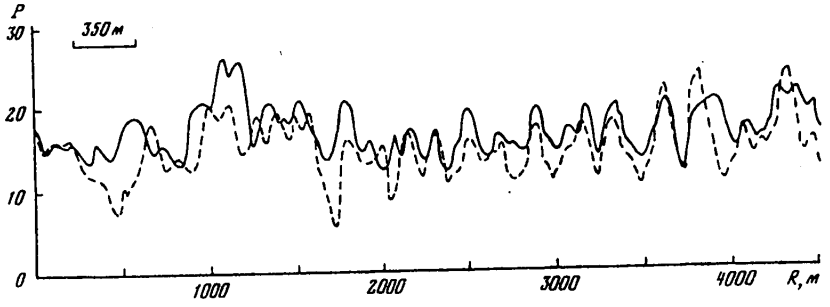

Fig. 2. Spatial variability of amplitude of reflected signals after filtering of process. Linear scale.

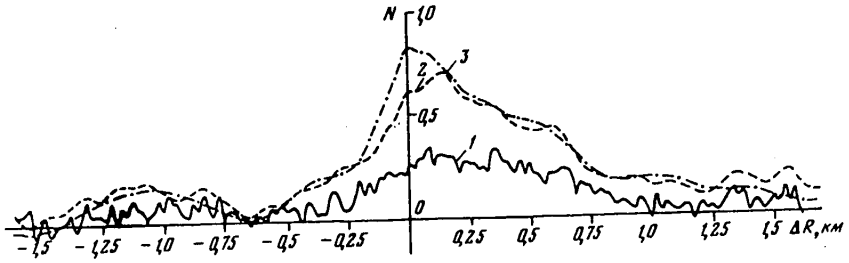

Fig. 3. Changes of cross-correlation coefficient of two processes in relation to spatial shift between them: 1) without averaging; 2) averaging using 7 values; 3) averaging using 21 values.

There is also a third, intermediate scale of variability of the reflected acoustic field which was already mentioned in [7]. This article is devoted to the results of an experimental investigation of precisely this scale.

Figure 1 shows a record of the normalized amplitude of the reflected wave (reflection coefficient) as a function of the movement of a ship lying at drift relative to the bottom. The two records correspond to the records for two hydrophones situated on one and the same ship and spaced by 60 m along its axis. It can be seen that in addition to the high-frequency fluctuations, which were mentioned above, there are considerable low-frequency components in the spectrum of the process. The thick lines in Fig. 1 represent variability of the latter kind after filtering of the high-frequency components. The measurements indicated that the spatial period of such variability in regions of the deep ocean with a level bottom is hundreds of meters to a kilometer and their intensity is approximately equal to the intensity of the high-frequency components [8]. It can also be seen from Fig. 1 that the correlation of the low-frequency components in processes registered by different detectors is very high. At the same time, the measurements indicate that there is virtually no correlation with respect to the high-frequency component, that is, the spacing of the detectors is much greater than the spatial correlation radius of these spectral components.

Available data indicate that the low-frequency spectral components are not governed by interference effects (like the high-frequency components), but by a considerable or complete change of the bottom region participating in the formation of the reflected signal and the associated change of the mean characteristics of the irregularities and nonuniformities of the bottom and also the physical properties of the sediments and the internal structure of the ground, which is especially important in the case of a stratified bottom. This conclusion is confirmed by the fact that the spatial correlation radius of the low-frequency components in order of magnitude coincides with the extent of the reflecting region of the bottom [1, 8].

Table 1

Degree of filtering	Maximum correlation coefficient	Correlation radius	Variation coefficient
Without filtering	0.35	462	44
Averaged for 7 values	0.70	450	31
Averaged for 21 values	0.82	455	28

Until recently such a spatial variability of the reflection coefficient was the least studied. We formulated special experiments for checking the fact of its universal existence in the abyssal regions of the ocean with a level bottom and its temporal stability. They were carried out using ships moving in the wake at speeds 11-11.5 knots at different, but each time fixed distances from one another, varying from 0.4 to 3.6 km. On each of the ships there was autonomous radiation and registry of the amplitude of the reflected signals using an echo sounder in a pulsed-tonal regime at a frequency of 9.6 KHz with a duration of the signals of 250 msec and a repetition rate of 1.5-4.0 sec. The objective of the experiment was identification of the pattern of variability at an intermediate scale, obtained on each of the ships, with a corresponding spatial shift, an evaluation of the depth of these fluctuations, and also the maximum correlation coefficient between

the two determined spatial processes in dependence on the degree of filtering of the high-frequency components of the initial processes. In Figure 2 the solid and dashed curves represent the records of the amplitudes of a reflected signal on different ships, averaged for 21 signals and displaced relative to one another with allowance for a time delay equal to the distance between the ships (in this case 3.6 km), divided by their speed. Figure 2 clearly shows fluctuations with a spatial scale of 200-400 m; the records for the different ships were highly correlated.

Figure 3 shows the correlation coefficient N of signals as a function of the uncompensated difference in the distance ΔR between the ships. The $\Delta R = 0$ value corresponds to the total compensation of the time delay when in computation of the correlation coefficient one record was displaced relative to the other for a time equal to the distance between the ships, divided by their speed. If it is assumed that the ships ideally follow in the wake of the other, the curves in Fig. 3 will coincide with the autocorrelation coefficients. The different curves correspond to different averaging intervals. Figure 3 shows that with impoverishment of the processes with high-frequency components the maximum of the correlation coefficient increases monotonically, in this case attaining a value 0.82. Some quantitative characteristics of the processes obtained with different degrees of filtering are given in Table 1.

It can be seen from the cited data that the filtering of processes leads to a sharp increase in their correlation, which is accompanied by a decrease in the variation coefficient. The spatial correlation radius of the processes is virtually not dependent on the degree of filtering. This indicates that the transformation of the processes by means of the averaging of the individual amplitude values, accomplished during processing, virtually does not affect their low-frequency part.

V. V. Krasnoborod'ko and V. A. Sechkin participated in the formulation and implementation of the experiment (Figures 2 and 3) and the authors express appreciation to them.

BIBLIOGRAPHY

1. AKUSTIKA OKEANA (Ocean Acoustics), Moscow, "Nauka," 1974.

2. Volovov, V. I. and Zhitkovskiy, Yu. Yu., OKEANOLOGIYA (Oceanology), Vol 6, No 6, 1086, 1966.

3. Volovov, V. I. and Lysanov, Yu. P., MORSKOYE PRIBOROSTROYENIYE, SER. AKUSTIKA (Marine Instrument Making. Acoustics Series), No 2, 25, 1972.

4. Brekhovskikh, L.M., et al., VOPROSY SUDOSTROYENIYA, SER. AKUSTIKA (Problems in Shipbuilding. Acoustics Series), No 10, 3, 1978.

5. Volovov, V. I., Lysanov, Yu. P., et al., OKEANOLOGIYA, Vol 17, No 1, 158, 1977.

6. Volovov, V. I., Lysanov, Yu. P., et al., AKUSTICH. ZHURN. (Acoustics Journal), Vol 25, No 2, 293, 1979.

7. Volovov, V. I., Lysanov, Yu. P. and Sechkin, V. A., AKUSTICH. ZHURN., Vol 19, No 1, 16, 1973.

8. Volovov, V. I., AKUSTICH. ZHURN., Vol 24, No 6, 934, 1978.

5303
CSO: 1865/224

SELECTED ABSTRACTS OF UNPUBLISHED ARTICLES ON GEOLOGY AND GEOPHYSICS

Moscow IZVESTIYA VYSSHIKH UCHEBNYKH ZAVEDENIY: GEOLOGIYA I RAZVEDKA in Russian
No 2, Feb 81 pp 54, 65, 74

UDC 543.05;551.48.018.6

USE OF DURABLE PLASTIC SHELLS FOR AUTONOMOUS INSTRUMENTS AND APPARATUS FOR GEOLOGICAL AND GEOPHYSICAL INVESTIGATIONS OF THE WORLD OCEAN

[Abstract of article by Kontar', Ye. A.]

[Text] The article gives the results of an analysis of the principal characteristics of durable tightly sealed plastic shells applicable to the problems involved in fabricating on their basis components and assemblies for autonomous instruments and apparatus for abyssal geological-geophysical investigations of the ocean. The author gives examples of the use of such shells in the construction of autonomous instruments and apparatus in the form of float elements, including abyssal autonomous samplers of the "Bentos" and "Bumerang-N" type, durable tightly sealed containers for sensors and recorders of bottom geophysical stations, durable tightly sealed housings for light and radio beacons of abyssal autonomous samplers of the "AP-6000" and "AP-passat" models, in systems for underwater hydroacoustic sounding used with autonomous instruments and apparatus, and also as power units for abyssal samplers of the "AP-bazal't" model and sources of elastic oscillations for deep seismic sounding in the ocean. 10 pages. Manuscript deposited at the All-Union Institute of Scientific and Technical Information, No 4525-80DEP, dated 27 October 1980.

UDC 550.837.05

METHOD FOR COMPUTING DIGITAL FILTERS FOR INTEGRAL TRANSFORMS IN ELECTRIC PROSPECTING

[Abstract of article by Belash, V. A.]

[Text] A method is proposed for computing digital filters making use of integral Bessel and Fourier transforms used in geoelectric prospecting. The transformed nuclear function is approximated by integration using a trinomial, after which numerical integration is carried out in intervals increasing in a geometric progression. The integration essentially involves a multiplication of the values of the nuclear function by precomputed filter coefficients and summation of the products. As a result, the process of integration on an electronic computer is accelerated by

hundreds of times. The realization of the filter for computing the impedance function made it possible to compute it with an accuracy to 0.1%. 14 pages. Manuscript deposited at the All-Union Institute of Scientific and Technical Information, No 4690-80DEP, dated 5 November 1980.

UDC 543.05;551.48.018.6

PROBLEMS IN OPTIMIZING 'BALLAST-BUOYANCY' SYSTEMS OF AUTONOMOUS INSTRUMENTS AND APPARATUS FOR ABYSSAL GEOLOGICAL-GEOPHYSICAL INVESTIGATIONS IN THE OCEAN

[Abstract of article by Kontar', Ye. A.]

[Text] A study was made of the principal characteristics of "ballast-buoyancy" systems of autonomous instruments and apparatus with and without floats for abyssal geological-geophysical investigations of the ocean. In the example of autonomous samplers of the "Bentos" type (United States), "Bumerang-N" (West Germany), "AP-6000," "AP-passat," "AP-kal'mar," and also an autonomous multishell bottom station of the "MADS-6" type (USSR) it is demonstrated that the improvement and use of "ballast-buoyancy" systems of autonomous instruments and apparatus is promising. 11 pages. Manuscript deposited at the All-Union Institute of Scientific and Technical Information, No 4524-80DEP, dated 27 October 1980.

5303
CSO: 1865/113

UDC 551.463.5:535.31

FEATURES OF DETECTION OF SEA SURFACE INHOMOGENEITIES BY THE RADAR METHOD

Moscow IZVESTIYA AKADEMII NAUK SSSR: FIZIKA ATMOSFERY I OKEANA in Russian Vol 17, No 7, Jul 81 (manuscript received 25 Feb 80, after revision 29 Jul 80) pp 754-761

[Article by A. I. Kalmykov and A. P. Pichugin, Institute of Radiophysics and Electronics, Ukrainian Academy of Sciences]

[Text]

Abstract: The article gives the amplitude (mean and fluctuation) and spectral characteristics of radar reflections of the uniform sea surface and inhomogeneities in the form of slicks. It is shown that reflections from slicks in a broad sector of angles of incidence are described within the framework of a model of selective scattering (two-scale model). Typical examples of the results are used in discussing the possibilities of processing of radar signals for the purpose of detecting slicks and determining their principal parameters.

One of the promising methods for the remote detection of spills of petroleum products on the water surface is the radar method. As is well known, the level of radar reflections by the sea surface is determined by the height of the ripples and the basis of contrast observation of spills of petroleum products is the extinction of ripples in these sectors. By use of the radar method it is possible to detect spills of petroleum products with a film thickness less than 0.1μm [1].

However, in addition to petroleum spills a wide range of phenomena transpiring both at the surface of the ocean and also in its depths is also observed in the form of a decrease (extinction) of the spectral density of the high-frequency components of surface waves. These inhomogeneities of the sea surface are usually called slicks.

As indicated by experiments, changes in the high-frequency components of waves can be caused by wind nonuniformities [2], the effects of emergence of internal waves [3], currents, etc. A peculiarity of slicks of such an origin is that most of them

appear when there are low waves (less than class 3); the slicks of spills of petroleum products also exist stably when there are waves of considerable height. Many of the effects creating slicks can be used in determining both the characteristics of these disturbing phenomena and the parameters of the ocean surface [4].

Most investigations of slicks until recently have had a descriptive character (for example, [5]). The detection and measurement of the parameters of slicks over great areas of the ocean is possible only by remote methods, the most sensitive of which, as noted above, is the radar method. In order to make broad use of this method it is necessary to know the laws of change of the radar reflections of inhomogeneities of this type -- slicks.

Comparative characteristics of radar reflections of the homogeneous sea surface and sectors of slicks. The radar reflections of a homogeneous sea surface were investigated in considerable detail. A model of these reflections [6] -- the selective scattering of the small-scale structure (ripples) and modulation by energy-carrying waves -- for the most part reliably describes the diversity of experimental data.

The appearance of slicks should lead to a change in the characteristics of radar reflections from the sea surface. Radar observations of slicks have had a sporadic character [1, 2]. These and other studies give only the changes of the mean values of the reflected signal in slicks; the fluctuation characteristics of reflections from slicks have virtually not been investigated. The principal measurements, whose results are cited below, were carried out in the radiohydrophysical polygon of the Marine Hydrophysical Institute Ukrainian Academy of Sciences. A feature of the mentioned polygon is the broad scanning sector and the diversity of the observed slicks, created by currents, the effects of emergence of internal waves, wind velocity fluctuations, etc. The instrumentation and the measurement method were discussed in [1]. The characteristics of the reflections from slicks cited below were obtained at a wavelength of $\lambda = 3.2$ cm with a sounder resolution $L\rho \approx 10$ m. Most of the experiments were carried out with sea waves with a class less than 3.

A typical record of the level of radar reflections E with antenna scanning in the space R is shown in Fig. 1. The operator places a mark over the record to indicate the place of intersection of the slick with the axis of the antenna diagram. There are reflections from a uniform sea to the left and right of the slick. The record in Fig. 1 was obtained with a vertical polarization with a glancing angle $\psi = 4.5°$; sea waves are of class 2. The slick zone, reflections from which are shown in Fig. 1, was formed by a current; the current velocity attained 0.5 $m \cdot sec^{-1}$. On this typical record there is a characteristic decrease in the mean level of reflections in the slick $\overline{E}_{sl}$ in comparison with reflections of the uniform sea $\overline{E}_{sea}$. The decrease in the level of reflections in the slick is characterized by the contrast

$$K_E = \overline{E}_{sea}/\overline{E}_{sl} \text{ or } K_E \text{ (db)} = 20 \lg (\overline{E}_{sea}/\overline{E}_{sl}). \quad (1)$$

In these experiments the K_E contrasts were varied in the range from 3-5 to 20 db or more. The lower values of the observed contrasts are limited by the characteristic fluctuations of reflections by a homogeneous sea. Under our conditions with scanning by the antenna the region of frequencies characterizing fluctuations of

reflections from slicks $F_{sl} < V/L_{sl}$ (V is the scanning rate, L_{sl} is the extent of the slick, $L_{sl} > L\rho$) is situated below 2-3 Hz and for it the fluctuations of the mean level of reflections from the sea in the case of waves up to class 3 is 2-3 db.

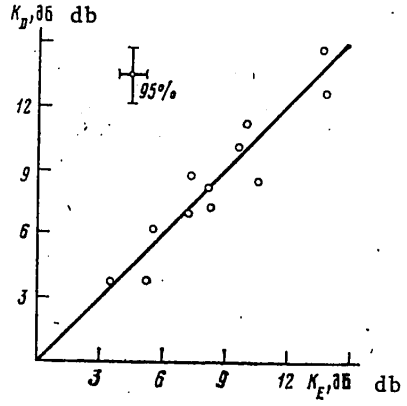

Fig. 2. Diagram used in comparing contrasts of reflections from slicks, determined from mean values (K_E) and dispersions (K_D). [Note: Figure 1 is not reproduced here. It shows a typical example of a record of the level of radar reflections from the sea with an inhomogeneity in the form of a slick. The slick is denoted by a mark.]

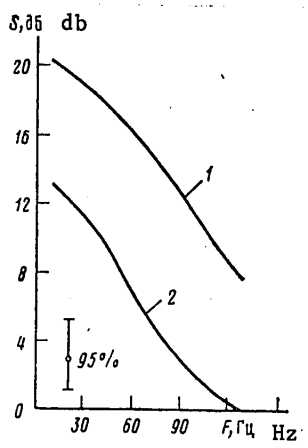

Fig. 3. High-frequency parts of spectra of fluctuations of reflections by a homogeneous sea (curve 1) and part of slick (curve 2).

Most slicks of natural origin are characterized by the presence of sharp boundaries of sea-slick and slick-sea reflections, whose extent in Fig. 1 corresponds to an element of resolution of the sounder $L_\rho \approx 10$ m. With a deterioration of resolution L_ρ the duration of the transition boundary increases, as corresponds to [1].

In the observation of slicks in the form of spills of petroleum products at radiowaves longer than $\lambda=3.2$ cm, for example, at $\lambda \approx 10$ cm [1], there can be a smoother dropoff of the mean level of reflections with transition from the homogeneous sea to a slick due to the relatively slow attenuation of long-wave ripples (wavelength $\Lambda \approx 5$ cm) in comparison with short-wave ripples ($\Lambda \approx 1.5$ cm); this smooth dropoff is observed only from the windward side of the slick. Thus, changes in the mean level of reflections from the slick against the background of reflections from the homogeneous sea have a pulselike character.

A distinguishing characteristic of reflections from slicks is also a decrease in the dispersion of fluctuations in comparison with a homogeneous sea. As indicated by radar observations of slicks, the contrasts

$$K_D = \sqrt{D_{sea}/D_{sl}} \text{ or } K_D \text{ (db)} = 10 \lg (D_{sea}/D_{sl}), \quad (2)$$

determined from the ratios of the dispersions of the levels of reflections from the homogeneous sea D_{sea} and slicks D_{sl}, were close to the values of the contrasts K_E, determined from (1). The discrepancies K_D and K_E fall within the limits of experimental accuracy. Figure 2 shows data from different experiments for the above-mentioned slicks of natural origin. It can be seen that the results of the experiments confirm the coincidence of the contrasts determined from (1) and (2). This coincidence is natural because within the framework of the model of selective scattering [6] both the mean level and the fluctuation characteristics of the reflections are dependent on the height of the ripples. Only with very glancing angles $\psi<1°$, when in addition to reflections from ripples, there are reflection bursts from the wave crests [7], can there be a difference between K_E and K_D.

As indicated by numerous investigations, a feature of radar reflections by the homogeneous sea is a single-mode character of the distributions of the levels of the reflections. In our experiments the distributions of levels of reflections by both the homogeneous sea and by slicks have a single-mode character. These distributions differ with respect to mean values and dispersions.

In choosing a model of radar reflections from the homogeneous surface of a sea with slicks it is of interest to examine the spectra of radar reflections. The nature of the spectra of reflections by a nonuniform sea is described completely by a model of selective scattering [6]: the low-frequency components of the spectrum are dependent for the most part on the energy-carrying waves, whereas the high-frequency components $F \gtrsim 10$ Hz (for $\lambda = 3$ cm) are determined only by ripples.

As indicated by recent experiments [8], the spectrum of rises of ripples has the character

$$S_h(F) \sim F^{-4} - F^{-5}. \quad (3)$$

The spectrum of fluctuations of the reflected signal $S_E(F)$ to the levels -20 - -30 db is determined for the most part by the orbital movements of the ripples and therefore

$$S_E(F) \sim F^2 S_h(F) \sim F^{-2} - F^{-3}. \quad (4)$$

This character of the high-frequency part of the spectrum is manifested in the spectra of reflections $S_E(F)$ shown in Fig. 3. Here we have shown only the high-frequency parts of the spectra of reflections from a homogeneous sea (curve 1) and a sector of the slick (curve 2). These spectra were obtained during scanning by the antenna and the spectral density of reflections from the slick in the frequency region $F \lesssim 10$ Hz is not statistically ensured.

The typical slopes of the high-frequency parts of the $S_E(F)$ spectra, which we observed with reflections from the sea and slicks, are close and fall in the range

$$S_E(F) \sim F^{-1.5} - F^{-3}.$$

This agrees well with the computational relationships (4). With respect to the levels of spectral density of reflections from the slicks, in accordance with the model [6], due to a decrease in the height of the ripples in the slicks there should be a contrast

$$K_S = \sqrt{S_{sea}/S_{sl}} \text{ or } K_S \text{ (db)} = 10 \lg (S_{sea}/S_{sl}), \quad (5)$$

where S_{sea} is the spectral density of reflections by the homogeneous sea, S_{sl} is the spectral density of reflections by a sector of the slick. In accordance with the model [6] we should have

$$K_E + K_D = K_S.$$

Figure 3 shows that the spectral density of the reflections from the slick S_{sl} on the average is 8 db lower than S_{sea}, that is, $K_S = 8$ db. The values of the contrasts $K_E = 7.43$ db and $K_D = 8.85$ db, computed in accordance with (1) and (2), with the confidence interval taken into account, coincide satisfactorily with K_S. The results of the processing of reflections from the slicks and other parameters confirm the data cited above. The similarity of these characteristics and the relationships of the levels of spectral density of the reflections by the homogeneous sea and slicks serve as an additional confirmation of the correctness of the mechanism of selective scattering [6] for reflection from slicks as well.

Thus, proceeding on the basis of the data cited above on the mean, fluctuation and spectral characteristics, the field reflected by a sea surface with slicks, can be represented as

$$E(R,t) = \begin{cases} E_{sea}(R, t) & \text{with } R \bar{\in} R_{sl}, \\ E_{sl}(R, t) = E_{sea}(R, t)/K & \text{with } R \in R_{sl}, \end{cases} \quad (6)$$

where $E_{sea}(R, t)$ is the field reflected by the homogeneous surface of the sea, which is described by the model [6], $E_{sl}(R, t)$ is the field reflected by a sector of the slick in the region of space R_{sl} and characterized by the contrast K

$$K = K_E = K_D = K_S.$$

Characteristics of reflections from an inhomogeneous surface. Taking into account the characteristics of separate reflections of the homogeneous sea surface and slicks cited above, it is possible to interpret the results of observation of

reflections from the nonuniform sea surface. Experimental investigations have indicated that the distributions of levels of signals reflected by the nonuniform sea have a two-mode character (Fig. 4). These distributions were obtained for one and the same slick with a different extent of the homogeneous sea. The first mode characterizes reflections from the slick; the second characterizes reflections by the homogeneous sea. Numerous observations have indicated that a two-mode distribution of the amplitudes of the radar reflections indicates a nonuniformity of this sector, that is, the presence of a slick.

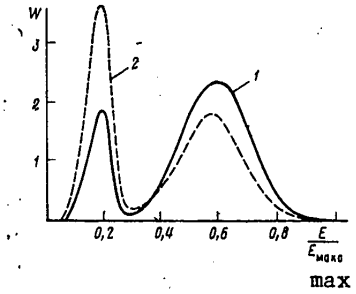

Fig. 4. Distributions of the levels of reflections by a nonuniform sea with different relative extents of the slick (L_{sl}/L_{obs}): 1) 0.22; 2) 0.47.

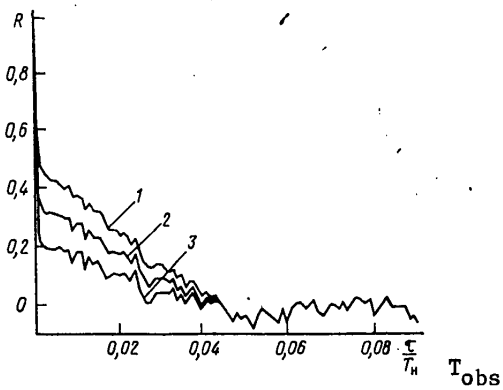

Fig. 5. Correlation functions of radar signals reflected by a nonuniform sea with a relative extent of the slick 0.045 and the contrasts: 1) 20; 2) 10; 3) 5.5 db.

On the basis of the model discussed above the ratio of the amplitudes corresponding to the maxima of the distributions determines the contrast of the reflections from the slick relative to the homogeneous sea K. Using distributions similar to those cited in Fig. 4 it is fundamentally possible to determine also the relative dimensions of the slicks as

$$L_{sl}/L_{obs} \approx \int_0^{A_0} w(A)\, dA, \qquad (7)$$

where L_{sl} is the extent of the sector of the slick, L_{obs} is the extent of the observed sector of the sea surface, $A = E/E_{max}$ is the relative level of the reflections, E_{max} is the maximum value of the level of reflections, A_0 is the level separating the reflections from the slick and the homogeneous sea (for Fig. 4 $A_0 \approx 0.3$), w(A) is the probability density of the relative level of reflections A. For the distributions cited in Fig. 4 the evaluations with (7) taken into account give K_E = 9.54 db, K_D = 9.82 db; L_{sl}/L_{obs} = 0.22 (continuous curve) and K_E = 9.54 db; K_D = 8.3 db; L_{sl}/L_{obs} = 0.47 (dashed curve); the corresponding parameters of the reflections from the slicks, computed on an electronic computer on the basis of a record of a signal similar to Fig. 1, are: K_E = 8.84 db, K_D = 9.63 db, L_{sl}/L_{obs} = 0.24 and L_{sl}/L_{obs} = 0.48.

As indicated by experiments for different slicks, the data from computations of the parameters of slicks on the basis of the proposed model correspond well to the results of computations of these characteristics on an electronic computer. The use of this method for determining the parameters of slicks is desirable with contrasts $K \geqslant 5$ db and $L_{sl}/L_{obs} \geqslant 0.1$, when the distributions of reflections from the slick and the homogeneous sea are separated reliably. The considered method can be realized using a level analyzer.

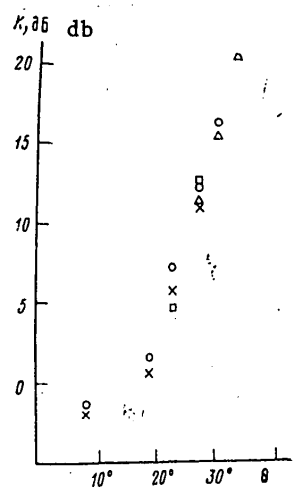

Fig. 6. Change in the contrasts of reflections from slicks with angle of incidence θ. The different symbols denote observational data for different slicks; waves up to class 3.

The appearance of slicks should also change the correlation function of radar reflections of the nonuniform sea surface. In accordance with the model of reflections from the nonuniform surface the correlation function of signals from the nonuniform sea R(r) should represent the characteristics of the correlation function of signals from the uniform sea and the pulsed character of reflections from the

slick (6). As is well known, the correlation function of a rectangular pulse has the shape of a triangle. This characteristic is also manifested in the correlation functions of reflections by a nonuniform sea.

Figure 5 shows typical correlation functions of signals reflected by a nonuniform sea, with different contrasts K and a relative extent of the slick L_{sl}/L_{obs} = 0.045. The correlation functions of the reflections from a nonuniform sector with a slick contrast K = 5.5 db were obtained as a result of processing of a real signal (curve 3). Processes with other contrasts (20 and 10 db) were modeled on an electronic computer using records with a contrast of 5.5 db in accordance with (6); the corresponding correlation functions are given in Fig. 5 (curves 1, 2). Figure 5 is characterized by the above-mentioned coincidence of fine-structured details in all the correlation functions. This is attributable to the use of one and the same record of reflections from the sea surface for the modeling of slicks with different contrasts on the surface. Figure 5 also shows the triangular character of the correlation function of reflections from a slick.

A change in the length of the slick leads to a change in the point of intersection of the triangular part of the correlation function with the axis of the normalized argument τ/T_{obs}. With $L_{sl}/L_{obs} \lesssim 0.1$ the values of the argument at the point of intersection $\tau/T_{obs} \approx L_{sl}/L_{obs}$ (T_{obs} is the observation time). Figure 5 shows that this parameter is not dependent on the contrast K. The value of the contrast K determines the place of intersection of the continuation of the triangular part of the correlation function with the axis R = 0. As indicated by experiments, using correlation processing it is possible to detect slicks and determine their principal parameters with the contrasts $K \geqslant 3$ db.

Region of applicability of radar method for detecting slicks. The region of angles of incidence in which the radar method for detecting slicks is applicable is determined by the region of applicability of the model of selective scattering by ripples [6]. As indicated above, for the detection of slicks with small glancing angles $\psi \lesssim 3°$ it is necessary to take into account the appearance of reflection bursts from the crests of waves prior to their collapse [7]. Reflection bursts are observed for the most part in horizontal polarization; in vertical polarization they are 15-20 db lower. Thus, for improvement of the conditions of radar observation of slicks in the case of small ψ angles (from a ship, from shore) it is desirable to use vertical polarization of radiation. This also increases the range of observation of reflections from the sea, that is, the range of detection of slicks.

The contrast observation of slicks from aerospace carriers is possible at angles of incidence $\theta > 15\text{-}20°$ ($\psi < 70\text{-}75°$). This limitation is related to an impairment of the applicability of a model of selective scattering with $\theta \lesssim 15\text{-}20°$ [9]. For the immediate checking of the effectiveness of the radar method for the detection of slicks with small angles of incidence $0° \leqslant \theta \lesssim 35°$ we carried out experiments also at a wavelength λ = 3.2 cm. This region of angles of incidence θ is of special interest since here there is a contribution to the reflected signal both by scattering by ripples and reflection by quasiplane surface elements.

Figure 6 shows experimental observational data for four typical slicks of natural origin. For angles $\theta \gtrsim 25°$ most of the detected slicks have a considerable contrast $K \geqslant 10$ db. In this region of angles it is common to observe slicks with contrasts $K \gtrsim 20$ db.

With a decrease in the angle of incidence θ the contrast K usually decreases in such a way that with $\theta \approx 20°$ the K value is $\lesssim$ 5 db. For virtually all slicks whose contrast is different with $\theta \gtrsim 25°$ the contrast value in the region $\theta \approx 15°$ is equal to zero, that is, reflections from the slick are not manifested against the background of reflections by the uniform sea.

Finally, with $\theta < 15°$ the contrast becomes negative, that is, the reflections from the slicks already exceed the reflections from the homogeneous sea; in this region of angles there is a predominance of quasimirror reflections. The angle $\theta \approx 15°$, for which K = 0, determines the transition region where scatterings from ripples and reflections by quasiplane elements are comparable. This agrees with data from special experiments [9], where it is noted that with average wave heights and angles of incidence $\theta < 6°$ there is a predominance of Kirchhoff reflection by quasiplane elements, with $\theta > 18°$ -- selective scattering by ripples, and the region of transition from one reflection mechanism to another is at angles $6° \lesssim \theta \lesssim 18°$.

Conclusions. Investigations of the statistical characteristics of radar reflections by a sea surface with slicks show:
1) the appearance of slicks can be reliably detected by the radar method,
2) the mean levels, dispersions and spectral densities of reflections in slicks decrease to an identical degree in comparison with the corresponding characteristics of reflections from a homogeneous sea,
3) in a wide range of angles of incidence from glancing to almost vertical ($\theta \gtrsim 15°$) the characteristics of the reflections from slicks are described in accordance with a model of selective scattering [6],
4) the statistical characteristics of reflections by an inhomogeneous sea can be used for the detection of slicks and determination of their principal parameters -- contrasts (the degree of extinction of ripples in them) and sizes.

In conclusion the authors express deep appreciation to B. A. Nelepo for stimulating discussions of the work.

BIBLIOGRAPHY

1. Galayev, Yu. M., Kalmykov, A. I., Kurekin, A. S., Lementa, Yu. A., Nelepo, B. A., Ostrovskiy, I. Ye., Pichugin, A. P., Pustovoytenko, V. V. and Terekhin, Yu. V., "Radar Detections of Petroleum Contaminations of the Sea Surface," IZV. AN SSSR: FAO (News of the USSR Academy of Sciences: Physics of the Atmosphere and Ocean), Vol 13, No 4, pp 406-414, 1977.

2. Ecklund, F., Nilsson, J. and Blomquist, A., "False Alarm Risks at Radar Detection of Oil Spills," PROC. URSI Com. II: MICROWAVE SCATTERING AND EMISSION FROM EARTH (BERNE 23-26 Sept 1974), edited by E. Schanda, Berne, 1974.

3. Ewing, G., "Slicks, Surface Films and Internal Waves," MARINE RES., Vol 9, No 3, pp 161-187, 1950.

4. Fedorov, K. N., "Observations of Oceanic Internal Waves From Space," OKEANOLOGIYA (Oceanology), No 5, pp 787-790, 1976.

5. Babkov, A. I., "Aerovisual Observations of the Sea Surface," METODY IZUCHENIYA MORSKIKH TECHENIY S SAMOLETA (Methods for Study of Sea Currents From an Aircraft), Moscow, Nauka, 1964.

6. Bass, F. G., Fuks, I. M., Kalmykov, A. I., Ostrovsky, I. E. and Rosenberg, A. D., "Very High Frequency Radio Wave Scattering by a Disturbed Sea Surface," IEEE TRANS. ANTENNAS PROPAG., Vol 16, No 5, pp 554-568, 1968.

7. Kalmykov, A. I. and Pustovoytenko, V. V., "On Polarization Features of Radio Signals Scattered From the Sea Surface at Small Grazing Angles," GEOPHYS. RES. (OCEAN AND ATMOSPHERE), Vol 81, No 12, pp 1960-1964, 1976.

8. Mitsujasu, H. and Honda, T., "The High-Frequency Spectrum of Wind-Generated Waves," OCEANOGR. SOC. JAPAN, Vol 30, No 4, pp 185-198, 1974.

9. Galaev, Yu. M., Bol'shakov, A. N., Yefimov, V. B., Kalmykov, A. I., Kurekin, A. S., Lementa, Yu. A., Nelepo, B. A., Ostrovskiy, I. Ye., Pichugin, A. P., Pustovoytenko, V. V. and Terekhin, Yu. V., NEKOTORYYE KHARAKTERISTIKI RADIOLOKATSIONNYKH OTRAZHENIY POVERKHNOST'YU MORYA PRI UGLAKH PADENIYA BLIZKIKH K VERTIKAL'NYM (Some Characteristics of Radar Reflections of the Sea Surface With Angles of Incidence Close to Vertical), Preprint No 1, MGI AN UkrSSSR, Sevastopol', 1978, 22 pages.

5303
CSO: 1865/222

UDC 551.466.81

RADIATIVE INSTABILITY OF SHEAR CURRENTS IN A STRATIFIED FLUID

Moscow IZVESTIYA AKADEMII NAUK SSSR: FIZIKA ATMOSFERY I OKEANA in Russian Vol 17, No 7, Jul 81 (manuscript received 7 Feb 80) pp 766-768

[Article by L. A. Ostrovskiy and L. Sh. Tsimring, Institute of Applied Physics, USSR Academy of Sciences]

[Text] The problem of the generation of internal waves by a shear current, as is well known, is extremely important for oceanography. This problem has already been examined in the literature (for example, see [1-3]). However, in all the considered models the radiated waves were generated due to instability of the Kelvin-Helmholtz type, possible in a stratified fluid only for quite short-wave disturbances. The energy losses from radiation from the shear layer lead to a partial stabilization of the instability.

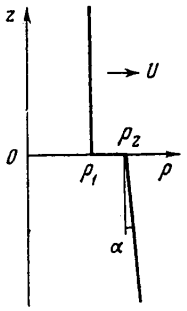

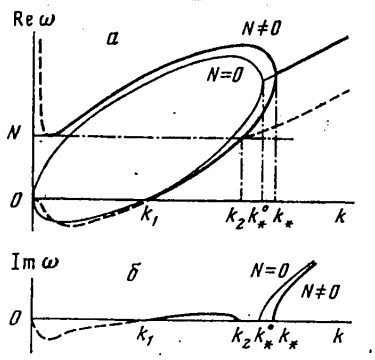

Fig. 1 (at left). Vertical density profile $\rho(z)$. Fig. 2. (at right). Dispersion curves. Dependence of real (a) and fictitious (b) parts of frequency on horizontal wave number with N = 0 (thin line) and N ≠ 0 (thick line).

Below we examine another mechanism for the radiation of internal waves associated with an increase or growth of negative energy waves. As is well known, the excitation of such waves does not increase, but decreases the total energy of the system.

In hydrodynamics waves of such a type were evidently examined for the first time by Benjamin [4] (also see [5-7]). The negative character of the energy means that introduction of any mechanism for the removal of energy will lead to its increase, that is, to current instability. As one of the possible mechanisms in [6] Cairns examined viscous friction. In our case the removal of energy was caused by the radiation of internal waves into a layer of stratified fluid. A fundamental difference from the cases examined in [1-3] is that here radiation does not suppress instability, but on the contrary, serves as a necessary condition for this.

We will formulate the problem in the following way. The plane $z = 0$ is a discontinuity above which ($z>0$) the fluid is homogeneous and moves with the velocity U relative to the lower region, where the fluid is fixed and also stratified there with respect to density ρ, and specifically

$$\rho = \rho_1 \ (z>0), \ \rho = \rho_2 - \alpha z \ \ (z<0), \tag{1}$$

where $\rho_2 > \rho_1$, $\alpha > 0$ (Fig. 1). We will assume that in the region of interest to us the Boussinesq approximation is correct; then it is possible to consider the Brent-Väisälä frequency $N = (-g\rho_z'/\rho)^{1/2} \approx (g\alpha/\rho_2)^{1/2}$. Here g is the acceleration of gravity.

A solution of the problem of the stability of such a current is found by the usual method. In the linearized Euler and continuity equations it is necessary to consider perturbations of all the parameters to be proportional to $\exp[i(kx + mz - \omega t)]$; then in the upper homogeneous half-space $m_{up} = ik$, whereas in the lower, stratified layer

$$m_{low} = k[(N^2/\omega^2) - 1]^{1/2}. \tag{2}$$

Using the boundary conditions at the discontinuity (continuity of pressure and normal velocity component) it is easy to demonstrate that ω and k satisfy the dispersion equation

$$\rho_1(\omega - kU)^2 + \rho_2(\omega^4 - N^2\omega 2)^{1/2} \tag{3}$$
$$-gk(\rho_2 - \rho_1) = 0.$$

Here we will add the conditions of disappearance of disturbances when $z \to +\infty$, which with $k>0$ is ensured by the relationship $m_{up} = ik$, and with $z \to -\infty$: Im $m_{low} < 0$. In addition, the vertical component of the energy flux S_z of the wave generated in the region $z<0$ should be directed downward (or is equal to zero when $\omega > N$). In this case

$$S_z = \overline{pw} = -\frac{\mathrm{Re}(\omega m_{low})}{k^2} \ \frac{\rho |w|^2}{2}, \tag{4}$$

where p and w are pressure perturbations and vertical velocity; the line denotes averaging for x. Accordingly, the generation (radiation) condition has the form

$$\mathrm{Re}(\omega m_{low}) = \mathrm{Re}(N^2 - \omega^2)^{1/2} > 0. \tag{5}$$

These conditions determine the signs on the roots in (2) and (3). The stability of the current is determined as usual by the sign on the fictitious part ω with real k. Figure 2,a shows the dependence of the real, and Fig. 2b shows the dependence

of the fictitious parts of ω on k with N = 0 and some $N \neq 0$. The continuous curves correspond to solutions satisfying all the mentioned boundary conditions. With N = 0 we arrive at the classical Kelvin-Helmholtz instability problem in a two-layer fluid [8]. The current is unstable with respect to quite short waves for which $k > k_*^0 = 2g(\rho_2 - \rho_1)/\rho_2 U^2$. However, we are interested in the region $k < k_*^0$, where ω is real with N = 0. It is important that in this region for one of the branches of the dispersion equation ω changes sign with $k = k_1 \approx k_*^0/2$. It is easy to show [5] that in the interval $k_1 < k < k_2$ the energy of the wave corresponding to the lower branch will be negative. The mechanism of removal of energy necessary for instability appears if $N \neq 0$; then with $\omega < N$ the tangential discontinuity radiates internal waves downward. This immediately leads to an increase in the perturbations in some range of wave numbers $k_1 < k < k_2$, where the mentioned interval is separated from the region of Kelvin-Helmholtz instability by the stable interval $k_2 < k < k_*$. It follows from (2) that with complex ω the vertical wave number m_{low} is also complex. In the presence of instability (that is, in the spectral interval $k_1 < k < k_2$) Im $m_{low} < 0$ and the amplitude decreases with increasing distance from the discontinuity, that is, there is a mode localized with respect to z. This ensures correctness of the formulation of the problem adopted here. The characteristic depth of the dropoff is the lesser the greater the instability increment. In the segments of the dispersion curve denoted by the dashed curve in Fig. 2 Im $m_{low} <$ 0 and the amplitude of the wave increases exponentially with depth for fixed x. Such structures of the wave field are known in optics [9] under the name "leaky waves." They are not characteristic solutions of the equations for a field without sources and therefore for a correct examination of such waves it is necessary to make the boundary and initial conditions more specific.

The radiative instability examined here has a direct analogy with the anomalous Doppler effect [10]. In this case an oscillator, moving with a velocity greater than the speed of light, radiates energy and in the process itself passes into a more excited state. In our problem the role of such oscillators moving at a speed greater than the speed of light is played by liquid particles oscillating in the vertical plane. The velocity of their translational motion, equal to the mean current velocity $U\rho_1/(\rho_1 + \rho_2)$, is greater than the phase velocity of the wave in the region of negative energy.

The increment of radiative instability is usually small in comparison with the maximum increment in the region of Kelvin-Helmholtz instability, but in our opinion this mechanism can play a definite role in the formation of the field of internal waves in the ocean. In actuality, for the ocean the tangential discontinuity considered here usually approximates some transition layer of the finite thickness h, which is possible under the condition $kh \ll 1$. This condition can be satisfied only for sufficiently long waves. In such a situation Kelvin-Helmholtz instability is manifested far more weakly. In addition, for $k > k_*$ the real part of the frequency is usually greater than N, so that even with $kh \to 0$ the waves generated in this region are propagated along the discontinuity without radiating into the depth of the ocean.

We will cite one evaluation of the characteristic scales of radiative instability. We will assume that U = 0.1 m/sec, $(\rho_2 - \rho_1)/\rho_2 = 10^{-3}$, N = 10^{-2} rad/sec. Then this instability is manifested in the interval of horizontal wavelengths 5.2-6.3 m.

The frequency of the radiated waves in this case varies from 0 to N and the vertical wave number, according to (3), varies from ∞ to 0. The greatest increment corresponds to a frequency $\omega = N/\sqrt{2}$ (the period in this example is 7 minutes); in this case m = k, that is, the wave is propagated at an angle 45° to the vertical. The time for increase of such a wave is about 1-2 hours.

BIBLIOGRAPHY

1. Lindzen, R. S. and Rosenthal, A. J., "On the Stability of Helmholtz Velocity Profiles in Stably Stratified Fluids When a Lower Boundary is Present," J. GEOPHYS. RES., Vol 81, No 9, pp 1561-1571, 1976.

2. Grimshaw, R. H. J., "On Resonant Overreflection of Internal Gravity Waves From a Helmholtz Profile," J. FLUID MECH., Vol 90, Pt 1, pp 161-178, 1979.

3. McIntyre, M. E. and Weissman, M. A., "On Radiating Instabilities and Resonant Overreflection," J. ATMOS. SCI., Vol 35, No 7, pp 1190-1196, 1978.

4. Benjamin, T. B., "The Threefold Classification of Unstable Disturbances," J. FLUID MECH., Vol 16, Pt 3, pp 436-450, 1963.

5. Voronovich, A. G. and Rybak, S. A., "Explosive Instability of Stratified Currents," DOKL. AN SSSR (Reports of the USSR Academy of Sciences), Vol 239, No 6, pp 1457-1460, 1978.

6. Cairns, R. A., "The Role of Negative Energy Waves in Some Instabilities of Parallel Flow," J. FLUID. MECH., Vol 92, Pt 1, pp 1-14, 1979.

7. Craik, A. D. D. and Adam, J. A., "Explosive Resonant Wave Interaction in a Three-Layer Fluid Flow," FLUID. MECH., Vol 92, Pt 1, pp 15-33, 1979.

8. Landau, L. D. and Lifshits, Ye. M., MEKHANIKA SPLOSHNYKH SRED (Mechanics of Continuous Media), Moscow, Gostekhizdat, 1954, 725 pages.

9. Fel'sen, L., "Quasioptical Methods in Diffraction," KVAZIOPTIKA (Quasioptics), Moscow, Mir, pp 11-62, 1964.

10. Nezlin, M. V., "Negative Energy Waves and the Anomalous Doppler Effect," UFN (Advances in the Physical Sciences), Vol 120, No 3, pp 481-496, 1976.

5303
CSO: 1865/222

TERRESTRIAL GEOPHYSICS

UDC 550.34.016

S AND P WAVE ATTENUATION OF THE CRUST AND UPPER MANTLE BENEATH THE WEST SIBERIAN PLATE AND SIBERIAN PLATFORM

Moscow IZVESTIYA AKADEMII NAUK SSSR: FIZIKA ZEMLI in Russian No 2, Feb 81 pp 37-50

[Article by A. V. Yegorkin, V. V. Kun and N. M. Chernyshev, Special Regional Geophysical Expedition, Scientific Production Association, Soyuzgeofizika, USSR Ministry of Geology]

[Text] The mean value of the figure of merit Q_p in Siberia increases from 227 in the range of depths of 0-150 km in the consolidated crust to 445 at H $\sim$ 150 km. The value of Q_p decreases to 190 at depths on the order of 150-210 km and then increases again, reaching 345 at H $\sim$ 400-450 km. The attenuation of P and S waves is essentially identical.

Considerable attention is devoted in the literature on the structure of the earth's lithosphere to parameters that characterize attenuation of P and S waves. However, the number of experimental data on these values is low, which one can judge, for example, from the summaries presented in [1-5]. The possibility of using data on attenuation of seismic energy during study of the earth's deep interior is limited in this regard.

One of the least investigated is the problem of ratio of P and S wave attenuation in the lithosphere. Data are presented in this article on the attenuation coefficients of S and P waves in the earth's crust and upper mantle (to a depth of 600 km), obtained from materials of explosion seismology during investigations in western and eastern Siberia. The results of studying the attenuation coefficients of P waves in the upper mantle to a depth of 100 km, obtained by the authors during similar investigations in regions of the Russian platform, the Caspian depression, the Urals and Kazakhstan, were published in [6]. Seismograms obtained in Siberia on two longitudinal profiles (Figure 1) were processed to calculate the attenuation parameters. Powerful industrial explosions that provide adequately intensive recording of P and S waves at epicentral distances up to 3,200 km (Figure 2) were used as the sources. A system of counter and overtaking hodographs was found on profiles I and II. The length of the hodograph from one explosion station was not less than 500 km. The distance between the points of recording the oscillations comprised 7-12 km. Three displacement components: one vertical and two horizontal (along the line of the profile and perpendicular to it), were recorded. The recordings were obtained by means of NSP-3 seismographs and Tayga stations with filtration having maximum frequency characteristic in the range of 4-5 Hz. The range of analyzed frequencies comprised 1-8 Hz.

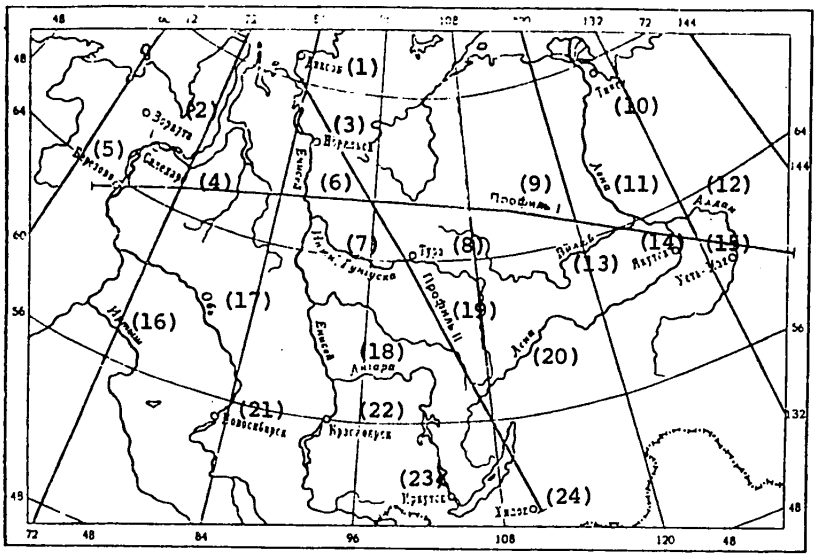

Figure 1. Layout of Profiles

Key:

1. Dikson
2. Vorkuta
3. Noril'sk
4. Salekhar
5. Berezovo
6. Yenisey River
7. Nizhnaya Tunguska River
8. Tura
9. Profile I
10. Tiksi
11. Lena River
12. Aldan River
13. Vilyuy River
14. Yakutsk
15. Ust'-Uda
16. Irtysh River
17. Ob' River
18. Angara River
19. Profile II
20. Lena River
21. Novosibirsk
22. Krasnoyarsk
23. Irkutsk
24. Khilok

The attenuation coefficients of P and S waves were determined by variations of their amplitude spectra as the distance R of the observation point from the source of the oscillations increased (by the decrease of the normalized spectral amplitude with distance). The method proposed by Vasil'yev [7] and used earlier in [1, 4, 6, 8] was used. The advantage of this method compared to others is that the effect of the divergence of the wave front and the different increase of the recording channels on the decrease of amplitude is eliminated in the calculations. The latter is especially important during observations on large legs of the profile by means of several seismic stations simultaneously. Each determination of $\alpha_{P,S}$ was made from seismograms of one explosion only at epicentral distances within which, judging by kinematic and dynamic parameters of seismic recordings, there is not wave shift [6]. Based on analysis of these parameters, the range of epicentral distances of 10-3,200 km is divided into seven legs: 10-200, 190-500, 350-850, 900-1,500, 1,500-2,200, 2,000-2,700 and more than 2,500 km.

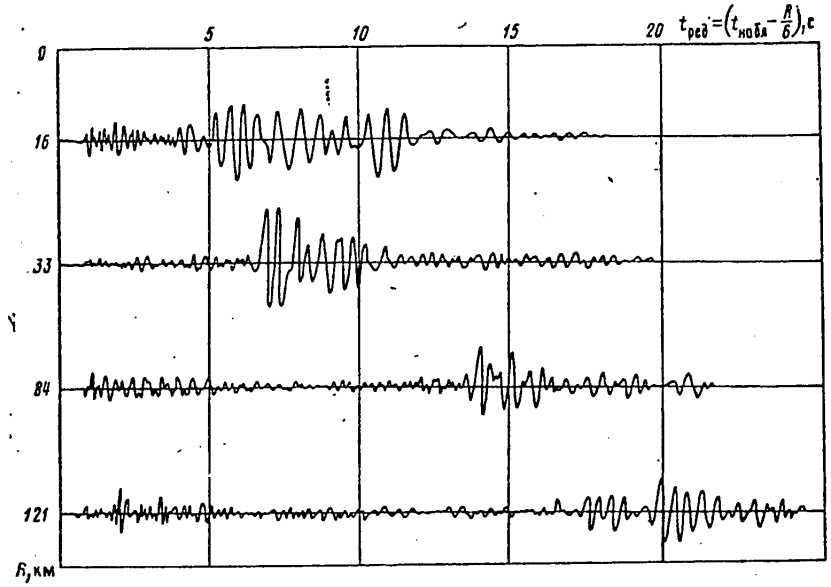

Figure 2. Example of S Wave Recordings Registered on Profile I

Refraction-refracted waves, called $P_k(S_k)$, $P_{n1}(Sn1)$, P_{n2}, P_{n3}, P_{n4}, P_{n5} and P_{n6}, respectively, are recorded within each leg. The first of them is propagated primarily in the upper part of the consolidated crust, penetrating to 15-30 km. The main part of the path of P_n waves is located in the upper mantle: P_{n1} from the Moho discontinuity to depths of 65-75 km, P_{n2} to 75-95 km, P_{n3} to 100-140 km, P_{n4} to 150-210 km, P_{n5} to 400-500 km and P_{n6} greater than 600 km.

The boundaries of the recording legs were determined for each explosion station on the basis of analyzing the amplitude graphs A(R), the graphs of the maximum spectral frequency $f_{max}(R)$ and the averaged graphs of the first onsets.

Special attention was devoted to correlation of waves recorded in the initial part of the seismograms and to determination of the legs where each of the P_n waves is determined in the simplest form (outside the interference zones with other waves) when selecting the profile interval on which the attenuation coefficients were calculated. The attenuation coefficients found in this case correspond to the depths at which the wave propagates in a direction close to horizontal (depths of maximum ray penetration) [9].

The results of calculating the parameters that describe the attenuation of P and S waves are presented in Tables 1-3. The following notations are used: ΔR is the interval of epicentral distances at which the wave was recorded, Δf is the frequency range for which the attenuation coefficient was calculated, K is the angular coefficient for the straight line that averages the dependence of the attenuation coefficient on frequency ($\alpha = Kf$), s/km, and it is equal in absolute value of the attenuation coefficient α at 1 Hz, σ_k is the mean square error of determining the values of K, ΔK is the range of values of K at fiducial probability of 0.9, Q is

the figure of merit ($Q = \pi/KV$), ΔQ is the range of values of Q with regard to the fiducial interval for K and V is the mean interval velocity of longitudinal (transverse) waves used when calculating Q. The geological structures within which attenuation was determined are indicated in the last column of the tables. The relative error of calculating the value of K fluctuates from 2.5 to 37.5 percent with a prevalent error of 6-8 percent. The actual error of determining the values of K and α is obviously greater since part of the pulse in some time interval Δt is used to calculate the spectra at each observation point; it is practically impossible to isolate the entire oscillation corresponding to each wave.

Attenuation of longitudinal waves in the consolidated crust (Table 1) in the investigated area varies within a considerable range: range K comprises $0.9 \cdot 10^{-3}$ to $7.05 \cdot 10^{-3}$ $s \cdot km^{-1}$ and Q comprises 69-562. The mean values for these parameters ($\bar{K}$, $\bar{Q}$) are equal to $3.28 \cdot 10^{-3}$ $s \cdot km^{-1}$ and 202, respectively. $\bar{K}_{p_1} = 2.78 \cdot 10^{-3}$ $s \cdot km^{-1}$ and $\bar{Q} = 227$ without abnormally high values ($K_p > 5.0 \cdot 10^{-3}$ $s \cdot km^{-1}$).

Relatively stable values of K ($3.0 \cdot 10^{-3}$ to $4.72 \cdot 10^{-3}$ $s \cdot km^{-1}$) and of Q (114-161) were found within the West Siberian plate (Nos. 1-4 of Table 1) and the Vilyuy syneclise (Nos. 14 and 15 of Table 1); the values of $\bar{K}$ for these regions comprise $3.84 \cdot 10^{-3}$ $s \cdot km^{-1}$ and $3.87 \cdot 10^{-3}$ $s \cdot km^{-1}$ and those of $\bar{Q}$ comprise 133 and 136. $\bar{K}$ is less ($2.60 \cdot 10^{-3}$ $s \cdot km^{-1}$) while $\bar{Q}$ is greater (212) in the region of profile II (the Tunguska syneclise, Angara-Lena stage), where the standard deviation of the considered values is also low.

The greatest variation of K and Q is noted within the central part of profile I (the Mirnyy-Aykhal saddle, Nos. 5-13 of Table 1). The maximum attenuation ($K = (6.01\text{-}7.05) \cdot 10^{-3}$ $s \cdot km^{-1}$ was found here from P_K waves that passed through the zones of a deep fault separating the Mirnyy-Aykhal saddle and the Vilyuy syneclise. For this region $\bar{K}$ is equal to $3.27 \cdot 10^{-3}$ $s \cdot km^{-1}$ and $\bar{Q} = 242$. $\bar{K} = 2.34 \cdot 10^{-3}$ $s \cdot km^{-1}$ and $\bar{Q} = 290$ without regard to the two maximum values.

Attenuation of longitudinal waves in the upper mantle. Based on analysis of Table 2, one can make the following conclusions.

1. The investigated ranges of the depths of the upper mantle (from 0 to 600 km from the M discontinuity) differ significantly by the values of the attenuation coefficients of longitudinal waves and by the nature of their variation in area.

2. High variability of the values of coefficient K in area and the figure of merit calculated by it is typical for the uppermost part of the upper mantle ($H \approx 0\text{-}20$ km). The value of $\bar{K}$, calculated from the data of two profiles, is equal to $1.80 \cdot 10^{-3}$ $s \cdot km^{-1}$; the range of its variation are relatively broad--$K = (1.02\text{-}3.60) \cdot 10^{-3}$ $s \cdot km^{-1}$. Deviations of K from the mean value are significant, on the order of 20-60 percent. The range of variation of the figure of merit is from 106 to 370 and $\bar{Q} = 241$. The wide range of the derived values of K and Q correlates to the significant variations of the boundary velocity through the surface of the upper mantle found in profiles I and II ($V_g = 8.2\text{-}8.7$ km/s). The existence of an inverse correlation of the dependence between the values of coefficient K and velocity V_p was shown earlier [6].

Table 1. Attenuation Coefficients and Figure of Merit of Earth's Crust (P-Waves)

(1) № п.п.	ПР	ПВ	ΔR, км	(2) Δf, Гц	$K_P \cdot 10^3$, с·км$^{-1}$ (3)	$\pm\sigma_K \cdot 10^3$, с·км$^{-1}$	$\Delta K \cdot 10^3$, с·км$^{-1}$	Q_P	ΔQ_P	V_P, км/с (4)	(5) Геологические структуры
1	I	V	13–110	1,8–6,2	3,64	0,41	3,42–3,86	134	120–150	6,5	Западно-Сибирская плита (6)
2	I	V	19–81	1,0–6,2	3,02	0,26	2,89–3,15	161	148–176	6,5	То же (6)
3	I	II	73–228	1,0–5,0	3,98	0,29	3,81–4,15	123	115–133	6,4	»
4	I	II	27–117	0,6–4,2	4,72	0,41	4,48–4,96	114	105–125	5,8	»
5	I	VI	21–79	2,8–6,8	5,25	0,47	4,98–5,52	97	89–107	6,2	Сибирская платформа, Мирнинско-Айхальская седловина (7)
6	I	VI	99–188	1,6–6,4	4,52	0,14	1,45–1,59	328	301–360	6,3	То же (7)
7	I	III	58–200	1,6–8,0	3,05	0,16	2,99–3,12	163	155–172	6,3	»
8	I	VII	16–127	3,6–7,2	1,39	0,14	1,31–1,47	370	320–392	6,1	»
9	I	VII	46–191	2,8–6,8	1,52	0,14	1,44–1,60	328	301–360	6,3	»
10	I	VII	48–99	1,0–4,6	0,90	0,09	0,86–0,94	562	514–622	6,2	»
11	I	VIII	50–101	1,0–5,0	7,05	0,41	6,81–7,29	69	66–74	6,4	»
12	I	IX	51–91	1,8–6,6	6,01	0,45	5,77–6,25	84	78–91	6,2	»
13	I	IX	98–155	1,0–8,2	2,73	0,25	2,61–2,85	179	164–198	6,4	» (8)
14	I	IV	63–206	1,2–3,6	4,05	0,85	3,42–4,68	128	106–162	6,1	Сибирская платформа, Вилюйская синеклиза
15	I	IV	16–176	1,0–4,0	3,70	0,38	3,52–3,88	144	130–160	5,9	То же (8)
16	II	II	33–157	1,5–8,0	1,69	0,04	1,67–1,71	300	295–303	6,3	Сибирская платформа, Тунгусская синеклиза (9)
17	II	III	22–70 (P^{oc})	1,0–8,0	2,81	0,25	2,67–2,95	190	182–201	5,9	То же (9)
18	II	III	39–164	1,5–8,0	3,49	0,16	3,41–3,57	148	143–150	6,1	»
19	II	IV	18–181	1,0–6,0	3,00	0,14	2,95–3,05	168	160–170	6,3	Сибирская платформа, Ангаро-Ленская ступень (10)
20	II	IV	9–148	1,0–8,0	2,00	0,16	1,91–2,09	254	243–266	6,2	То же (10)

Key:

1. Number of item
2. Hertz
3. $s \cdot km^{-1}$
4. km/s
5. Geological structures
6. West Siberian plate
7. Siberian platform, Mirnyy-Aykhal saddle
8. Siberian platform, Vilyuy syneclise
9. Siberian platform, Tunguska syneclise
10. Siberian platform, Angara-Lena stage

Table 2. Attenuation Coefficients and Figure of Merit of Upper Mantle (P-Waves)

(1) Профиль	ПВ	ΔR, км	(2) Δf, Гц	$K_P \cdot 10^3$ с·км$^{-1}$ (3)	$\pm\sigma_K \cdot 10^3$	$\Delta K \cdot 10^3$, с·км$^{-1}$	Q_P	ΔQ_P	V_P, км/с (4)	(5) Геологические структуры
I	I	220–627	0,8–4,0	1,13	0,083	1,09–1,17	335	312–361	8,30	Западно-Сибирская плита (6)
II	III	256–351	1,0–6,0	3,6	0,23	3,49–3,71	106	103–110	8,20	Сибирская платформа, Тунгусская (7) синеклиза
II	III	309–541	1,0–5,0	1,26	0,058	1,23–1,29	303	294–314	8,30	То же (7)
II	IV	242–428	1,0–8,0	1,20	0,23	1,07–1,33	310	280–350	8,40	»
I	IV	203–345	1,4–5,8	2,24	0,42	2,01–2,47	169	142–208	8,40	Сибирская платформа, Вилюйская (8) синеклиза
I	III	327–453	1,0–7,0	1,46	0,12	1,40–1,52	263	252–274	8,20	То же (8)
I	III	215–296	1,6–6,4	2,51	0,30	1,36–1,58	151	135–171	8,30	Сибирская платформа, Мирненско- (9) Айхальская седловина
I	III	223–335	1,0–7,0	2,81	0,18	2,72–2,90	133	125–142	8,40	То же (9)
II	II	363–445	1,5–10	2,85	0,16	2,77–2,93	132	130–137	8,30	Таймырский массив, Енисей-Хатанг- (10) ский прогиб
II	II	215–475	1,0–8,0	1,02	0,06	0,98–1,06	370	360–386	8,30	
II	V	189–280	2,0–8,0	1,50	0,05	1,47–1,53	242	235–245	8,70	Ангаро-Ленская ступень (11)
I	II	421–620	0,4–5,2	0,72	0,071	0,68–0,76	525	494–601	8,35	Западно-Сибирская плита (6)
I	II	459–768	0,8–5,0	1,04	0,21	0,95–1,12	363	302–455	8,35	То же (6)
I	III	349–684	2,0–8,8	0,71	0,03	0,70–0,72	530	508–553	8,35	Сибирская платформа, Тунгусская (7) синеклиза
I	II	504–629	0,6–6,2	1,42	0,142	1,35–1,50	264	240–293	8,35	То же (7)
I	III	567–752	2,0–7,6	1,31	0,05	1,29–1,33	267	277–298	8,35	»
II	II	400–488	1,0–5,5	6,54	0,29	6,41–6,67	57	57–61	8,40	»
II	II	506–705	1,0–5,5	1,86	0,16	1,78–1,94	200	193–210	8,40	»
II	IV	512–728	1,0–3,0	0,97	0,28	0,80–1,15	385	330–470	8,40	»
II	III	483–632	1,0–6,0	1,86	0,26	1,73–1,99	201	190–218	8,40	»
I	III	658–867	1,4–6,2	1,00	0,08	0,96–1,04	376	362–392	8,35	Сибирская платформа, Вилюйская (8) синеклиза
I	III	479–638	1,0–7,0	1,22	0,07	1,19–1,25	308	292–326	8,35	То же (8)
I	IV	369–590	0,2–3,4	1,14	0,19	1,02–1,25	331	284–396	8,35	Сибирская платформа, Мирненско- (9) Айхальская седловина
II	V	435–647	1,5–6,5	1,03	0,061	0,97–1,09	350	330–370	8,70	Сибирская платформа, Ангаро- (12) Ленская ступень

[Continued on following page]

APPROVED FOR RELEASE: 2007/02/09: CIA-RDP82-00850R000400050037-2

FOR OFFICIAL USE ONLY

Table 2 [Continued from preceding page]:

Профиль	ПВ	ΔR, км	Δf, Гц	$K_P \cdot 10^8$, с·км$^{-1}$	$\pm\sigma_K \cdot 10^8$	$\Delta K \cdot 10^8$, с·км$^{-1}$	Q_P	ΔQ_P	V_P, км/с	Геологические структуры
I	IV	1054–1377	1,6–5,0	0,876	0,08	0,84–0,91	424	387–469	8,45	Сибирская платформа, Тунгусская (7) синеклиза
II	V	984–1270	1,0–7,0	0,70	0,21	0,58–0,82	528	452–640	8,50	То же(7)
II	II	1211–1401	0,5–5,0	1,67	0,35	1,46–1,88	221	209–268	8,50	»
I	II	912–1135	0,4–4,0	0,61	0,15	0,52–0,70	612	490–817	8,45	Сибирская платформа, Мирнинско-Айхальская седловина, Западно-Сибирская плита (13)
I	I	897–1485	0,4–4,6	0,99	0,10	0,95–1,04	375	330–420	8,45	Сибирская платформа, Мирнинско-Айхальская седловина (9)
I	II	1044–1473	0,8–2,6	0,67	0,11	0,60–0,73	557	479–666	8,45	
II	III	904–1125	1,0–6,0	0,89	0,13	0,83–0,95	408	380–435	8,70	Сибирская платформа, Ангаро-Ленская ступень Прибайкальский прогиб (14)
I	III	1697–2117	0,6–4,0	2,25	0,22	2,15–2,35	164	149–182	8,50	Западно-Сибирская плита (6)
I	IV	2080–2232	0,2–2,4	2,40	0,60	2,06–2,74	154	123–205	8,50	То же
II	V	1676–1902	0,9–2,9	2,28	0,23	2,15–2,41	160	150–175	8,60	Сибирская платформа, Тунгусская (7) синеклиза
I	II	1521–1696	0,6–3,4	1,68	0,20	1,58–1,79	219	196–249	8,50	Сибирская платформа, Вилюйская (8) синеклиза
I	II	1684–1894	0,8–3,0	1,66	0,29	1,50–1,82	223	190–269	8,50	То же
I	I	1990–2110	0,2–2,6	1,59	0,40	1,35–1,83	232	186–310	8,50	Сибирская платформа, Мирнинско-Айхальская седловина (9)
II	II	1542–1906	0,5–5,0	1,31	0,23	1,17–1,45	280	249–308	8,70	Сибирская платформа, Ангаро-Ленская ступень (12)
I	III	2070–2297	0,4–5,0	1,24	0,08	1,21–1,27	266	246–280	9,50	Западно-Сибирская плита (1)
I	IV	2251–2601	0,2–3,2	2,58	0,15	2,51–2,65	128	119–133	9,50	То же
I	II	1979–2126	0,4–2,6	2,12	0,41	1,89–2,35	156	128–190	9,50	Сибирская платформа (15)
II	I	2209–2382	1,0–2,6	0,92	0,11	0,85–0,99	359	317–400	9,50	То же
	V	2307–2677	1,0–3,8	~0,40	0,15	0,32–0,48	825	700–1000	9,50	»
I	IV	2581–2975	0,4–4,0	1,97	0,17	1,89–2,05	156	133–158	10,50	Западно-Сибирская плита (1)

[Key on following page]

[Key continued from preceding page]:

1. Profile
2. Hertz
3. $s \cdot km^{-1}$
4. km/s
5. Geological structures
6. West Siberian plate
7. Siberian platform, Tunguska syneclise
8. Siberian platform, Vilyuy syneclise
9. Siberian platform, Mirnyy-Aykhal saddle
10. Taymyr massif, Yenisey-Khatanga downwarp
11. Angara-Lena stage
12. Siberian platform, Angara-Lena stage
13. Siberian platform, Mirnyy-Aykhal saddle, West Siberian plate
14. Siberian platform, Angara-Lena stage, Baykal downwarp
15. Siberian platform

The range of values of K and Q calculated by P_{n2} waves and corresponding to depths of 30-50 km (from the M discontinuity) is narrower than for P_{n1} waves; the absolute values of K are lower and those of Q are higher; $\bar{K} = 1.19 \cdot 10^{-3}$ $s \cdot km^{-1}$ and $\bar{Q} = 345$. The deviations of the values of K from $\bar{K}$ are less than in the first interval.

The very large value of K equal to $6.54 \cdot 10^{-3}$ $s \cdot km^{-1}$, found on profile I on the leg of the Verkhnetembenchinskiy uplift of the Tunguska syneclise,* should be especially noted. The high attenuation and the reduced figure of merit of the upper mantle on this leg were apparently determined by the existence of a zone of deep tectonic disturbance penetrating into the upper mantle. This is confirmed indirectly by the abnormally high value of K ($3.6 \cdot 10^{-3}$ $s \cdot km^{-1}$) found on this same leg from the P_{n1} wave at the other explosion station.

4. The values of α_P and Q calculated by the P_{n3} wave correspond to depths on the order of 60-95 km below the M discontinuity. Attenuation is less here than for the other intervals, while the figure of merit is higher. The value of K varies from $0.607 \cdot 10^{-3}$ to $1.67 \cdot 10^{-3}$ $s \cdot km^{-1}$, $\bar{K} = 0.910 \cdot 10^{-3}$ $s \cdot km^{-1}$ and $\bar{Q} = 445$; deviation of single determinations from the mean value are less than 30 percent. An exception is the region of the Katanga saddle of the Tunguska syneclise, for which an abnormally high value of K ($1.67 \cdot 10^{-3}$ $s \cdot km^{-1}$) was found.

5. The value of $\bar{K}$ increases to $1.98 \cdot 10^{-3}$ $s \cdot km^{-1}$ while that of $\bar{Q}$ decreases to 193 at depths of 150-210 km, where attenuation was studied from the amplitude spectra of the P_{n4} wave. Individual values of K are included in a rather narrow range ($1.59 \cdot 10^{-3}$ to $2.40 \cdot 10^{-3}$ $s \cdot km^{-1}$) and are close to those found for the mass lying near the Moho discontinuity.

6. The values of K determined from the P_{n5} wave and which characterize attenuation at depths of 400-500 km differ significantly from data of different detonation stations (from $0.40 \cdot 10^{-3}$ to $2.58 \cdot 10^{-3}$ $s \cdot km^{-1}$) and $\bar{K} = 1.45 \cdot 10^{-3}$ $s \cdot km^{-1}$. The maximum deviations from the mean value are 80 percent and $\bar{Q} = 347$.

7. A single value of $K = 1.97 \cdot 10^{-3}$ $s \cdot km^{-1}$ and $Q = 145$ was found from the P_{n6} wave.

*This value was eliminated when calculating K for P_{n2} waves.

Table 3. Attenuation Coefficients and Figure of Merit of Earth's Crust and Upper Mantle (S-Waves)

№ п.п (1)	ПР	ПВ	Δh, км	Δf, Гц (2)	$K \cdot 10^3$, с·км$^{-1}$ (3)	$\pm\sigma_K \times 10^3$, с·км$^{-1}$	$\Delta K \cdot 10^3$, с·км$^{-1}$	Q_S	ΔQ_S	V_S, км/с (4)	Геологические структуры (5)	$K_P \cdot 10^3$	Q_P	K_P/K_S	Q_P/Q_S
						(6) Волна S_k					(7)				
1	I	VI	28–29	2,8–6,8	3,28	0,41	3,05–3,51	260	231–297	3,7	Сибирская платформа, Мирнинско-Айхальская седловина	5,25	97	1,60	0,37
2	I	X	49–159	2,8–11,2	2,80	0,07	2,77–2,83	305	297–313	3,7	То же(7)	3,05	163	1,14	0,51
3	I	III	78–215	2,4–5,6	2,67	0,28	2,50–2,84	320	289–357	3,7	»				
4	I	III	112–194	1,2–8,0	3,21	0,37	3,04–3,38	266	238–300	3,7	»				
5	I	VII	34–162	3,2–8,0	2,85	0,14	2,77–2,93	300	285–314	3,7	»	1,39	370	0,49	1,23
6	I	VIII	8–79	2,0–8,8	2,53	0,06	2,50–2,56	337	329–345	3,7	»	7,05	69	2,79	0,20
7	I	VIII	31–173	2,8–8,8	2,35	0,11	2,30–2,4	363	347–380	3,7	»				
8	II	II	33–192	2,0–6,5	2,49	0,13	2,41–2,57	350	336–358	3,6	Сибирская платформа, Тунгусская синеклиза (8)	1,69	300	0,68	0,86
9	II	III	30–180	1,0–5,0	1,90	0,22	1,83–2,03	450	432–478	3,6	То же (8)	3,49	148	1,84	0,33
10	II	IV	18–181	1,0–7,0	2,62	0,21	2,42–2,82	343	315–367	3,5	Сибирская платформа, Ангаро-Ленская ступень (9)	3,00	168	1,14	0,49
11	II	IV	9–114	0,5–6,5	1,77	0,23	1,64–1,90	505	470–547	3,5	То же (9)	2,00	254	1,13	0,50
						(10) Волна S_{n1}					(8)				
12	I	II	272–601	1,0–3,8	1,24	0,08	1,20–1,28	539	506–567	4,7	Сибирская платформа, Тунгусская синеклиза				
13	II	II	235–339	1,5–6,0	2,42	0,20	2,32–2,52	260	248–270	5,0	То же (8)				
14	II	II	400–514	2–5,5	1,58	0,21	1,46–1,70	400	368–428	5,0	»				
15	II	II	400–514	1,0–6,0	1,92	0,11	1,87–1,97	326	318–335	5,0	»	6,54	59	3,40	0,18
16	II	III	309–495	0,5–6,0	1,68	0,24	1,55–1,81	375	347–405	5,0	»	1,26	303	0,75	0,82
17	II	III	208–507	1,0–6,5	1,36	0,19	1,25–1,46	460	430–500	5,0	»	3,60	106	2,65	0,23
18	II	IV	175–307	0,5–5,5	2,58	0,91	2,45–2,71	240	227–252	5,1	»	1,50	242	0,58	1,01
19	II	IV	193–428	1,5–6,0	1,24	0,22	1,12–1,36	510	470–560	5,0	»	1,20	310	0,97	0,61

Key:

1. Profile
2. Hertz
3. s·km^{-1}
4. km/s
5. Geological structures
6. S_k wave
7. Siberian platform, Mirnyy-Aykhal saddle
8. Siberian platform, Tunguska syneclise
9. Siberian platform, Angara-Lena stage
10. S_{n1} wave

The ratios of the mean values of $\bar{K}$ and $\bar{Q}$, calculated for depth ranges of II-V, to the mean values $\bar{K}_1$ and $\bar{Q}_1$ found for the uppermost part of the upper mantle are equal to $\bar{K}_2/\bar{K}_1 = 0.66$, $\bar{K}_3/\bar{K}_1 = 0.50$, $\bar{K}_4/\bar{K}_1 = 1.10$ and $\bar{K}_5/\bar{K}_1 = 0.80$; $\bar{Q}_2/\bar{Q}_1 = 1.43$, $\bar{Q}_3/\bar{Q}_1 = 1.90$, $\bar{Q}_4/\bar{Q}_1 = 0.80$ and $\bar{Q}_5/\bar{Q}_1 = 1.44$. Similar values of $\bar{K}_2/\bar{K}_1$ (0.60) and $\bar{Q}_2/\bar{Q}_1$ (1.55) were also found in [6] from materials of seismic investigations within the Urals, the Turan plate and the Russian platform.

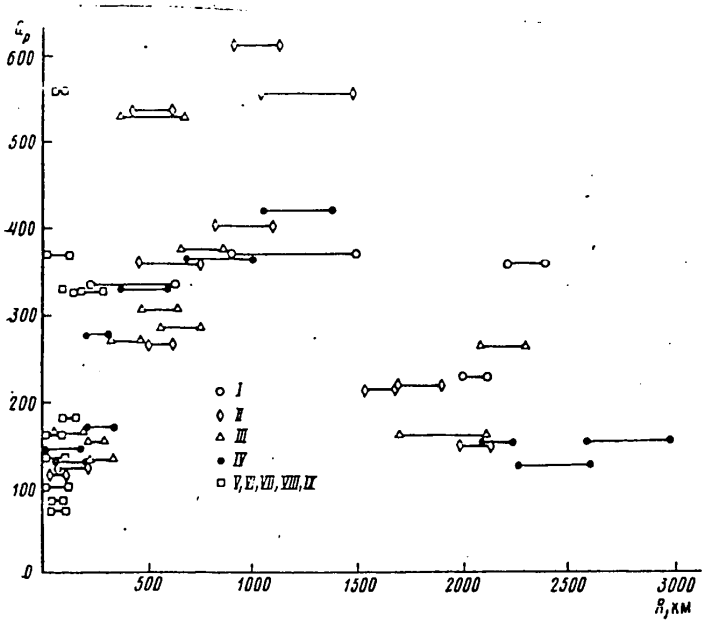

Figure 3. Dependence of Figure of Merit Q_P of Consolidated Crust and of Upper Mantle on Profile I on the Distance of the Range of Determination of Q_P to the Source (detonation point): I-IX correspond to the indices of the detonation points on profile I (Tables 1 and 2, Appendix 1)

It must be noted that the derived values of the attenuation coefficients characterize only layers with relatively increased velocities of body waves. And it is those very layers to which the refracted waves emerging during the first onsets are related. The figures presented in the article do not give an idea of the degree of attenuation of seismic energy in layers with reduced S and P wave propagation velocities.

Analyzing the data given in Table 2 and in [6], one may note (also see Figure 3):

1. The maximum attenuation ($K_1 = 2.40\text{-}2.96)\cdot 10^{-3}$ s·km^{-1} and $Q_1 = 130\text{-}160$) in the uppermost layer of the upper mantle was found for the Urals, the Kazakh folded country, the Turan plate, the Taymyr massif and the Mirnyy-Aykhal uplift. These regions are usually characterized either by relatively low values of P wave propagation velocity (7.8-8.1 km/s) or by a developed network of tectonic disturbances that encompass the upper mantle. The values of $\bar{K}_1$ and $\bar{Q}_1$ are similar to the mean

values (K_1 = (1.70-2.02)·10^{-3} s·km^{-1} and Q_1 = 220-240) in the Moscow, Tungusska and Vilyuy syneclises, where $V_P \geq 8.2$ km/s. The maximum figure of merit (Q_1 = = 250-290) is observed in the Caspian depression and the Baykal downwarp, i.e., in regions with higher velocity of P waves (V_P > 8.4 km/s).

2. Attenuation in the second depth range (75-95 km) depends to a lesser degree on the region of investigations. According to available data, an inverse ratio is noted between Q_1 and Q_2: reduced values of Q_2 correspond to zones of increased values of Q_1 (higher than the mean value). Thus, the mean value of this parameter is equal to 258 in the Caspian depression, 275 in the Tungusska syneclise, on the order of 320 in the Urals and in central Kazakhstan and 330 in the Mirnyy-Aykhal uplift.

3. The lowest attenuation in the entire mass of the upper mantle occurs in the third depth range (100-140 km). It is still difficult to talk about any principles in the distribution of $Q_3(K_3)$ with regard to the small amount of available data. One can note only that the mean value of Q_3 (five determinations) is equal to 450 for the Siberian platform and it is equal to 495 (two determinations) for the west Siberian plate. A single determination for the Moscow syneclise [6] yielded a value of Q_3 = 430.

4. The figure of merit of the layers of the upper mantle, corresponding to the fourth (150-210 km) and fifth (400-500 km) depth ranges, is somewhat higher on the Siberian platform (Q_4 = 225 and Q_5 = 260-450) than on the west Siberian plate (Q_4 = = 160 and Q_5 = 200).

Attenuation of transverse waves and comparison of it to attenuation of longitudinal waves. The attenuation of S-waves was determined from the amplitude spectra of S_k and S_{n1} waves. Recordings of the X- and Y-channels were used. Graphs of the dependence of $\ln[A(f_i)/A(f_m)](R)$, plotted from the S-wave spectra for X- and Y-channels separately, hardly differ from each other. The attenuation calculated from them is essentially identical with regard to confidence intervals. Therefore, attenuation by the spectra of the X- and Y-recordings processed jointly was calculated in the final version. Data on the values of K and Q are reduced in Table 3. Unlike Tables 1 and 2, four columns are added to Table 3 in which the values of K and Q are presented for P waves found approximately in the same intervals of the profile as K_S and Q_S. It is obvious from Table 3 that the accuracy of determining K_S and Q_S is the same as for P-waves.

The values of K_S for S_k waves, i.e., for the consolidated crust, are included in the range from 1.77 to 3.28·10^{-3} s·km^{-1}. Their mean value is equal to 2.60·10^{-3} s·km^{-1}. The figure of merit of the consolidated crust varies from 260 to 505 and $\bar{Q}_S$ = 345. The main part of the calculations of K_S was carried out within the Mirnyy-Aykhal saddle, where $\bar{K}_S$ = 2.81·10^{-3} s·km^{-1} and $\bar{K}_S$ = 310. Somewhat lower values of $\bar{K}_S$ were found for the Tungusska syneclise and the Angara-Lena stage, but there are only two determinations each in these regions.

Attenuation of S waves in the upper part of the upper mantle was studied only for the Tungusska syneclise. The value of K_S varies from 1.24·10^{-3} to 2.58·10^{-3} s·km^{-1}, the figure of merit varies from 260 to 539, $\bar{K}_S$ = 1.75·10^{-3} s·km^{-1} and $\bar{Q}_S$ = 390.

Analysis of the data (Tables 1-3) shows that the attenuation coefficients of P and S waves are approximately identical in the consolidated crust and in the upper part of the upper mantle, while the figure of merit for S-waves is higher. The ratio $\bar{K}_P/\bar{K}_S$ ($\bar{Q}_P/\bar{Q}_S$) is equal to 1.07 (0.66) for the crust and 1.03 (0.62) for the upper mantle. Considering these ratios only for cases when K_P and K_S was calculated on the same interval of the profile (Table 3), one may note: a) single determinations of K_P/K_S lie within the range of 0.49-2.79 for the consolidated crust and 0.58-3.40 for the upper mantle; b) the maximum values of K_P/K_S were found in zones of tectonic disturbances, which is in agreement with the data of other investigators [10]; and c) the mean value of $\bar{K}_P/\bar{K}_S$ ($\bar{Q}_P/\bar{Q}_S$) is equal to 1.07 (0.65) for the consolidated crust and 1.24 (0.67) for the upper mantle without maximum values.

Comparison of the data with the results of previous investigations is made difficult to a significant degree with regard to the different degree of detail of the measurements, the different method of calculations, the use of recordings of different types of waves and so on.

The value of K_P fluctuates from $0.98 \cdot 10^{-3}$ to $6.50 \cdot 10^{-3}$ $s \cdot km^{-1}$ for P waves and Q_P fluctuates from 70 to 525 in the consolidated crust, according to the figures (on the order of 30) presented in [1, 3, 7, 11-16]. The mean values of $\bar{K}_P = 2.70 \cdot 10^{-3}$ $s \cdot km^{-1}$ and $\bar{Q}_P = 185$. Thus, the range of variation of the parameters in Siberia that characterize attenuation in the crust (Table 1) and the mean values of $\bar{K}_P$ and $\bar{Q}_P$ are similar to the published experimental data for other regions of the earth.

Data on the attenuation parameters of P-waves are available in [1, 6, 7, 13-16] for the first 10-20 km of the upper mantle. According to the literature (40 determinations), the value of K fluctuates from $0.8 \cdot 10^{-3}$ to $6.67 \cdot 10^{-3}$ $s \cdot km^{-1}$ and Q fluctuates from 60 to 530. The mean values are equal to $2.15 \cdot 10^{-3}$ $s \cdot km^{-1}$ and 180, respectively. The mean value of K, calculated from the seismograms of large explosions [1], is equal to $1.9 \cdot 10^{-3}$ $s \cdot km^{-1}$. Thus, good agreement between published data and the data which we found is also observed for the mean values of parameters that characterize attenuation in the uppermost part of the mantle.

Determinations of Q_P were made by a number of investigators in rather thick masses for greater depths. Thus, Berzon et al [8] give $Q_P = 220$, Kanamori [17] gives 100 and Dorman [18] gives 475 for the 0-100 km layer; the following figures were found for a thickness of 0-760 km: 530 ± 150 [7], 150 [17] and 166-272 [19]. Moreover, curves of the dependence of Q_P on depth were published. A summary of these data is available in [20]. The results of calculating Q_P in the upper mantle of Siberia are in quite satisfactory agreement with the data of [6], the results for thickness of 0-100 km are in agreement with those presented in [8] and the results for the 0-760 km layer are in agreement with those presented in [19].

The mean value of Q_P in the investigated area of Siberia is similar to data of Antonova et al and Veith and Clawson (220, 240 and 260, respectively, on the graphs Q_P (H) [20, 21] in the depth range of 250-700 km. At the same time there are appreciable differences in the values of Q_P and in the nature of their variation with depth at $H < 200$ km. Thus, the maximum values of the figure of merit (approximately 450, according to the models of $Q_P(H)$ indicated above, are confined to the uppermost part of the mantle (near the Moho discontinuity) and decrease gradually

to a depth on the order of 100-120 km (a layer with reduced propagation velocity of elastic oscillations), the figure of merit then begins to increase and becomes equal to 240-260 at H ≈ 350 km. The figures presented in Table 2 show that if the layer with reduced velocity, present in the upper part of the mantle of the Siberian platform [22] is excluded, then one can talk about an increase of Q_P from 260 near the Moho discontinuity to 440 at a depth of approximately 200 km. Thus, the distribution of the figure of merit which we found for the upper 160 km of the mantle in layers with relatively increased velocity of body waves is directly opposite to that which is presented in [20, 21].

Comparison to MM8 and SL 1, 2, 3 models [5, 23] permits one to note the following: a) Q_P used in these models for the earth's crust is 5-20 times higher than the values determined in the Soviet Union and b) the mean value of the figure of merit in the first 160 km of the mantle are similar to those found in Siberia for SL 1, 2, 3 models and is lower by approximately a factor of 1.5 for the MM8 model. The nature of variation of Q_P with depth is approximately the same in SL models as that shown in [20, 21]; and c) the values of Q_P in the considered models are appreciably higher (by a factor of 1.5-3) than on the Siberian platform for the depth range of 200-700 km.

The reason for the disagreement of the data of different authors on the figure of merit of the earth's crust and the upper mantle may be the use of different methods of calculation and different types of waves and also the horizontal inhomogeneity in distribution of the attenuating properties of the object under study [6, 20, 24]. Moreover, some fixed value of Q_P/Q_S (usually $Q_P = 3/4(V_P/V_S)^2 Q_S$ [5, 20, 23]), not having adequate experimental substantiation, is used in some cases when plotting the functions of $Q_P(H)$.

The problem of the ratio of the attenuation coefficients (figure of merit) of longitudinal and transversal waves in the crust and upper mantle has been discussed repeatedly in the geophysical literature. Very different conclusions were made in this case. For example, $\alpha_P \approx \alpha_S$ and $Q_P < Q_S$ [15, 16, 25], $\alpha_S \approx 1.7\ \alpha_P$ and $Q_P = Q_S$ [4, 17] and $\alpha_S \approx 4.25\ \alpha_P$ and $Q_P \approx 2.5\ Q_S$ [26]. These differences can be explained by factors used previously to explain the differences in the values of Q_P. However, we feel that the main reason is the calculation of Q_P/Q_S by values determined from seismograms of P- and S-waves with significantly different trajectories. There are very few data on the values of α_P/α_S and Q_P/Q_S for the crust and mantle obtained by using an identical method on longitudinal and transversal waves with similar propagation paths. Thus, I. P. Pasechnik found the following values for the upper mantle of Central Asia (the region of recording refracted waves at 200-1,000 km): $K_P/K_S = 1.03$ and $Q_P/Q_S = 0.5$ [1] and E. P.Sumerina determined that $K_P/K_S \approx 0.8$ and $Q_P/Q_S \approx 0.75$ [16] from P^m_{pr} and S^m_{pr} waves in the North German depression. According to Khalturin's materials [11], $K_P/K_S = 1.1$ and $Q_P/Q_S = 0.53$ in the consolidated crust. E. P. Sumerina cites the following figures for the consolidated crust of the North German depression and the region of Tashkent [15, 16]: K_P/K_S is included in the range of 1.18-1.33 while Q_P/Q_S is included in the range of 0.45-0.50.

A considerable number of determinations of α_P and α_S in the frequency band of 0.4-24.0 Hz is presented in [27] for the crust and upper mantle (depth from 26 to 160

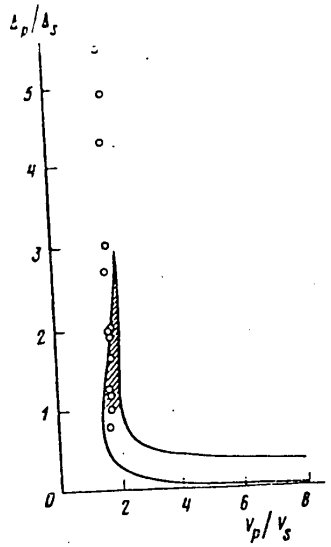

Figure 4. Dependence of Ratio of P- and S-Wave Attenuation Decrements on V_P/V_S: Points--experimental data for the crust and upper mantle of Siberia. The region of the most probable values of $\Delta P/\Delta S$ for hard rock according to [3, 29] is cross-hatched.

km) of Kamchatka. It follows from these data that α_P/α_S varies from 0.82 to 1.22 in the crust with a mean value of 0.99. The mean value of the considered parameter is equal to 1.00 (range of 0.50-1.87) at depths of 26-54 km and is equal to 1.02 (range of 0.29-2.0) in the range of 55-84 km, it is equal to 0.98 (range of 0.42-1.75) at 85-120 km and it is equal to 1.13 (range of 0.75-1.80) at 120-160 km. A direct estimate of the value of $(\alpha_P - \alpha_S)$ was also made along with measurement of α_P and α_S. It was shown that attenuation of longitudinal waves is more intensive than of transverse waves along routes passing through a region of modern volcanism and that attenuation of shear waves is no less than that of compression waves on routes through the focal layer.

Direct analysis of the ratio of coefficients K_P and K_S was also made for Siberia [28]. It was established that $K_P/K_S \approx 1$ for the consolidated crust and the upper 20-30 km of the upper mantle.

The region of possible values of the ratio of P- and S-wave attenuation decrements Δ_P/Δ_S at different values of V_P/V_S is outlined in Figure 4 from data of [29] based on Gurevich's analysis and generalization of the summary of experimental results presented in [3, 29, 30]*; $\Delta_{P,S} = \alpha_{P,S}\lambda_{P,S} = K_{P,S}V_{P,S}$. All our results of

*Editor's note. The sources of the experimental data are incorrectly shown in the summaries of [3] and [29] borrowed mainly from [30].

[Footnote continued on following page]

determining k_P and k_S in the crust and mantle according to Table 3 are presented in this same figure. As can be seen, with few exceptions they are in good agreement with Gurevich's theoretical function. Incidentally, we note that since $Q_S/Q_P = \Delta_P/\Delta_S$, from Figure 4 for "compact" rock, according to Gurevich, at $\Delta_P/\Delta_S > 1$ immediately follows $Q_S > Q_P$, which corresponds to many of the experimental results mentioned above.

Summarizing available data on the considered values, one may note that the experimental values of α_P/α_S and Q_P/Q_S for the consolidated crust and upper mantle are characterized by a significant spread, but the mean values of these parameters found in different regions are very similar and $\alpha_P/\alpha_S \approx 1$ and $Q_P/Q_S \approx 0.6$.

Conclusions

1. The figure of merit of the consolidated crust and supper mantle in Siberia differ significantly in area. The degree of its variation decreases somewhat as depth increases.

2. The mean figure of merit $\bar{Q}_P$ of the upper mantle increases from 241 to 445 as the depth increases to approximately 150 km (one has in mind layers with relatively increased velocities to which refracted waves emerging during the first onsets are related). The value of $\bar{Q}_P$ decreases to 190 at $H \approx 150$-210 km and $\bar{Q} = 345$ at depths of 400-500 km.

3. The attenuation coefficients of longitudinal and transversal waves in the consolidated crust and upper part of the upper mantle vary with depth, remaining practically equal to each other, while the mean value of Q_P is approximately 1.7 times less than the mean value of Q_S.

[Footnote continued from preceding page]
Table 7, page 413 in the column "Source" in [3] should read: [65] instead of [213], [213] instead of [219], [219] instead of [139], [139] instead of [119] for the sedimentary mass and for granite and [102] instead of [119] for loess, [119] instead of [99, 100] and [99] instead of [175] for granite and [175] for rock of the earth's mantle. Moreover, reference [16] should be replaced by [8] from [20]; all figures are from the bibliography in [3].

The table in the column "Source" in [29] should read: [12] instead of [13], [13] instead of [14], [14] instead of [15], [15] instead of [16] [16] instead of [17], [18] instead of [19], [19] instead of [20] and [20] instead of [21]. Moreover, reference [18] should be replaced by [8] from [1]; all the figures are from the bibliography of [29].

The entire bibliography in [20] is shown correctly.

We note in passing that "the most accurate and reliable results" of determining the attenuation coefficients of longitudinal and transverse waves in granites (for that time) noted in Figure 2 in [30] by the large circle: $\alpha_P = \alpha_S$, were presented in [8] from [30]. When these materials were processed, the method of interpretation was both developed and used for the first time which is also used by the authors of this article.

BIBLIOGRAPHY

1. Pasechnik, I. P., "Kharakteristika seysmicheskikh voln pri yadernykh vzryvakh i zemletryaseniyakh" [Characteristics of Seismic Waves During Nuclear Explosions and Earthquakes], Moscow, Nauka, 1970.

2. Jackson, D. D. and D. L. Anderson, "Physical Mechanisms of Seismic Wave Attenuation," REVIEW OF GEOPHYSICS AND SPACE PHYSICS, Vol 3, No 1, 1970.

3. Gurevich, G. I., "Deformiruyemost' sred i rasprostraneniye seysmicheskikh voln" [The Deformability of Media and Propagation of Seismic Waves], Moscow, Nauka, 1974.

4. Kogan, S. Ya., "Seysmicheskaya energiya i metody yeye opredeleniya" [Seismic Energy and Methods of Determining It], Moscow, Nauka, 1975.

5. Anderson, D. L. and R. S. Hart, "Attenuation Models of the Earth," PHYSICS OF THE EARTH AND PLANETARY INTERIORS, 1978.

6. Yegorkin, A. V. and V. V. Kun, "Attenuation of Longitudinal Waves in the Earth's Upper Mantle," IZVESTIYA AN SSSR, FIZIKA ZEMLI, No 4, 1978.

7. Berzon, I. S., A. M. Yepinat'yeva, G. N. Pariyskaya and S. P. Starodubovskaya, "Dinamicheskiye kharakteristiki seysmicheskikh voln v real'nykh sredakh" [Dynamic Characteristics of Seismic Waves in Real Media], Moscow, Nauka, 1962.

8. Berzon, I. S., I. P. Pasechnik and A. M. Polikarnov, "Determining the Parameters of P-Wave Attenuation in the Earth's Mantle," IZVESTIYA AN SSSR, FIZIKA ZEMLI, No 2, 1975.

9. Berzon, I. S., I. P. Pasechnik and A. M. Polikarnov, "Supplement to the Article 'Determination of the Parameters of P-Wave Attenuation in the Earth's Mantle [1, 2]'," IZVESTIYA AN SSSR, FIZIKA ZEMLI, No 10, 1979.

10. Pustovitenko, B. G. and T. G. Rautian, "Investigating the Attenuation of Seismic Waves in the Crimea and the Regional Characteristics of Focal Radiation Through the Crust," Proceedings of the Symposium "Modern Methods of Recording and Interpretation of Seismic Observations," Report Topics, Yalta, 1979.

11. Khalturin, V. I. and N. B. Urusova, "Estimating the Attenuation of Longitudinal and Transversal Waves in the Earth's Crust From Observations of Local Earthquakes," TRUDY INSTITUTA FIZIKI ZEMLI AN SSSR, No 25 (192), 1962.

12. Tulina, Yu. V. and G. A. Yaroshevskaya, "Vnutrennyaya struktura Zemnoy kory" [The Internal Structure of the Earth's Crust], Moscow, Nauka, 1976.

13. "Glubinnoye seysmicheskoye zondirovaniye zemnoy kory v SSSR" [Deep Seismic Sounding of the Earth's Crust in the USSR], Leningrad, Gostoptekhizdat, 1962.

14. Vol'vovskiy, I. S. and V. S. Vol'vovskiy, "Razrezy zemnoy kory territorii SSSR po dannym glubinnogo seysmicheskogo zondirovaniya" [Profiles of the Earth's Crust in the USSR From Deep Seismic Sounding Data], Moscow, Sovetskoye radio, 1975.

15. Sumerina, E. P., "Determining the Attenuation and Scattering Coefficients of Longitudinal and Transversal Waves Recorded by 'Zemlya' Stations," in "Razvedochnaya geofizika" [Exploratory Geophysics], Issue 59, Moscow, Nedra, 1973.

16. Sumerina, E. P., "Attenuation of Longitudinal and Transversal Waves," in "Sostoyaniye i perspektivy razvitiya metodov poperechnykh i obmennykh voln v seysmorazvedke" [The State and Prospects for Development of Methods of Transversal and Body Waves in Seismic Prospecting], Moscow, Rotaprint, VNIIGeofizika, 1977.

17. Kanamori, H., "Spectrum of P and PcP in Relation to the Mantle-Core Boundary and Attenuation in the Mantle," JOURNAL OF GEOPHYSICAL RESEARCH, Vol 72, 1967.

18. Dorman, L. M., "Anelasticity and the Spectra of Body Waves," JOURNAL OF GEOPHYSICAL RESEARCH, Vol 73, No 12, 1968.

19. Mikumo, T. and T. Kurita, "On Distribution for Longperiod P-Waves in the Mantle," JOURNAL OF PHYSICS OF THE EARTH, Vol 16, 1968.

20. Antonova, L. V., F. F. Aptikayev, R. I. Kurochkina et al, "Eksperimental'nyye seysmicheskiye issledovaniya nedr Zemli" [Experimental Seismic Investigations of the Earth's Interior], Moscow, Nauka, 1978.

21. Veith, K. F. and G. E. Clawson, "Magnitude from Short-Period P-Wave Data," BULLETIN OF THE SEISMOLOGICAL SOCIETY OF AMERICA, Vol 69, No 2,1972.

22. Vinnik, L. P. and A. V. Yerogkin, "Wave Fields and Models of the Lithosphere and Asthenosphere from Seismic Observation Data in Siberia," DOKLADY AN SSSR, Vol 250, No 2, 1980.

23. Anderson, D. L., A. Ben-Menahem and C. B. Archambeau, "Attenuation of Seismic Energy in the Upper Mantle," JOURNAL OF GEOPHYSICAL RESEARCH, Vol 70, No 6, 1965.

24. Vinnik, L. P., "Issledovaniya mantii Zemli seysmicheskimi metodami" [Investigations of the Earth's Mantle by Seismic Methods], Moscow, Nauka, 1976.

25. Attewell, P. B. and J. V. Ramana, "Wave Attenuation and Internal Friction as a Function of Frequency in Rocks," GEOPHYSICS, 1966.

26. Kovach, R. L., "Attenuation of Seismic Body Waves in the Mantle," GEOPHYSICS JOURNAL OF THE ROYAL ASTONOMICAL SOCIETY, 1967.

27. Boldyrev, S. A., "Spectre of Elastic Waves from Weak Earthquakes and Analysis of Attenuation Under Kamchatka," in "Seysmichnost' i seysmicheskiy prognoz, svoystva verkhney mantii i ikh svyaz' s vulcanizmom na Kamchatke" [Seismicity and Seismic Forecasting, the Properties of the Upper Mantle and Their Relationship to Volcanism on Kamchatka], Novosibirsk, Nauka, 1974.

28. Yegorkin, A. V. and G. V. Yegorkina, "Transversal Waves During Deep Investigations," GEOLOGIYA I GEOFIZIKA, No 6, 1980.

29. Vasil'yev, Yu. I. and G. I. Gurevich, "The Ratios Between the Attenuation Decrements and Propagation Velocities of Longitudinal and Transversal Waves," IZVESTIYA AN SSSR, SERIYA GEOFIZIKA, No 12, 1962.

30. Vasil'yev, Yu. I., "Two Summaries of Attenuation Constants of Elastic Oscillations in Rock," IZVESTIYA AN SSSR, SERIYA GEOFIZIKA, No 5, 1962.

6521
CSO: 8144/1489

COLLECTION OF ARTICLES ON DYNAMIC THEORY OF SEISMIC WAVE PROPAGATION

Moscow VOPROSY DINAMICHESKOY TEORII RASPROSTRANENIYA SEYSMICHESKIKH VOLN in Russian
No 20, 1981 (signed to press 7 Jan 81) pp 3, 212

[Foreword and table of contents from collection of articles "Problems in the Dynamic Theory of Seismic Wave Propagation", edited by G. I. Petrashen', Izdatel'stvo "Nauka", Leningradskoye otdeleniye, 1300 copies, 216 pages]

[Text] Foreword. The articles contained in this number of the series are naturally subdivided into groups relating to extremely important directions in modern seismics, to wit: 1) study of wave processes in anisotropic and isotropic elastic media; 2) algorithms and methods for computing seismic fields; 3) theoretical and experimental investigations in the field of seismic prospecting, and finally, 4) statistical approaches in evaluating geophysical information. As a result of the abundance and diversity of articles it would be very difficult here to attempt to give a detailed description of their contents. This, to be sure, is not required, since a general idea concerning their content can be obtained from the abstracts.

The most important feature of this collection of articles is its international character, being a direct result of our scientific contacts with the geophysicists of the countries of the Socialist Economic Bloc, who with each passing year are becoming more and more close. For example, this collection contains a long article by our colleagues from Czechoslovakia V. Cerveny and J. Zahradnik and from West Germany K. Fuchs and G. Muller, as well as two articles by our colleagues from East Germany G. Peschel, H. Poppitz, A. E. Gotz and P. Kolyschkov. It will undoubtedly be of interest to familiarize our Soviet readers with these articles.

Another feature of the collection of articles to which it is evidently fitting to draw attention is that its appearance is related to the beginning of our scientific attack on all that is unclear in the field of seismic anisotropy. The fact of a need for taking into account the anisotropy of seismic media in the choice of their sufficiently adequate models is scarcely in need of argumentation. However, the anisotropy of seismic media until now has been poorly taken into account in modern seismics. And this occurs primarily due to the widespread opinion that allowance for the anisotropy of media in wave propagation processes is unreliable due to "insuperable" mathematical difficulties and the excessive unwieldiness of any analytical solutions of wave propagation problems.

We resolutely dispute such a point of view and it is our purpose to show that with some departure from the traditional classical approaches to problems the obtaining of effective quantitative solutions of the main problems of wave propagation in anisotropic elastic media becomes an entirely real task, not requiring even a great expenditure of time and work. We have presented a full proof of such an assertion

in a special monograph. [G. I. Petrashen', RASPROSTRANENIYE VOLN V ANISOTROPNYKH UPRUGIKH SREDAKH (Wave Propagation in Anisotropic Elastic Media), Leningrad, "Nauka," 1980.]

To be sure, here I would like to devote attention to each article in the collection and characterize its merits with at least one or two sentences. But I will limit myself solely to directing the attention of readers to the articles of M. M. Popov and L. G. Tyurikov, devoted to computation of the geometrical divergence of beams of rays in arbitrary inhomogeneous isotropic media. These articles give a very refined and simple solution of the problem and therefore great satisfaction can be obtained from their reading.

G. Petrashen'

Contents

5303
CSO: 1865/227

PAPERS ON MATHEMATICAL METHODS FOR INTERPRETING GEOPHYSICAL OBSERVATIONS

Novosibirsk MATEMATICHESKIYE METODY INTERPRETATSII GEOFIZICHESKIKH NABLYUDENIY in Russian 1979 (signed to press 26 Dec 79) pp 2-3, 175-177

[Annotation, table of contents and abstracts from collection of articles "Mathematical Methods for the Interpretation of Geophysical Observations," edited by Anatoliy Semenovich Alekseyev, Vychislitel'nyy tsentr SO AN SSSR, 600 copies, 178 pages]

[Text] Annotation. This collection of articles is devoted to problems related to the development, validation and numerical application of methods for solving direct and inverse problems in the theory of wave propagation and diffraction and photogrammetry. The collection is of interest for specialists in the fields of geophysics and mathematical physics, and also for students and graduate students specializing in the field of geophysics.

Contents

Abstracts

UDC 550.344

COMPUTATION OF GEOMETRICAL DIVERGENCE IN CARTESIAN COORDINATES

[Abstract of article by Belonosova, A. V. and Tsetsokho, V. A.]

[Text] The article gives a system of six ordinary differential equations for determining the geometrical divergence of the central field of seismic waves in a medium without discontinuities. In contrast to the studies of other authors, in deriving the equations use was made only of a Cartesian coordinate system in which the characteristics of the medium are stipulated. It is also demonstrated in the study that the advantage of any system of differential equations for the numerical determination of geometrical divergence is related not so much to the number of equations in the system as to the number of arithmetical operations required for computing the right-hand side of the system at one point.

UDC 517.948:519.6

NUMERICAL SOLUTION OF THE TWO-DIMENSIONAL PROBLEM OF DIFFRACTION OF AN ELASTIC WAVE ON AN ELASTIC BODY III

[Abstract of article by Voronin, V. V.]

[Text] The author in general features describes an algorithm for the numerical application of a method proposed and validated in the earlier articles of the author. The elimination of singularities is used in computing the coefficients of the matrix obtained after discretization of a system of singular integral equations. The results of numerical experiments are given. Figures 5; references 4.

UDC 517.544

RESTORATION OF THE COEFFICIENTS ON THE LOWER DERIVATIVES IN THE ACOUSTIC EQUATION

[Abstract of article by Yelinov, V. D.]

[Text] The article examines the problem of the uniqueness of determination of the coefficients on the lower derivatives in the acoustic equation. The initial problem is reduced to the known problem of integral geometry. References 3.

UDC 517.945

ON THE PROBLEM OF STABILITY IN DETERMINATION OF RADIATING POINT OBJECTS

[Abstract of article by Yerokhin, G. N.]

[Text] A study was made of the stability of solution of the inverse problem in determination of "brightness" and coordinates of a finite number of luminescent sources on the basis of the information stipulated in the form of some blurred image. In two special cases a function characterizing this stability was determined in explicit form.

UDC 550.345

METHODS FOR COMPUTING TSUNAMI WAVES WITHIN THE FRAMEWORK OF APPROXIMATE MODELS

[Abstract of article by Marchuk, A. G.]

[Text] The author proposes a number of methods for computing the problems involved in the generation, propagation and breaking of tsunami waves on the shore. The generation problem is solved within the framework of a nonlinear system of equations for shallow water. A model of an ideal incompressible fluid is also proposed for use in solving generation problems. Numerical experiments were used in investigating the dependence of the characteristics of tsunami waves on the parameters of bottom movements. A method for separate calculations in deep and shallow parts of the basin was developed for computing the problems involved in the propagation of tsunami waves in a basin of variable depth. Also discussed in the article is the problem of the energy of tsunami waves and its relationship to focal energy. A refined formula is proposed for estimating this energy. An original method related to transformation to an oblique coordinate system is proposed for computing the problems involved in the rolling of tsunami waves onto a sloping shore. The results of numerical computations by the mentioned methods are given. Figures 22, references 9.

UDC 518.61.550.344

NUMERICAL MODELING OF THE PROPAGATION OF ELASTIC WAVES IN ANISOTROPIC INHOMOGENEOUS MEDIA (CASE OF A HALF-SPACE AND SPHERE)

[Abstract of article by Martynov, V. N. and Mikhaylenko, B. G.]

[Text] The article gives algorithms using finite integral transforms in combination with numerical methods for solving problems in the propagation of elastic waves in a transversally isotropic half-space. A method is also developed for a radially inhomogeneous tangentially isotropic model of the earth. Also examined is the problem of the use of finite integral time transforms for solving the problem of the propagation of elastic waves in inhomogeneous anisotropic media with absorption. References 10.

UDC 518.61.550.344

NUMERICAL SOLUTION OF THE LAMB PROBLEM FOR AN INHOMOGENEOUS BOLTZMANN MEDIUM WITH AN ELASTIC AFTEREFFECT

[Abstract of article by Fat'yanov, A. G. and Mikhaylenko, B. G.]

[Text] The article consists of two parts. The first gives a solution of the Lamb problem for an inhomogeneous (with respect to depth) half-space filled with a Boltzmann medium with an exponential function of the aftereffect. The second proposes an approximate method for solving this problem for an arbitrary function of the aftereffect. The convergence of the methods for a homogeneous medium is demonstrated. Theoretical seismograms are given for a layer on a half-space with different absorption. Figures 8, references 22.

UDC 513.73

ON GEOMETRICAL DIVERGENCE

[Abstract of article by Sharafutdinov, V. A.]

[Text] It is demonstrated in this study that the computation of geometrical divergence can be reduced to solution of the Cauchy problem for the Jacobi equation and the symmetry of geometrical divergence is also demonstrated for the case of an anisotropic medium. References 4.

5303
CSO: 1865/209

PHYSICS OF ATMOSPHERE

UDC 551.507.551.513:551.507.551.508.551.513.590.2

PAPERS ON ROCKET SOUNDING OF THE ATMOSPHERE

Moscow TRUDY TSENTRAL'NOY AEROLOGICHESKOY OBSERVATORII: FIZIKA VERKHNEY ATMOSFERY, SERIYA A: RAKETNOYE ZONDIROVANIYE in Russian No 144, 1981 (signed to press 23 Jan 81) pp 2, 133

[Annotation and table of contents from collection of articles "Transactions of the Central Aerological Observatory: Physics of the Upper Atmosphere, Series A: Rocket Sounding", edited by G. A. Kokin, doctor of physical and mathematical sciences, Izdatel'stvo Moskovskoye otdeleniye Gidrometeoizdata, 370 copies, 134 pages]

[Text] Annotation. This collection of articles contains papers devoted to methods for carrying out a rocket experiment in the upper atmosphere. For the most part the authors examine problems involved in the method for determining small components in the atmosphere and also the problem of aerodynamic modeling of processes of interaction of measuring instruments with a flow of supersonic rarefied gas. Some results of rocket sounding are discussed. The collection is of interest for scientific specialists interested in problems relating to physics of the upper atmosphere, the aerodynamics of rarefied gas, and also specialists concerned with the development of scientific rocket and laser instrumentation.

Contents

5303
CSO: 1865/201

UDC 551.593+551.510.536

COLLECTION OF PAPERS ON ATMOSPHERIC OPTICS

Moscow TRUDY INSTITUTA EKSPERIMENTAL'NOY METEOROLOGII: OPTIKA ATMOSFERY in Russian No 10(84), 1981 (signed to press 28 Jan 81) pp 2, 102

[Annotation and table of contents from collection of articles "Transactions of the Institute of Experimental Meteorology: Atmospheric Optics", edited by V. N. Lebedinets, Izdatel'stvo Moskovskoye otdeleniye Gidrometeoizdata, 430 copies, 102 pages]

[Text] Annotation. This collection of articles includes 12 original and review articles devoted primarily to instrumental-methodological problems in the following principal research directions: development of instrumentation for optical investigations of the atmosphere and accompanying measurements of ionospheric parameters; calibration of radiometric apparatus and computation of measurement errors; methods for remote optical sounding of the atmosphere; results of measurements of composition of the upper atmosphere and the optical characteristics of atmospheric formations. The authors describe a number of instruments for surface and rocket investigations of the atmosphere developed at the Institute of Experimental Meteorology at the level of the best Soviet and foreign models. The papers give the results of the first systematic investigations of the layer of Ca^+ ions in the USSR near the mesopause by the method of surface spectral twilight observations. The collection is intended for a wide range of specialists in the field of atmospheric optics, physics of the upper atmosphere and optical methods for remote sounding of the atmosphere.

Contents

5303
CSO: 1865/200

COLLECTION OF PAPERS ON INVESTIGATION OF THE IONOSPHERE AND MAGNETOSPHERE BY ARTIFICIAL MODIFICATION METHODS

Apatity ISSLEDOVANIYE IONOSFERY I MAGNITOSFERY METODAMI AKTIVNOGO VOZDEYSTVIYA in Russian 1977 (signed to press 8 Jul 77) pp 2, 81

[Annotation and table of contents from collection of papers "Investigation of the Ionosphere and Magnetosphere by Artificial Modification Methods", edited by Ye. M. Filatov, Uchastok operativnoy poligrafii Ordena Lenina Kol'skogo Filiala imeni S. M. Kirova AN SSSR, 300 copies, 82 pages]

[Text] Annotation. The authors of the papers in this collection of articles describe the principles of operation and give the principal technical specifications of an apparatus for modification of the polar ionosphere by powerful short-wave radiation and also the results of experiments carried out during the period 1975-1977 using this and similar apparatus, in particular, the results of observations of radiation at combined frequencies in the auroral zone, measurements of the polarization of signals at combined frequencies, investigations of the effects of scattering of a radio signal from the region of the ionosphere subjected to the influence of powerful short-wave radiation, and the effects observed during vertical sounding of this region. Also examined are possible mechanisms of the influence of a powerful radio wave on the ionosphere and magnetosphere, as well as the probable mechanisms of the influence of this wave on the generation of VLF emissions.

Contents

5303
CSO: 1865/220

ARCTIC AND ANTARCTIC RESEARCH

UDC 551.510.536

LASER SOUNDING OF THE UPPER ATMOSPHERE AT THE ANTARCTIC STATION MOLODEZHNAYA

Moscow DOKLADY AKADEMII NAUK SSSR in Russian Vol 258, No 2, 1981 (manuscript received 2 Feb 81) pp 334-335

[Article by M. F. Lagutin, Yu. Ye. Megel', N. N. Petrov, A. A. Zarudnyy, V. N. Kuznetsov, V. Ye. Mel'nikov, N. P. Mustetsov and N. G. Baranov, Khar'kov Institute of Radioelectronics]

[Text] In accordance with the national program for investigating the middle atmosphere, systematic experiments for laser sounding of the upper atmosphere of the south polar region were initiated for the first time in world practice in May 1979 at the Antarctic station Molodezhnaya (69°S) during the 24th Soviet Antarctic Expedition. The purpose of this study was an investigation of dynamic processes for measuring the concentration and vertical distribution of the natural sodium layer in the Antarctic mesosphere under polar night conditions.

The atmosphere was sounded using a lidar of original design based on a tunable laser with a radiation line width 0.1 A. The surface antenna used was a telescope with a dish having a diameter of 80 cm and an angle of the field of view $5 \cdot 10^{-3}$ rad. The photodetector with an interfilter bandwidth 25 A operated in a photon-counting regime. The registry system is a 100-channel memory system with digital elements; the width of the sounded range interval was 1 km; the routine display of information for a single sounding and in an accumulation regime was on a screen of an original design; the documentation of information was on a digital magnetic recorder. The normalization of the sounding results was accomplished using molecular scattering signals from an altitude of 30-40 km, where aerosol scattering is not observed.

A preliminary analysis of information during the observation period (May-October 1979) indicated that the sodium concentration in the south polar region 69°S is subject to the influence of a number of dynamic processes. The observed vertical distribution decreases sharply in the sector 3-5 km due to the influence of turbulent diffusion. The turbulence coefficient, computed on the basis of the character of the change in concentration with altitude, corresponds to the values characteristic for the middle latitudes. The mean altitude of the layer is 91 ± 1 km.

The dynamics of the upper part of the layer at an altitude of about 100 km and the sodium concentration in a column is probably due to the influence of meteor streams. At individual moments there is a considerable stratification in the distribution with a width of the layers ~ 1 km in which the concentration substantially exceeds

the mean value, indicating a presence of atmospheric disturbances specific for the auroral zone, for example, due to the leakage of energetic particles. A periodic modulation of density is also observed in the pattern of molecular scattering signals. The method of digital filtration of signals revealed waves of the vertical gravitational waves type with a period of 12, 8, 6, 4, 3.6 and 2.8 km. There is a change in the phase of waves with a velocity of 0.6-3 km/hour propagating both downward and upward, which indicates a different nature of the sources of their excitation.

Thus, the results determine the fundamental possibility of carrying out extensive laser investigations of the atmosphere in Antarctica with the use of resonance luminescence, molecular and aerosol scattering of laser radiation.

It is of special interest to carry out complex investigations by radiometeor, rocket and other methods with simultaneous laser sounding for the purpose of studying dynamic processes caused by stratomesospheric interactions with the discrimination of phenomena of auroral origin.

5303 - END -
CSO: 8144/1581